

1N-09  
158532  
P.66

NASA Technical Memorandum 103920

---

# Performance and Test Section Flow Characteristics of the National Full-Scale Aerodynam- ics Complex 80- by 120-Foot Wind Tunnel

---

Peter T. Zell

---

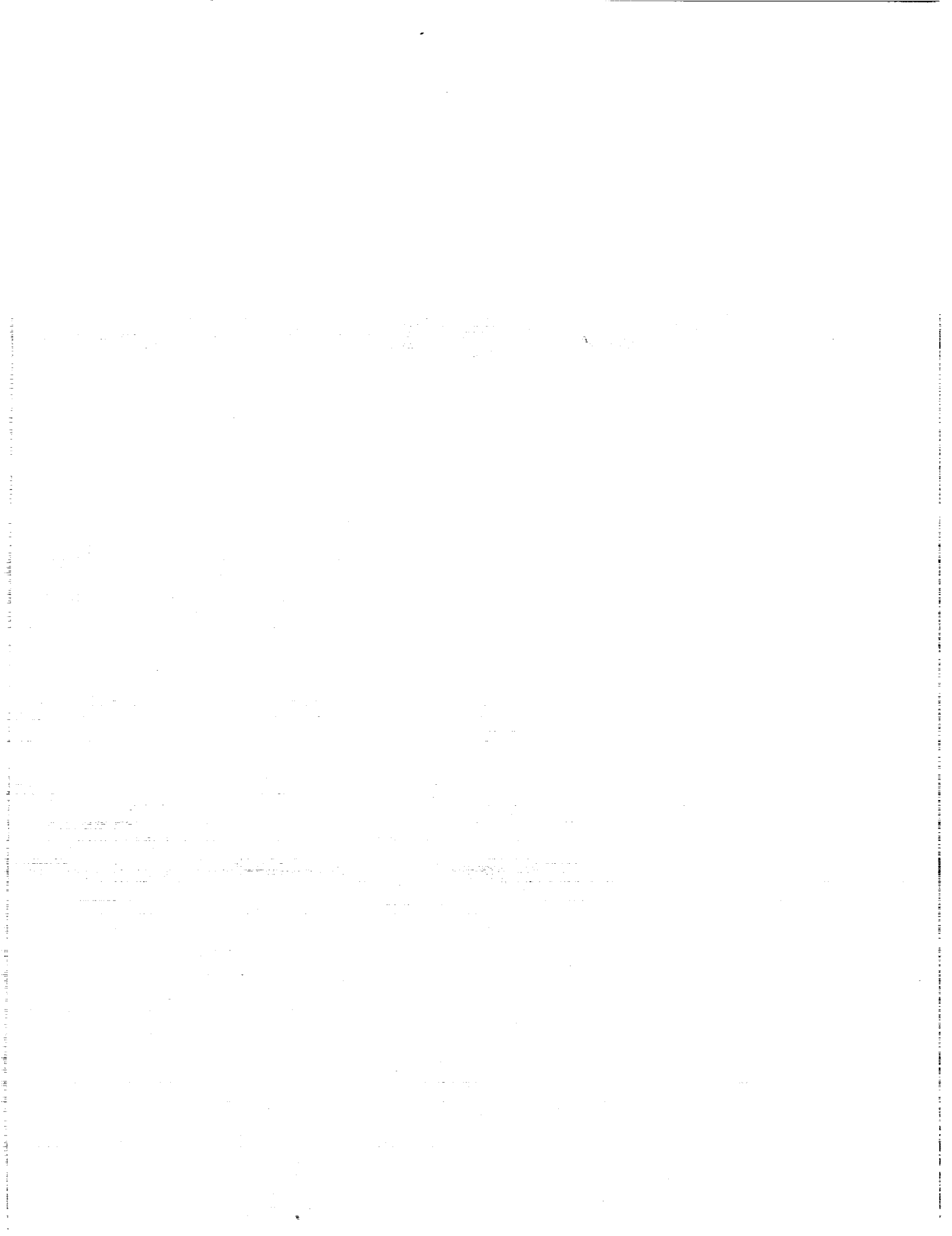
January 1993

(NASA-TM-103920) PERFORMANCE AND  
TEST SECTION FLOW CHARACTERISTICS  
OF THE NATIONAL FULL-SCALE  
AERODYNAMICS COMPLEX 80- BY  
120-FOOT WIND TUNNEL (NASA) 66 p

N93-23420

Unclass

G3/09 0158532



---

# Performance and Test Section Flow Characteristics of the National Full-Scale Aerodynam- ics Complex 80- by 120-Foot Wind Tunnel

---

Peter T. Zell, Ames Research Center, Moffett Field, California

January 1993



National Aeronautics and  
Space Administration

**Ames Research Center**  
Moffett Field, California 94035-1000



# Table of Contents

	Page
Nomenclature .....	v
Summary .....	1
Introduction .....	1
Facility Description .....	1
Apparatus .....	2
Instrumentation Support Hardware .....	2
Instrumentation .....	3
Data System .....	3
Dynamic Pressure Calibration .....	3
Performance Calibration .....	4
Dynamic Pressure and Velocity Versus Fan Blade Angle .....	4
Dynamic Pressure and Velocity Versus Tunnel Power .....	4
Dynamic Pressure Decay .....	5
Time Averaged Flow Quality Parameters .....	5
Pressure and Velocity Distributions .....	5
Streamwise Static Pressure Distributions .....	6
Flow Angle Distributions .....	6
Temperature Distributions .....	6
Boundary Layer Profiles .....	7
Dynamic Flow Quality Parameters .....	7
Turbulence Intensity Distributions .....	7
Axial Turbulence Intensity Energy Spectra .....	7
Flow Meander .....	7
Atmospheric Wind Effects .....	7
Summary of Results .....	8
Recommendations .....	9
References .....	9
Tables .....	10
Figures .....	14



## Nomenclature

BA	fan blade angle	$q_{cse}$	dynamic pressure measurement corrected for scale errors only, $q_{cse} = q_u - \Delta q_{sc}$ , psf
$C_p$	flow field static pressure coefficient, $C_p = (p_s - p_{s,cl}) / (q_{cse})$	$\Delta q_{sp}$	static plate correction to measured dynamic pressure, psf
$C_{p,w}$	test section wall static pressure coefficient, $C_{p,w} = (p_{s,w} - P_s) / (q_{cse})$	$q_{clu}$	dynamic pressure measurement corrected for scale errors and static plate errors only, $q_{clu} = q_{cse} - \Delta q_{sp}$ , psf
$I_u$	axial turbulence intensity component, $I_u = u'/u$ , percent	$\Delta q_\eta$	compressibility correction to measured dynamic pressure, psf
$I_v$	lateral turbulence intensity component, $I_v = v'/u$ , percent	$q_c$	fully corrected dynamic pressure measurement, $q_c = q_{clu} - \Delta q_\eta$ , psf
$I_w$	vertical turbulence intensity component, $I_w = w'/u$ , percent	T	total temperature measured in the test section, °F
$P_{atm}$	atmospheric pressure, psf	$T_T$	tunnel total temperature measured at the wind tunnel inlet, °F
$p_s$	static pressure, psf	u	axial velocity component, ft/sec
$p_{s,cl}$	static pressure measured on the test section centerline, psf	$u'$	axial rms velocity component, ft/sec
$p_{s,w}$	static pressure measured on the test section wall, psf	U	flow velocity, knots
$P_s$	measured test section static pressure from the scale system, psf	$\bar{U}$	average flow velocity, knots
$p_t$	total pressure, psf	$U_{ts}$	test section flow velocity, knots
$p_{t,cl}$	total pressure measured on the test section centerline, psf	$v'$	lateral rms velocity component, ft/sec
$P_t$	measured test section total pressure from the scale system, psf	$w'$	vertical rms velocity component, ft/sec
q	dynamic pressure, $q = 1/2\rho U^2$ , psf	X	streamwise coordinate, ft (positive downstream)
$\bar{q}$	average dynamic pressure, psf	Y	cross-stream coordinate, ft (positive to the right looking upstream)
$q_u$	uncorrected dynamic pressure from the scale system, $P_t - P_s$ , psf	Z	vertical coordinate, ft (in. if specified, positive up)
$\Delta q_{sc}$	scale correction to measured dynamic pressure, psf	$\alpha$	upflow angle, degrees
		$\beta$	crossflow angle, degrees
		$\rho$	air density, slugs/ft <sup>3</sup>





## Summary

Results from the performance and test section flow calibration of the 80- by 120-Foot Wind Tunnel are presented. Measurements indicating the 80- by 120-ft test section flow quality were obtained throughout the tunnel operational envelope and for atmospheric wind speeds up to approximately 20 knots. Tunnel performance characteristics and a dynamic pressure system calibration were also documented during the process of mapping the test section flow field.

Experimental results indicate that the test section flow quality is relatively insensitive to dynamic pressure and the level of atmospheric winds experienced during the calibration. The dynamic pressure variation in the test section is within  $\pm 0.75\%$  of the average. The axial turbulence intensity is less than 0.5% up to the maximum test section speed of 100 knots, and the vertical and lateral flow angle variations are within  $\pm 0.5^\circ$  and  $\pm 0.7^\circ$ , respectively. Atmospheric winds were found to affect the pressure distribution in the test section only at high ratios of wind speed to test section speed.

## Introduction

The 80- by 120-Foot Wind Tunnel is part of the National Full-Scale Aerodynamics Complex (NFAC) located at the NASA Ames Research Center (fig. 1). It is an open circuit wind tunnel with a closed, rectangular test section. The maximum test section flow speed is approximately 100 knots (51 m/sec). Figure 2 shows a schematic of the wind tunnel circuit.

The 80- by 120-Foot Wind Tunnel shares a portion of its flow circuit with the 40- by 80-Foot Wind Tunnel. A schematic of the tunnels in 40- by 80-mode is shown as figure 3. Both tunnels use the same fan drive system. It consists of six fans rated at 135,000 maximum combined horsepower (101 MW) as shown in figure 4.

The 40- by 80-Foot Wind Tunnel was constructed in the 1940s and used extensively for over three decades for a variety of large-scale subsonic tests. The tunnel was then brought off-line for modifications necessary to meet the current and future requirements of large-scale aerodynamic and aeroacoustic testing. The drive system was repowered to increase the test section velocity from 200 to 300 knots. The new nonreturn leg with an 80- by 120-ft test section was also added to the tunnel circuit at this time.

The quality of the flow passing through the test chamber of the 80- by 120-Foot Wind Tunnel is determined by the performance of the atmospheric inlet and contraction. The performance of the wind tunnel depends on the quality of

the flow in the entire tunnel circuit. Much experimental and theoretical work was done during the tunnel modification to improve circuit aerodynamics. The results of this work are described by Olson et al. (ref. 2).

Before research testing could begin in the new 80- by 120-Foot Wind Tunnel, a performance and test section flow calibration was required. This report presents the results of the calibration concluded in June of 1988. A similar calibration of the 40- by 80-Foot Wind Tunnel was concluded in June of 1987 (ref. 1).

The primary goal of the flow calibration (FLOCAL) test was to measure the 80- by 120-ft test section flow quality throughout the tunnel operational envelope and for various atmospheric wind conditions. This was done by examining the distributions of total and static pressure, velocity (including magnitude and direction), turbulence, and temperature. A limited assessment of unsteady flow characteristics was also made. Wind tunnel performance results consisted of calibration curves of test section dynamic pressure and velocity versus fan blade angle and net power delivered to the fans. A dynamic pressure system calibration was also performed. Table 1 contains the FLOCAL test matrix.

## Facility Description

The flow path of the 80- by 120-Foot Wind Tunnel is described here, beginning outside the atmospheric inlet and proceeding through the circuit to the atmospheric exhaust. It is important to note that the 80- by 120- and 40- by 80-Foot Wind Tunnels share portions of their flow paths (figs. 2 and 3). Selection between the two tunnels is accomplished by adjusting a set of large movable tunnel walls and flow-deflection vanes. These walls and deflection vanes are discussed in the order that they are encountered by the flow in the 80- by 120-circuit.

Atmospheric air is drawn toward the inlet of the wind tunnel. Air in the vicinity of the inlet edges is guided into the tunnel by a 17-ft radius cowl. The flow then encounters a set of acoustically treated vanes. The acoustic treatment reduces the noise generated by the fan drive and models to the surrounding community. The inlet guide vanes are splayed as shown in figure 5. A bird screen is attached to the leading edge of the vanes. A flow treatment screen is attached to the trailing edge to reduce turbulence generated by the presence of the vanes. More information about the design and development of the 80- by 120-inlet is contained in references 3-5.

Most of the flow nonuniformity and turbulence outside of the tunnel is reduced by the inlet guide vanes and 5:1 area ratio contraction cone ahead of the test section. Before the

flow enters the test section, it encounters the dynamic pressure measurement system which will be described later.

The flow then enters the 80-ft-high by 120-ft-wide by 120-ft-long rectangular test section and can reach a speed of approximately 100 knots. The height and width have been reduced to 78.5-ft high by 118-ft wide from their original dimensions by the addition of an acoustic liner on the walls, ceiling, and floor of the test section. The liner was contoured into the existing tunnel wall surface.

As the flow exits the test section, it passes through a constant area duct. A 5-ft-high debris fence is located at the end of the duct. The flow then encounters the six flat-plate doors of vane set no. 4 that serve as a large valve which walls off the 80- by 120-Foot Wind Tunnel when the 40- by 80-Foot Wind Tunnel is operated. The doors of vane set no. 4 are aligned with the tunnel flow (they do not turn the flow) and have structural trusses which stiffen them against bending. The trusses are constructed of aerodynamically shaped structural members. After the flow leaves vane set no. 4, the east side of the circuit is formed by vane set no. 3, which walls off the 40- by 80-Foot Wind Tunnel. Figure 6 shows the intersection of the 40- by 80- and 80- by 120-Foot Wind Tunnels.

The next vane set, vane set no. 5, turns the flow 45° into the fan drive. In the 40- by 80-mode, the flow passes through vane set no. 5 without turning. This vane set has uniquely shaped, fixed vanes with good drag characteristics over 55° of onset flow angle (ref. 2). Vane set no. 5 is also equipped with a 3-ft debris fence on the floor at the trailing edge.

The flow now enters the fan drive. The six fans have a combined power consumption at full speed of 135,000 hp (fig. 4). Each fan is 40 ft in diameter and has 15 rotor blades and 23 stator blades. The fan speed and blade angle are adjustable to alter tunnel dynamic pressure. Each fan has a faired contraction and diffuser to guide the flow from the rectangular cross section ahead of the fans to the rectangular cross section after the fans.

The fan diffuser guides and slows the flow to the low-speed, south end of the tunnel. Vane set no. 6 is equipped with a 6-ft chord trailing-edge flap that adjusts to turn the flow 90° in the 40- by 80-mode or allows the flow to pass unturned in the 80- by 120-mode (fig. 7). The fixed portion of the vane set is acoustically treated to absorb noise from the fan drive.

At the south end of the wind tunnel is louver no. 7. This adjustable set of flat plate doors allows the flow from the 80- by 120-Foot Wind Tunnel to exhaust into the atmosphere (fig. 2). The flow exits the circuit and is deflected 45° upward by an exhaust ramp on the ground. The

exhaust ramp reduces surface winds at the south end of the wind tunnel.

## Apparatus

### Instrumentation Support Hardware

Optimum instrumentation support hardware for a flow calibration would position the instrumentation at all locations in the test chamber instantaneously, with no interference to the flow. In a large-scale wind tunnel, this goal is impossible to meet. The compromise chosen for this project was to use fixed measurement stations that were distributed as shown in figures 8 and 9.

The advantage of using fixed stations over, for example, traversing a single probe, is that measurements can be made at several locations at the same time. Past problems with low-frequency variations in flow quality made it desirable to collect the data in this way. Also, because of the nature of the tests conducted in this facility, collecting "fine grid" distributions of the flow quality was not required.

Size and flow speed of the 80- by 120-ft test section also influenced the hardware design. In particular, deflections of large instrumentation supports caused by aerodynamic loads had to be minimized without causing significant flow interference.

**Instrument boom**— A fixed instrument boom with five probe stations was used to span the center 75% of the test section. This "rake" could be moved to four vertical positions. Photographs of the boom at the  $Z = 25$ -, 40-, and 60-ft heights are shown as figures 10 through 12 (the  $Z = 10$ -ft height is not shown). The boom was mounted on the main struts of the 80- by 120-Foot Wind Tunnel model support system. Aerodynamic fairings were used to cover the large cylinders of the main struts when the boom was at the  $Z = 40$ - and 60-ft heights. No fairings were used at the  $Z = 10$ - and 25-ft boom heights.

The boom itself was a symmetric airfoil with a truncated trailing edge. Five multiple instrument probes (multiprobes) were sting mounted approximately 7 ft ahead of the boom (fig. 13). This minimized aerodynamic measurement interference that originated from the model support struts and boom. Two additional multiprobes were mounted on 15-ft cantilevered supports at each end of the boom (fig. 8).

The leading edge of the boom was equipped with a rake of forty-one total pressure probes (fig. 13). This rake spanned the center 50% of the test section. A vertical rake of 10 total pressure probes was also mounted on the boom

at the  $Y = -22.5$  ft station. The rake extended 10 ft above and below the boom.

**Boundary layer rakes**— Two fixed rakes of pressure probes were used to measure the thickness and shape of the boundary-layer on the floor of the test section. The rake mounting locations are shown in figure 9. A 48-in.-tall rake was mounted 38 ft upstream from the center of the turntable and 25 ft east of the tunnel centerline. A taller 64-in. rake was mounted 34 ft downstream of the center of the turntable and 25 ft east of the centerline.

**Wall pressure taps**— Static pressure taps were mounted on both walls and the ceiling of the test section. The taps were placed in the center of a 12-in. square sheet metal plate. The tap and plate surface were made smooth to provide a good static pressure measurement. The locations of the pressure plates are given in table 2.

**Atmospheric Weather Tower**— A weather tower with measurement stations 30, 60, and 100 ft above ground level was used to determine the magnitude and direction of atmospheric winds. The tower is located 328 ft upstream of the inlet face and 27 ft east of tunnel centerline.

## Instrumentation

**Wind tunnel instrumentation**— Most of this instrumentation is used to set wind tunnel speed. Measurements include dynamic pressure, total temperature, relative humidity, barometric pressure, fan drive power, fan speed, and fan blade angle.

Figure 14 shows locations of the wind tunnel instrumentation. Dynamic pressure is measured using a ganged ring of four total pressure probes and a ganged ring of four wall static pressure taps located just ahead of the test section. The pressure is measured with a bellows and scale system. Tunnel temperature is measured at the start of the inlet contraction on the wind tunnel centerline. Relative humidity is measured on the floor in the test section. Barometric pressure is measured outside of the wind tunnel.

**Multiprobes**— The multiprobe is a compact combination of measuring instruments that was developed for the FLOCAL. It contains a pitot-static probe, a hot-wire probe, a total-temperature probe, and a set of pitch and yaw vanes. All of these components were assembled and mounted on a central sting, as shown in figure 15. Multiprobes were mounted at the measurement stations on the instrument boom.

The pitot-static, total-temperature, and hot-wire probes used in the multiprobe were standard, commercially

available instruments. The pitch and yaw vanes were developed in-house (described in ref. 6). The multiprobe was designed to rotate  $180^\circ$  for measuring pitch and yaw angle tares. Alignment jigs were used to set the pitch and yaw vanes at a reference zero position. An alignment jig is installed on the pitch vane of the multiprobe shown in figure 15.

**Wind instrumentation**— The weather tower upstream of the inlet is equipped with three propellor/vane wind speed and direction sensors. An additional pair of three-cup wind speed anemometers were mounted to the cowls of the inlet as shown in figure 16.

Specifications on all of the probes that were used for the FLOCAL are given in table 3.

## Data System

Two independent data systems were used during the FLOCAL. The standard wind tunnel data system was used to collect data from individual pressure transducers, hot-wire anemometers, temperature probes, flow-direction vanes, and wind tunnel instrumentation. Additional pressure data were collected using a stand-alone electronically scanned pressure (ESP) system. This system is described in detail in reference 7. An HP 9836 computer ran the ESP system. Figure 17 is a data-system flow chart for a typical multiprobe.

The quality of a test section flow calibration depends on the accuracy of the measurements made. Every measurement has both fixed and random measurement errors that contribute to the overall measurement uncertainty. To reduce measurement errors during the FLOCAL, steady-state measurements were averaged over a 30-sec time interval and data from repeat runs were also compared to assess the amount of data scatter.

## Dynamic Pressure Calibration

A critical element of a wind tunnel calibration is the calibration of the dynamic pressure measurement system. The 80- by 120-Foot Wind Tunnel system was described earlier in the Apparatus section. The method used to calibrate the dynamic pressure system is similar to the method used for calibrating the 40- by 80-Foot Wind Tunnel system and is described by Tolhurst in reference 8.

In the 80- by 120-ft section, a measurement of dynamic pressure on the centerline of the tunnel, directly above the turntable, was used to calibrate a set of total and static pressure measurement rings located just ahead of the test section. Rae and Pope (ref. 9) suggest that this calibration should be done with the test section empty, with model

support struts in, with a ground plane in, and with any other baseline test section configurations that will be used. Since emptying the test section was not possible, this calibration was done with the instrumentation supports installed. Blockage of the supports was accounted for in the calibration of the dynamic pressure system.

The difference between the total and static pressure ring measurements is approximately equal to the dynamic pressure just ahead of the test section. Although this measurement of dynamic pressure is not equal to the dynamic pressure in the test section, it is repeatable over the speed range of the tunnel. Corrections can be applied to adjust these measurements to the dynamic pressure at the centerline.

The first step was to make an accurate measurement of dynamic pressure from the total and static rings. A mechanical bellows-type pressure transducer attached to a Toledo scale was used. An in-place calibration of this transducer was performed. Figure 18 is a plot of the current scale correction ( $\Delta q_{sc}$ ) plotted against the uncorrected dynamic pressure measured with the scale ( $q_u$ ). A new parameter can then be defined:

$$q_{cse} = q_u - \Delta q_{sc}$$

where  $q_{cse}$  is the dynamic pressure corrected for scale errors. This parameter will be used as a reference pressure for flow-quality assessment.

A static plate correction ( $\Delta q_{sp}$ ) was then measured. This correction is the difference between the dynamic pressure measured on the centerline ( $q_{cl}$ ) and the dynamic pressure measured by the scale ( $q_{cse}$ ). A plot of  $\Delta q_{sp}$  versus  $q_{cse}$  is shown as figure 19. Several runs of the FLOCAL were averaged to obtain  $\Delta q_{sp}$ . This correction takes into account the increase in  $q$  due to the reduction in the tunnel cross-sectional area between the static ring location and the model mounting location. An interim parameter can be defined such that

$$q_{clu} = q_{cse} - \Delta q_{sp}$$

A final correction was then applied to account for compressibility ( $\Delta q_{\eta}$ ). This correction is derived in reference 8. Figure 20 is a plot of  $\Delta q_{\eta}$  versus  $q_{clu}$ . The resulting equation for the corrected dynamic pressure on the centerline is

$$q_c = q_{clu} - \Delta q_{\eta}$$

The test section windspeed can then be determined from this corrected dynamic pressure, using the relationship

$$U_{ts} = (2q_c/\rho_{ts})^{1/2}$$

The test section density ( $\rho_{ts}$ ) is calculated using the method described in reference 8. The tunnel temperature,

barometric pressure, relative humidity, and static pressure values in the test section are required.

## Performance Calibration

A wind tunnel performance calibration was done during the FLOCAL. The variations of test section dynamic pressure and velocity with changes in fan blade angle and fan drive power were documented. These performance curves were generated for two fan drive power modes. The decay of test section dynamic pressure after a fan drive shutdown at full speed was also documented.

Two fan drive power modes are available. These include the induction frequency control (IFC) system, which uses a motor-generator set to provide power up to 24 MW, and the Utility power system. In the IFC mode, the fan speed and blade angle can be varied. The fan speed range is 0 to 175 rpm and the fan blade angle range is  $-18$  to  $24^\circ$  ( $-5^\circ$  is flat pitch). When operating in Utility mode, the fans are connected directly to line power and rotate at a fixed 180 rpm. The fan blade angle is adjusted between  $-18^\circ$  and  $49^\circ$  to vary tunnel speed. The tunnel was not run at blade angles below flat pitch ( $-5^\circ$ ) during the FLOCAL.

### Dynamic Pressure and Velocity Versus Fan Blade Angle

The corrected test section dynamic pressure ( $q_c$ ) is plotted against the fan blade angle for Utility and IFC modes in figures 21 and 22, respectively. The data shown incorporate all FLOCAL runs performed with the boom at the  $Z = 40$ -ft height. The purpose of these plots is to provide an estimate of dynamic pressure for a particular fan blade angle and fan rpm.

Figures 23 and 24 are plots of test section velocity versus fan blade angle for Utility and IFC modes, respectively. Figure 25 is a plot of test section velocity versus fan blade angle for low speed operation (0 to 11 knots, IFC – 36 rpm). This performance curve is based on data collected at a single point, 10.5 ft above the floor, using a cup anemometer wind speed indicator.

### Dynamic Pressure and Velocity Versus Tunnel Power

The corrected dynamic pressure ( $q_c$ ) is plotted against the net power delivered to the fans for Utility and IFC modes in figures 26 and 27, respectively. Data shown incorporate all of the FLOCAL runs. Figures 28 and 29 are plots of test section velocity versus fan drive power for Utility and IFC modes, respectively.

## Dynamic Pressure Decay

The dynamic pressure decay following a maximum dynamic pressure tunnel shutdown was measured. This documented how quickly the tunnel reaches a no-flow level when the electric power is suddenly disconnected from the fans. Figure 30 shows that after a fan drive shutdown, the dynamic pressure dropped to 5% of maximum in 32 sec. Tunnel shutdowns performed at conditions other than maximum dynamic pressure will have different decay profiles.

## Time-Averaged Flow-Quality Parameters

### Pressure and Velocity Distributions

Another goal of the FLOCAL was to obtain the spatial distributions of total, static, and dynamic pressure in the test section. Pitot-static probes were used to measure the total and static pressure. The dynamic pressure was then calculated as total minus static pressure. These measurements were made to document variations in the level and distribution of total and static pressure caused by tunnel speed setting, tunnel geometry, power mode, and other factors.

Flow velocity in the test section establishes the static pressure level. If all of the flow in the test section is aligned with the tunnel centerline, then the static pressure will be uniform. Static pressure gradients are associated with flow curvature in potential flow. The flow curvature in the test section may be caused by boundary-layer growth or the flow interference of support structures. Support structures obstructing the flow also affect the overall flow velocity and thus the static pressure level.

Total pressure is a measurement of the energy of the flow. The fans generate a total pressure rise while all of the tunnel components (i.e., vane sets, contractions, diffusers, etc.) cause total pressure losses. Variations in the total pressure distribution in the test section can be caused by a wind tunnel component, such as a vane set, that has a nonuniform pressure loss. The slower flow in the boundary layer causes a total pressure gradient near the test section wall.

Levels and distributions of both total and static pressure influence the dynamic pressure level and distribution in the test section. All factors that affect the total and static pressure affect the dynamic pressure.

The pitot-static probe measurement of total pressure is not highly sensitive to probe damage or alignment. The static pressure measurement, however, may be significantly affected by these factors and by density changes due to

variations in atmospheric pressure, temperature, and humidity.

The total and static pressure distributions for each point of the FLOCAL were plotted. These plots were then analyzed to examine the data for trends in the distributions. Runs and points that illustrated important trends were then selected and plotted for this report.

**Total Pressure**— Figure 31 shows how the indicated total pressure on the test section centerline referenced to atmospheric pressure ( $p_{t, cl} - P_{atm}$ ) varies with tunnel dynamic pressure. The dynamic pressure corrected for scale errors ( $q_{cse}$ ) is used as the reference for flow quality plots because it is nearly independent of the test section set-up. All FLOCAL runs at the  $Z = 40$ -ft height were used to generate figure 31.

Figures 32 and 33 show the horizontal total pressure distribution in the test section at a velocity of 50 knots and 100 knots, respectively. Data from the multiprobe pitot static probes and the horizontal rake of total pressure probes were used to generate these plots. The distributions are referenced to the total pressure measured by the pitot static probe on centerline. Figure 33 shows wakes at the  $Y = \pm 10$  ft locations from a pair of large structural vanes located at the inlet face. Figure 34 illustrates how the absolute total pressure distribution changes with tunnel speed. The vertical distribution of total pressure is shown as figure 35.

**Static pressure**— Absolute static pressure is a difficult parameter to measure in a wind tunnel. It is affected by the blockage of the instrumentation supports, aerodynamic interference of supports, density variations, and probe geometry.

The hardware required to position the instruments at the four vertical locations had different amounts of blockage. This is illustrated in figures 10 through 12. Since it was not possible to obtain data with the test section completely empty, no attempt was made to define absolute static pressure distributions. Instead, the emphasis was on examining distributions of static pressure referenced to the static pressure at the tunnel centerline.

Figure 36 shows how the static pressure on centerline varies with tunnel dynamic pressure. Figure 37 shows the static pressure coefficient distribution at the  $Z = 25$ -, 40-, and 60-ft locations. The effect of the instrumentation support fairings on the static pressure readings made at the  $Y = \pm 15$ -ft stations at the  $Z = 40$ -ft height is visible. Since the fairings were not present at the  $Z = 25$ -ft height, and were far from the measurement locations at the  $Z = 60$ -ft height, the instrumentation support interference was negligible. The static pressure error produced by the

fairings was estimated by subtracting the Z= 40-ft data from the average of the Z = 25- and 60-ft data (fig. 38).

**Dynamic pressure**– Horizontal dynamic pressure distributions at  $U_{ts} = 50$  knots and 100 knots are shown as figures 39 and 40. The splayed configuration of the inlet guide vanes is the most probable cause for the sloping distribution of dynamic pressure on either side of centerline (fig. 40). The dynamic pressure distribution was found to be within  $\pm 0.75\%$  of the average (of the seven pitot static measurements) up to maximum tunnel speed. No significant effect of tunnel speed on the distribution of dynamic pressure was found.

**Velocity**– The velocity at each measurement location was also calculated from the measured pressures. Horizontal velocity distributions at a  $U_{ts}$  of 50 knots and 100 knots are shown as figures 41 and 42. The velocity distribution is within  $\pm 0.5\%$  of the average (of the seven pitot static measurements) up to maximum tunnel speed.

### Streamwise Static Pressure Distributions

The streamwise wall pressure distribution in the test section was measured along the west wall, east wall and ceiling (fig. 6). The wall pressure distribution was not affected by tunnel speed or boom position. Figure 43 is a set of representative plots of the wall static pressure coefficient versus the streamwise location (X). The wall static pressure coefficient was referenced to scale system pressures and is defined as

$$C_{p,w} = (P_{s,w} - P_s) / (q_{cse})$$

The distribution of wall static pressure coefficient over the 120-ft test section length was found to be within  $\pm 0.02$ . Variations in the distribution of ceiling static pressure can be attributed to ramps that fair the acoustic liner into the test section ceiling.

### Flow Angle Distributions

Upflow and crossflow angles were measured using the free-trailing flow direction vanes described earlier. Flow angle measurements were made at the locations shown in figure 5 for all points in the test matrix (table 1).

The sign convention used for flow angle measurements made during the FLOCAL was as follows. A positive upflow angle indicates flow directed towards the ceiling of the test section. A positive crossflow indicates flow directed toward the left wall of the test section facing upstream. The upflow and crossflow angles are absolute angles. The upflow angle was referenced to the local gravitational waterline with a propeller protractor. The

crossflow angle was referenced to the geometric centerline of the test section.

Several factors affected the average flow angle data quality during the FLOCAL. Corrections were made to account for structural misalignments of the large probe support structure, aerodynamic effects on the vane fin, and drifts in the output of the vane transducers due to temperature. Flow angles induced by the probe support structure were estimated and also applied as a correction to the data. Deflection of the support structure under aerodynamic load was negligible.

Review of the data showed significant data scatter. A combination of instrumentation errors and the other errors discussed above caused this scatter. It was impossible to resolve small variations in flow angle distributions due to variations in tunnel speed. For this reason, flow angle data collected at each boom position were divided into four speed ranges and averaged to obtain the overall free-stream angle distributions. The speed ranges were 25 to 50 knots, 50 to 80 knots, 80 to 100 knots, and 97 to 100 knots.

FLOCAL flow angle results indicate that the mean upflow angle is within  $\pm 0.5^\circ$  at tunnel speeds above 97 knots. Figure 44 shows the upflow angle distributions for the Z = 10-, 25-, 40-, and 60-ft boom heights at  $U_{ts} > 97$  knots. Symbols represent the mean value at each location and bars show the range of data scatter. The upflow angle distributions at the Z = 10-, 25-, 40-, and 60-ft boom heights show an irregular upflow of approximately  $0.5^\circ$  in the test section. Figure 45 shows the same series of plots for the crossflow angle. The mean crossflow angle is within  $\pm 0.7^\circ$  at tunnel speeds above 97 knots.

The upflow and crossflow angle distributions for the three speed ranges at the Z = 40-ft boom height are shown in figures 46 and 47, respectively. As shown, the data scatter bars become smaller with increasing tunnel speed. The mean value however, does not vary much with increasing speed.

### Temperature Distributions

Total temperature measurements were made at each multiprobe station to document cross-stream variations in temperature. In addition, these measurements provided a local temperature measurement for the calculation of local density. As expected, there was no significant temperature gradient in the 80- by 120-ft test section.

## Boundary Layer Profiles

Two rakes of pressure probes were used to measure the thickness, shape, and streamwise growth of the boundary layer on the test section floor. Rake locations are shown in figure 6.

Figure 48 shows dynamic pressure profiles measured at the two rake locations. Four repeat points are shown at maximum test section velocity ( $U_{TS} = 100$  knots). Velocity profiles were calculated using the same data set (fig. 49). The boundary layer thickness or shape was not found to vary significantly with test section speed.

The boundary layer thickness grows from approximately 30 in. to 44 in. between the two rakes. This represents a growth of about 14 in. over a distance of 72 ft. The boundary layer shapes are smooth, showing no signs of flow distortions near the test section floor.

## Dynamic Flow Quality Parameters

### Turbulence Intensity Distributions

Axial turbulence intensity was measured at each multiprobe location using independent hot wires. Lateral and vertical turbulence intensity were measured on the centerline using a cross-wire probe.

A constant-temperature, DISA, hot-wire system was used during the FLOCAL. Instrumentation setup diagrams for the 9- $\mu$ m single and cross-wire probes are shown as figure 50. A 1-kHz low-pass filter was placed on the output of the linearizer. A spectrum analyzer was positioned on the output of the anemometer unit.

Data are presented for three speed ranges. Figure 51 shows the axial turbulence intensity distribution below  $U_{TS} = 50$  knots for the 10-, 25-, 40-, and 60-ft boom heights. Figures 52 and 53 are the same plot groups for  $U_{TS} = 50$ - to 75-knots and  $U_{TS} = 75$ - to 100-knots, respectively. The axial turbulence intensity had a mean level of about 0.4% in the  $U_{TS} = 75$ - to 100-knot speed range.

The plots of figures 51 through 53 also show the lateral turbulence intensity on the centerline. The cross wire on the centerline was rotated 90° to measure the difference between lateral and vertical turbulence intensity. There was no discernible difference between lateral and vertical turbulence intensity. Both had a mean level of around 0.6% at the top speed range. The higher level of lateral and vertical turbulence intensity compared to axial turbulence intensity is typical of subsonic wind tunnels.

Figure 54 shows the variation of turbulence intensity with test section velocity for each station on the boom. Data from all runs of the FLOCAL were used to generate these

plots. The arrow on the right side of each plots indicates the average turbulence intensity measured above  $U_{TS} = 75$ -knots at the  $Z = 40$ -ft height.

### Axial Turbulence Intensity Energy Spectra

Axial turbulence intensity energy spectra were recorded from the hot wire located at the center station of the boom. These data were collected to determine the frequency range of the highest energy flow disturbances.

The nonlinear output of the hot-wire anemometer was fed directly to a spectrum analyzer. An assumption was made that since the turbulence levels were low, the RMS voltage fluctuation was linear over the range of anemometer output. The analyzer was set up to provide power spectral density plots with a decibel (dB) range from 0 to -60 and a linear frequency range from 0 to 2000 Hz.

Spectra recorded at various boom positions were compared and no significant differences were visible. Figure 55 shows spectra taken with the hot wire located on the tunnel centerline at six test section speeds up to 100 knots.

The spectra grew to incorporate higher-frequency flow disturbances as the speed of the tunnel was increased. There was also a rapid decay in energy between 0 and 200 Hz. This is typical of most large-scale subsonic wind tunnels where most of the flow unsteadiness is caused by large-scale velocity fluctuations. Large-scale flow disturbances could be caused by the fan drive, the vane sets, or areas of flow separation in the circuit. The most important feature of the spectra recorded during the FLOCAL was that they were smooth and had no significant peaks.

### Flow Meander

Time histories of pitch and yaw angle were collected during the FLOCAL. No significant meander was observed during data sampling periods lasting in excess of two minutes.

## Atmospheric Wind Effects

Another goal of the FLOCAL was to determine the effects of atmospheric winds on test section flow quality. This problem was originally addressed during the early development of the 80- by 120-Foot Wind Tunnel (ref. 3). Based on the intended testing requirements for the facility, small-scale model studies, and the prevailing winds at the site, the potential impact of atmospheric winds on test section flow quality was evaluated. The development of the current inlet and inlet flow treatment is described in reference 5. A detailed description of the inlet is given as

well as comparisons between theoretical, small-scale model, and full-scale tunnel flow quality results.

Atmospheric winds and the large-scale turbulence they generate provide a complex flow field ahead of the inlet. Winds can gust, rapidly changing direction, or they can blow steadily from one prevailing direction. Winds are also seasonal. The FLOCAL was conducted during a limited portion of the year and at a limited time of day. The number of FLOCAL runs and the locations of wind and flow quality measurements were also limited.

The approach used was to sample wind conditions and test section flow quality during all FLOCAL runs and then examine these data for trends. An attempt was made to obtain at least two runs per boom location with atmospheric wind speeds exceeding 10 knots.

After the FLOCAL, the entire data set was examined for flow quality trends that could be attributed to atmospheric wind effects. Wind speed and direction measurements from the 100 ft wind tower station were used to create a wind rose for the FLOCAL (fig. 56). It shows that the winds are mostly from the northwest at between 0 and 20 knots. It also illustrates that the wind tunnel is well aligned with the prevailing winds at the site. Figure 57 shows the variation of wind speed and direction recorded during the operation of a typical FLOCAL run.

During early runs of the wind tunnel in windy conditions, persons walking in front of the inlet noticed a difference between the flow velocity around the east cowl and the velocity around the west cowl. This difference in near cowl velocity was also found to vary with wind conditions. A pair of wind cup anemometers was installed on the inlet cowls (fig. 16) in an attempt to document this effect. The idea was to correlate flow quality in the test section with the difference in cowl velocity. This would be much simpler than trying to correlate with the infinite combinations of wind speed and direction.

The difference in cowl velocity was plotted against the horizontal wind velocity component aligned perpendicular to the tunnel centerline (fig. 58). Winds aligned with the tunnel centerline should not produce a difference between the east and west cowl velocity. Winds from the west produced higher cowl velocities on the west cowl. Winds from the east increased the cowl velocity on the east cowl. Data scatter can be attributed to gusty winds and the difference in the measurement location between the weather tower and the cowls.

The most notable wind effect was a spanwise variation in total pressure in the test section. Figure 59 shows total pressure distributions in percent of average dynamic pressure for three speed ranges at various wind conditions. These data were collected using the horizontal rake on the

leading edge of the boom. The slope of the total pressure distribution did not correlate well with cowl velocity measurements or wind measurements. This is likely due to a time lag between the wind condition and the development of the pressure distribution tilt.

All of the horizontal rake total pressure distributions and corresponding wind data recorded during the FLOCAL were used to generate Figure 60. This plot compares total pressure distribution distortion to test section velocity for three resultant wind cases: dead calm, less than 10 knots, and 10 to 20 knots. Figure 60 shows that above  $U_{ts} = 70$  knots, the total pressure distribution was not significantly affected by winds up to 20 knots.

A pitot-static probe located in the test section recorded simultaneous variations in total and static pressure when the tunnel was not operating and when the tunnel was operating at low test section speeds (less than 10 knots). Local static pressure fluctuations outside the inlet caused by gusting winds are believed to be the source of this effect. The fluctuations become negligible as test section speed is increased above 10 knots. No variations in flow angle due to wind could be resolved from the data.

## Summary of Results

Objectives of the 80- by 120-Foot Wind Tunnel performance and test section FLOCAL were to:

1. calibrate the dynamic pressure system,
2. document tunnel performance, and
3. document the spatial variations in test section flow quality parameters throughout the tunnel operational envelope and for various atmospheric wind conditions

The dynamic pressure measurement system was calibrated to accurately measure dynamic pressure on the centerline, directly above the center of the turntable. This calibration was performed in the presence of the instrumentation supports and fairings.

The tunnel performance calibration documented how the dynamic pressure and velocity in the test section vary with fan blade angle, fan speed and tunnel power.

Flow quality data were collected for the typical operating range of the tunnel including a variety of atmospheric wind conditions. Atmospheric winds were found to have negligible effects on flow quality at high test section speeds ( $U_{ts} > 70$  knots). At test section speeds below 70 knots, off-axis winds produced non-uniform pressure distributions in the test section. No effects of wind on flow angle or turbulence distributions could be resolved.



## Recommendations

Free-stream flow disturbances in the test section should be well documented. These disturbances have the potential of affecting steady and dynamic measurements made in the wind tunnel. The author recommends that the pressure, temperature, and turbulence-intensity fluctuations with time be measured.

Tests in the 80- by 120-Foot Wind Tunnel that are highly sensitive to total pressure gradients should be conducted during low wind conditions. The plot of total pressure disturbance versus velocity for various wind conditions contained in this report should be used to determine when it is appropriate to run.

For more detailed information about any particular section of this report, consult the NFAC Documentation Archives located at NASA Ames Research Center.

## References

1. Zell, Peter T.; and Flack, Karen: Performance and Test Section Flow Characteristics of the National Full-Scale Aerodynamics Complex 40- by 80-Foot Wind Tunnel. NASA TM-101065, 1989.
2. Olson, Lawrence E.; Zell, Peter T.; Soderman, Paul T.; Falarski, Michael D.; Corsiglia, Victor R.; and Edenborough, H. Kipling: Aerodynamic Flow Quality and Acoustic Characteristics of the 40- by 80-Foot Test Section Circuit of the National Full-Scale Aerodynamic Complex. SAE Tech. Paper 872328, 1987.
3. Eckert, William T.; and Mort, Kenneth W.: Earth Winds, Flow Quality, and the Minimum-Protection Inlet Treatment for the NASA Ames 80- by 120-Foot Wind Tunnel Nonreturn Circuit. NASA TM-78600, 1979.
4. Ross, James C.; Olson, Lawrence E.; Meyn, Lawrence A.; and van Aken, Johannes M.: A New Design Concept for Indraft Wind-Tunnel Inlets with Application to the National Full-Scale Aerodynamics Complex. NASA TM-88226, 1986.
5. van Aken, Johannes M.; Ross, James C.; and Zell, Peter T.: Inlet Development for the NFAC 80- by 120-Foot Indraft Wind Tunnel. AIAA Paper 88-2528, 1988.
6. Zell, Peter T.; and McMahon, Robert D.: A Free-Trailing Vane Flow Direction Indicator Employing a Linear Output Hall Effect Transducer. Proc. 34th Intern. Instrumentation Symp., 1988, pp. 429-436.
7. Pressure Systems Incorporated: Model 780B/T Pressure Measurement System Users Manual. Sept. 1983.
8. Tolhurst, W. H.: The Fundamentals of Measuring Dynamic Pressure and Velocity in the Ames 40- by 80-Foot Wind Tunnel. NFAC Documentation Archives, Dec. 1987.
9. Rae, William H., Jr.; and Pope, Alan: Low-Speed Wind Tunnel Testing, Second Ed. John Wiley and Sons, 1984.

**Table 1. 80- by 120- FLOCAL2 test matrix**

Date 1988	Run no.	Boom pos., ft	Power mode	RPM	Blade angle, °	Max. vel., kn	Wind vel., kn	Comments
3/22	1	40	Utility	180	12-49	100	0-20	Vanes inverted
3/23	2	40	Utility	180	12-49	100	0-15	
4/26	3	40	Utility	180	12-49	100	0-15	
4/26	4	40	-	-	-	-	-	Run cancelled
4/27	5	40	Utility	180	12-49	100	0-10	Low speed operation
4/27	6	40	IFC	36	0-24	11	0-5	
				90	12-24	25		
				135	12-24	38		
				175	12-24	49		
4/28	7	40	Utility	180	12-49	100	0-10	New boom position
5/16	8	60	Utility	180	12-49	100	0-15	
5/17	9	60	Utility	180	12-49	100	0-20	
5/17	10	60	IFC	90	12-24	25	0-10	
				135	12-24	38		
				175	12-24	49		
5/18	11	60	Utility	180	12-49	100	0-10	New boom position
5/26	12	25	Utility	180	12-49	100	0-15	
5/26	13	25	Utility	180	12-49	100	0-15	
5/26	14	25	IFC	90	12-24	25	0-10	
				135	12-24	38		
				175	12-24	49		
5/31	15	25	Utility	180	12-49	100	0-15	New boom position
6/2	16	10	Utility	180	12-49	100	0-15	
6/3	17	10	Utility	180	12-49	100	0-15	
6/6	18	10	IFC	90	12-24	25	0-15	
				135	12-24	38		
				175	12-24	49		
6/6	19	10	Utility	180	12-49	100	0-5	

**Table 2. Wall pressure tap locations<sup>a</sup>**

No.	Ceiling taps, feet	East wall taps, feet	West wall taps, feet
1	-120	-119.7	-125.7
2	-100	-101.7	-101.7
3	-68.7	-78.0	-75.7
4	-48.7	-61.8	-59.7
5	-38.7	-42.5	-43.7
6	-28.7	-34.5	-35.7
7	-18.7	-26.5	-27.7
8	-8.7	-18.5	-19.7
9	+1.3	-10.5	-11.7
10	+8.8	-3.5	-3.7
11	+13.8	+3.5	+4.3
12	-18.8	+10.5	+12.3
13	-23.8	+18.5	+20.3
14	-28.8	+26.5	+28.3
15	-33.8	-34.5	-36.3
16	-41.3	-42.5	-44.3
17	-51.3	-50.5	-52.3
18	-71.3	-57.6	-68.3
19	-100	-73.9	-84.3
20	-120	-108.7	-113.3
21	-144	-139.2	-144.2

<sup>a</sup>The turntable centerline is the zero reference. Positive is towards the fans and negative is towards the inlet.

**Table 3. Probe descriptions**

<b>Pitot/static probe</b>	
Manufacturer	United Sensor
Specifications	Model PAE-12-M-W Probe length, 12 in. Sensing stem diameter, 1/4 in.
Accuracy	±0.5% of reading
Additional information	Part of multiprobe assembly
<b>Thermocouple</b>	
Manufacturer	United Sensor
Specifications	Model TU-12-C/C-36-F Wire Type, CU/CON Maximum temperature, 400°F Probe diameter, 1/4 in.
Accuracy	±1°F
Additional information	Part of multiprobe assembly
<b>Hot-wire probe</b>	
Manufacturer	DISA Electronics
Specifications	Model 55P01 (single sensor) Model 55P51 (dual sensor) Platinum-plated tungsten wire-diameter = 9 μm
Additional information	Part of multiprobe assembly
<b>Flow-angle vanes</b>	
Manufacturer	Specially designed and built in-house
Specifications	Airspeed range, 5 to 300 knots Angle range, ±40°
Accuracy	Angle resolution, ±0.1°
Additional information	Part of multiprobe assembly pitch and yaw vanes contained on each multiprobe
<b>Wall pressure tap</b>	
Manufacturer	In-house design
Specifications	1-ft-square plate with 1/8-in.-diameter orifice in center
Accuracy	±0.5% of reading
Additional information	Sixty-three static pressure taps mounted flush on the west test section wall
<b>Static pressure probe</b>	
Manufacturer	In-house design
Specification	0.250 diameter × 0.035 wall tubing Four pressure ports, radially 90° apart, 10 diameters from the tip of the probe
Accuracy	±0.5% of reading
Additional information	Probes were mounted on two fixed rakes, 48 in. and 32 in. tall.
<b>Total pressure probe</b>	
Manufacturer	In-house design
Specification	0.125 diameter × 0.028 wall tubing 12 in long, 30° beveled tip
Accuracy	±0.5% of reading
Additional information	Probes were mounted on; two fixed rakes, 48 in. and 32 in. tall; boom leading edge rake; vertical rake

**Table 3. Concluded**

---

<b>Humidity sensor</b>	
Manufacturer	General Eastern
Specifications	Model 400 CD Range: 0-100% relative humidity Temperature span for relative humidity, 0-140°F
Accuracy	±3%, between 15% and 95% relative humidity
Additional information	Temperature-induced humidity changes are eliminated by employing a compensating thermistor
<b>Barometer</b>	
Manufacturer	Datametrix
Specifications	Type 1400 Electronic Manometer
Additional information	Located in control room
<b>Atmospheric wind sensor</b>	
Manufacturer	S/P Weathermeasure
Specifications	Model W 102 P/HF Skyvane Wind Sensor
Accuracy	±0.25 mph
Additional information	Located on weather tower at three stations
<b>Cup anemometer airspeed sensor</b>	
Manufacturer	Weathertronics
Specifications	3-cup wind speed sensor
Accuracy	±1% of reading
Additional information	Mounted in test section to document low speed tunnel operation (<10 knots); mounted on inlet cowls

---



Figure 1. Aerial view of the NASA 40- by 80-/80- by 120-Foot Wind Tunnels at Ames Research Center.

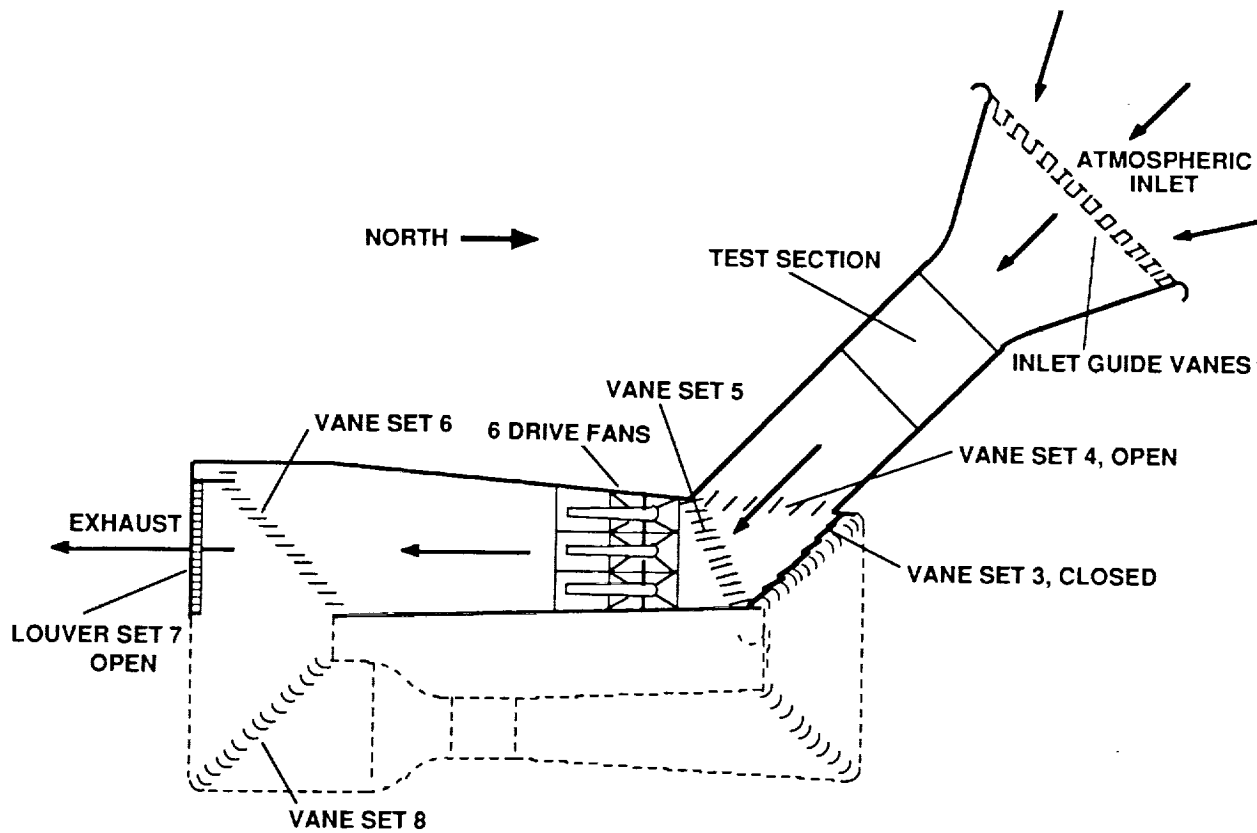


Figure 2. 80- by 120-Foot Wind Tunnel circuit.

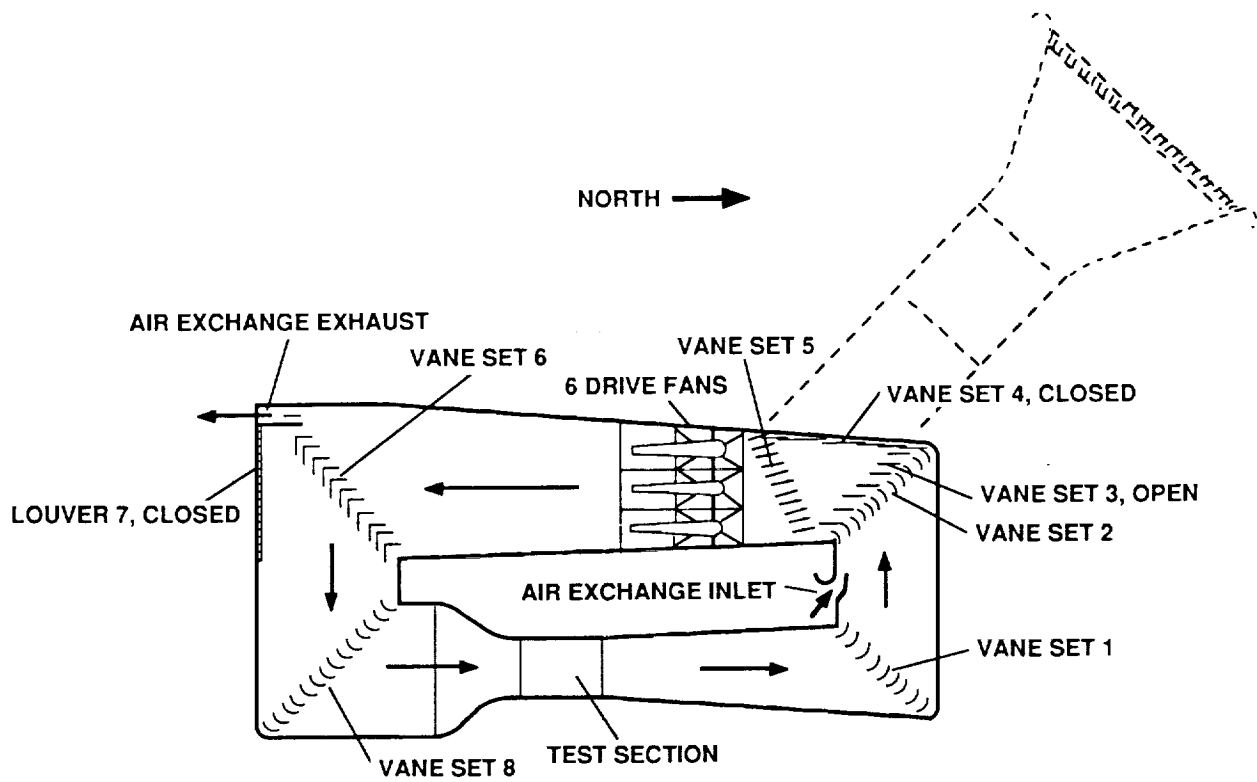


Figure 3. 40-by 80-Foot Wind Tunnel circuit.

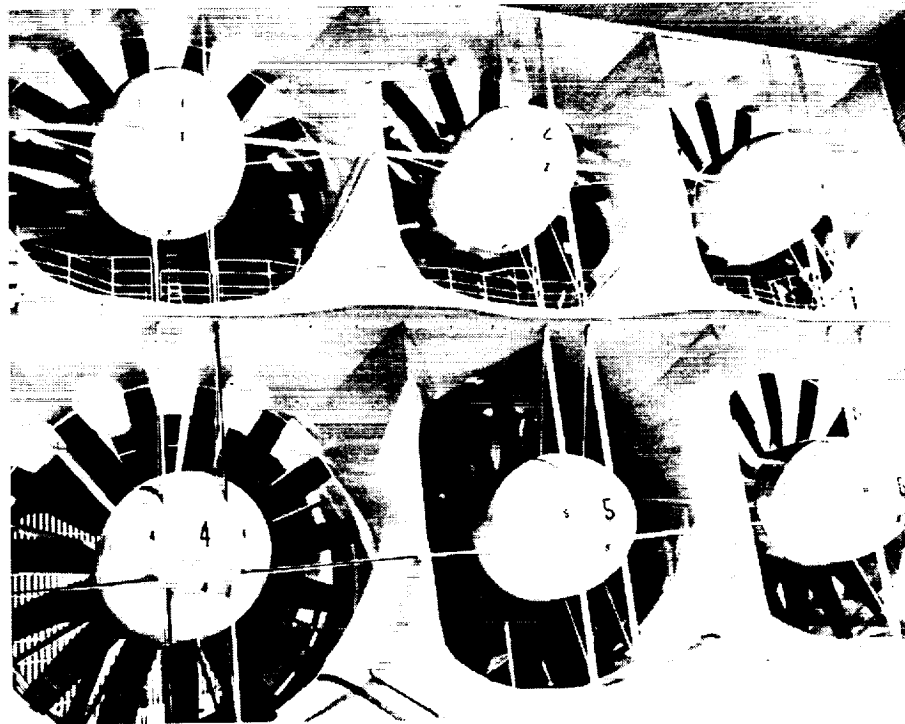


Figure 4. NFAC fan drive system.

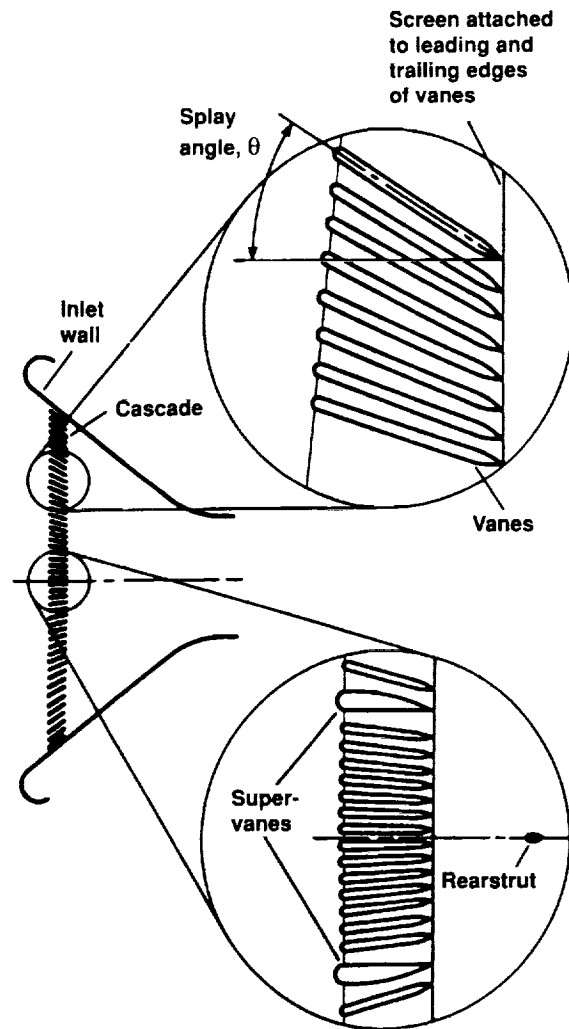


Figure 5. Details of inlet cascade (guide vanes) and screen.



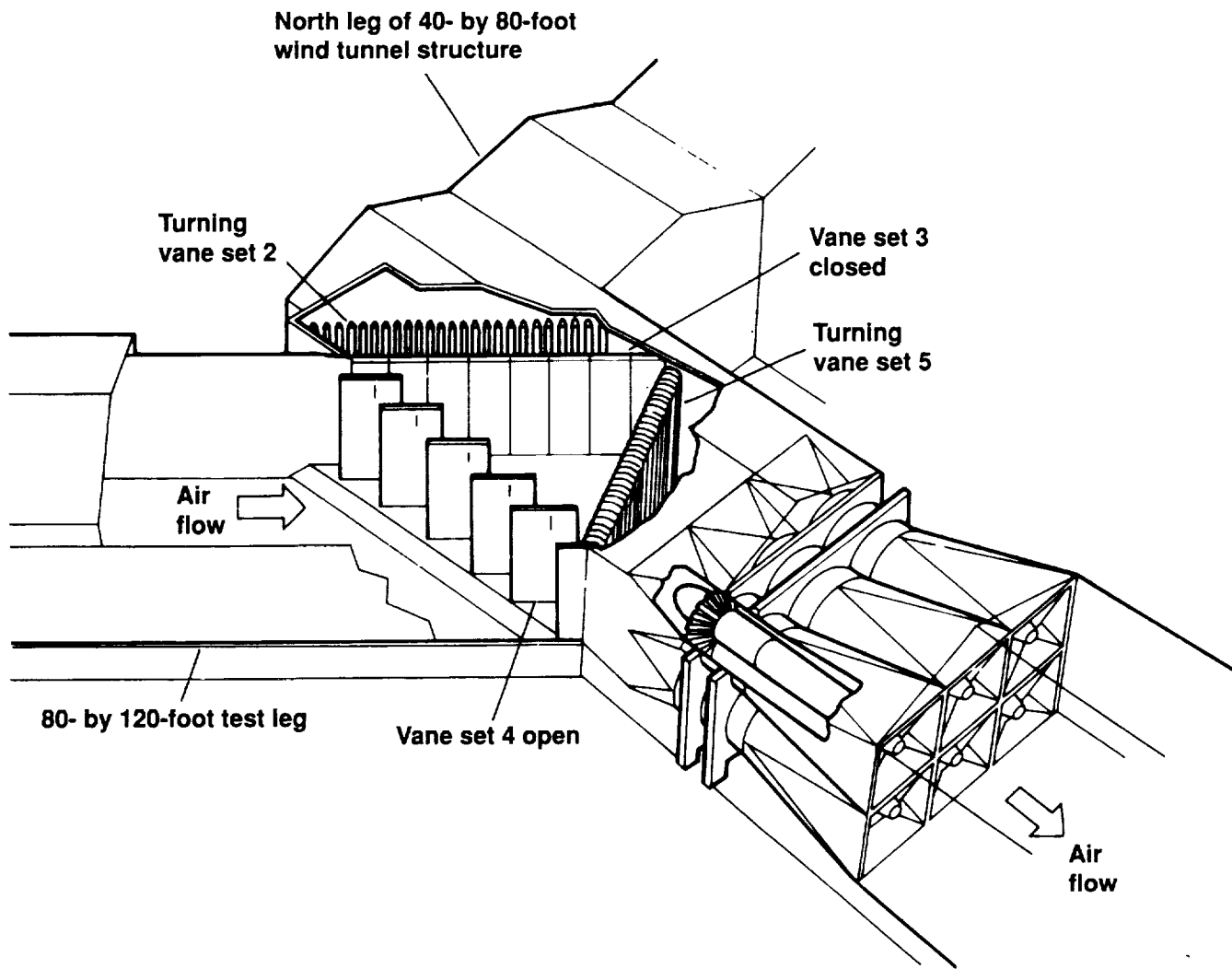


Figure 6. Intersection between the 40- by 80-Foot and 80- by 120-Foot Wind Tunnels (80- by 120-Foot Wind Tunnel mode).

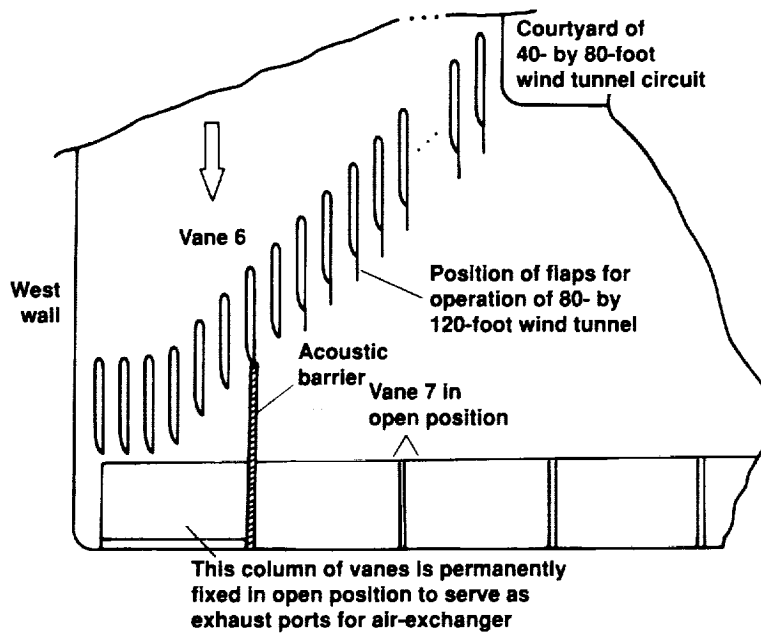
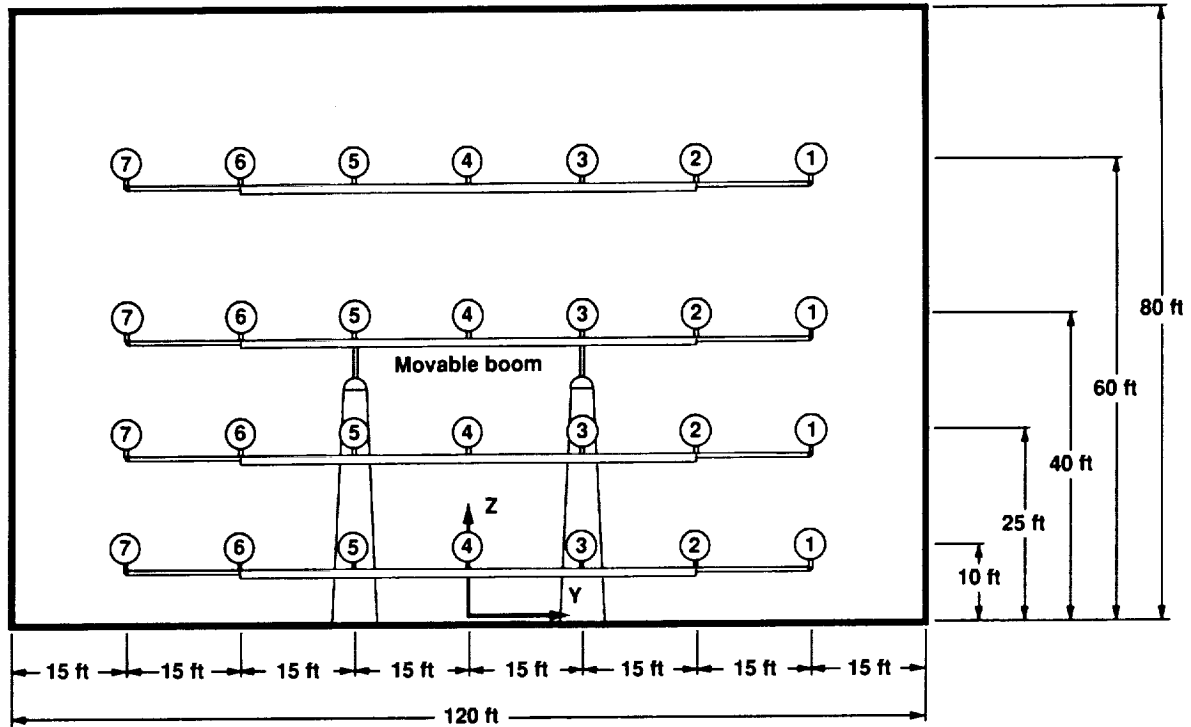


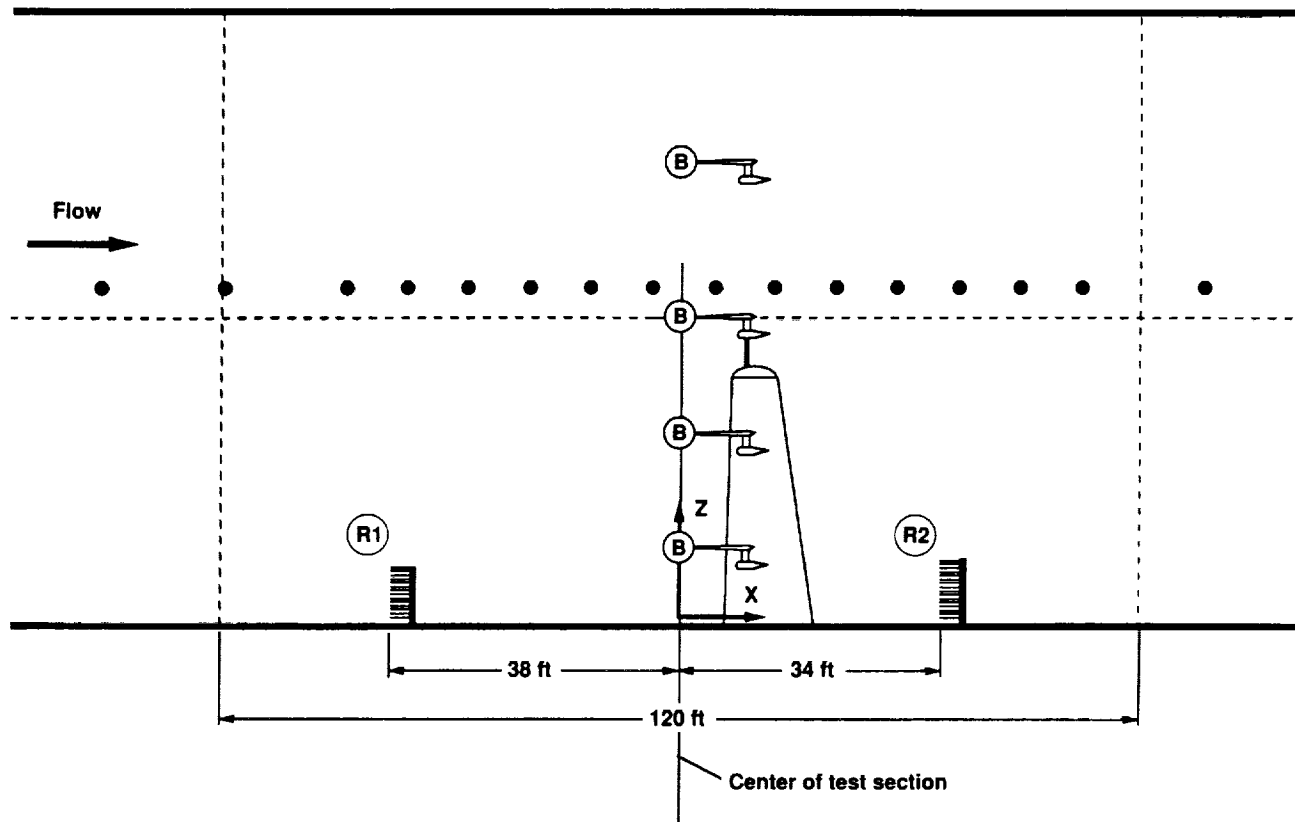
Figure 7. Vane set no. 6, louver no. 7, and the atmospheric exhaust (positioned for 80- by 120-Foot Wind Tunnel operation).



Instrumentation distribution (view looking upstream-pilot's view)

Station	Pitot-static probe	Pitch/yaw vanes	Thermocouple	Hot wire X probe	Hot wire single
1	X		X		X
2	X	X	X		X
3	X	X	X		X
4	X	X	X	X	
5	X	X	X		X
6	X	X	X		X
7	X		X		X

Figure 8. Location of instrumentation in the 80- by 120-Foot Wind Tunnel test section (pilot's view).



Instrumentation distribution

Station	Instrumentation
B	7 sting mounted multi-probes (see figure 8)
R1	1 48 in., 19 tube boundary layer rake (19 totals & 5 statics)
R2	1 64 in., 25 tube boundary layer rake (25 totals & 7 statics)
●	Wall static pressure taps (east wall, west wall, ceiling, 21 ea.)

Figure 9. Location of instrumentation in the 80- by 120-Foot Wind Tunnel test section (view looking east).

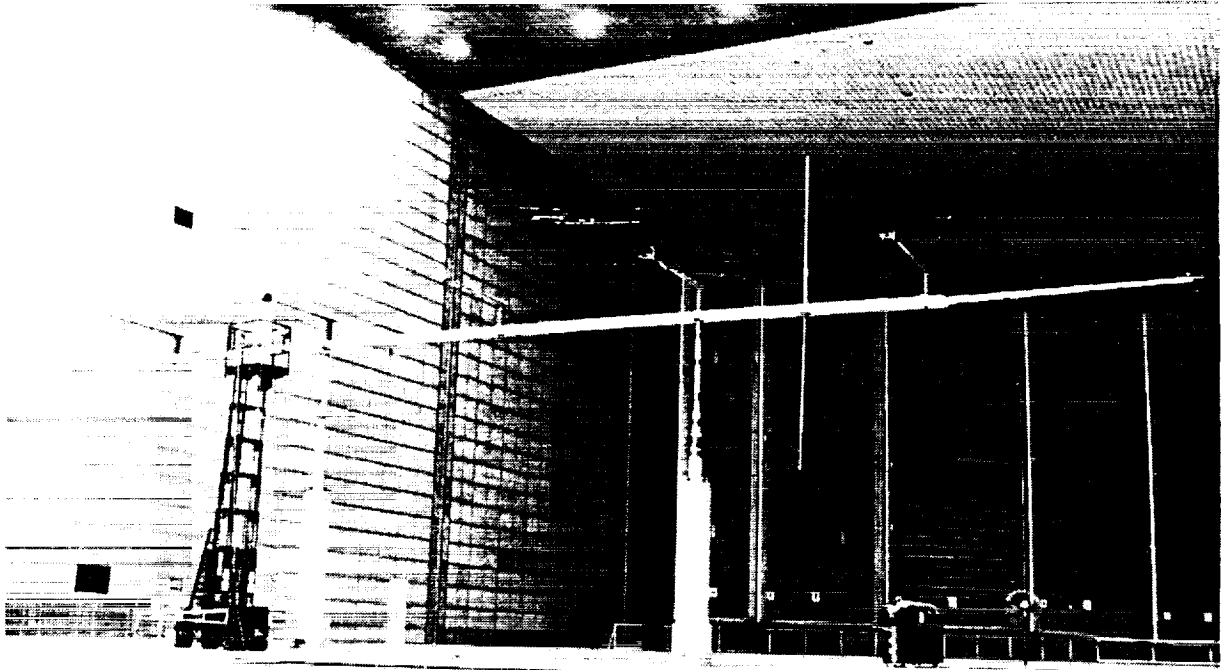


*Figure 10. Instrumentation boom at Z = 25 ft height.*

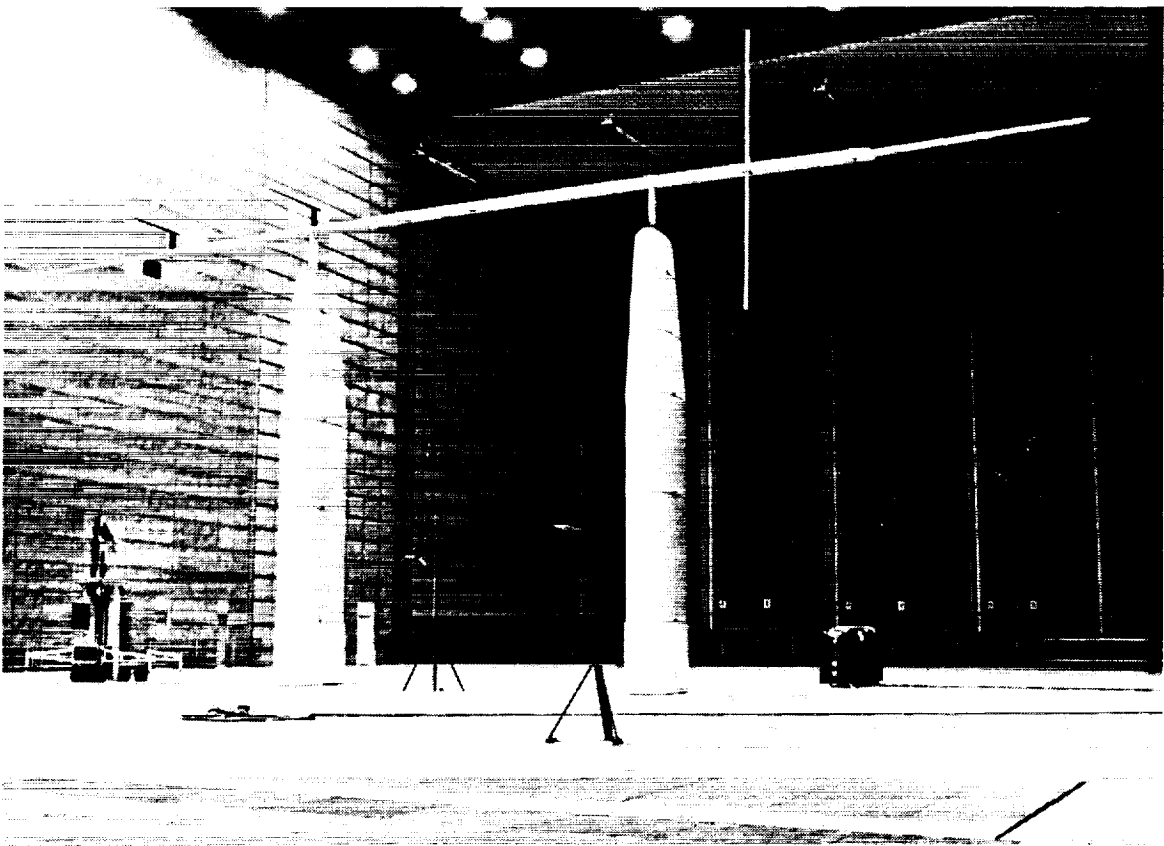


*Figure 11. Instrumentation boom at Z = 40 ft height.*

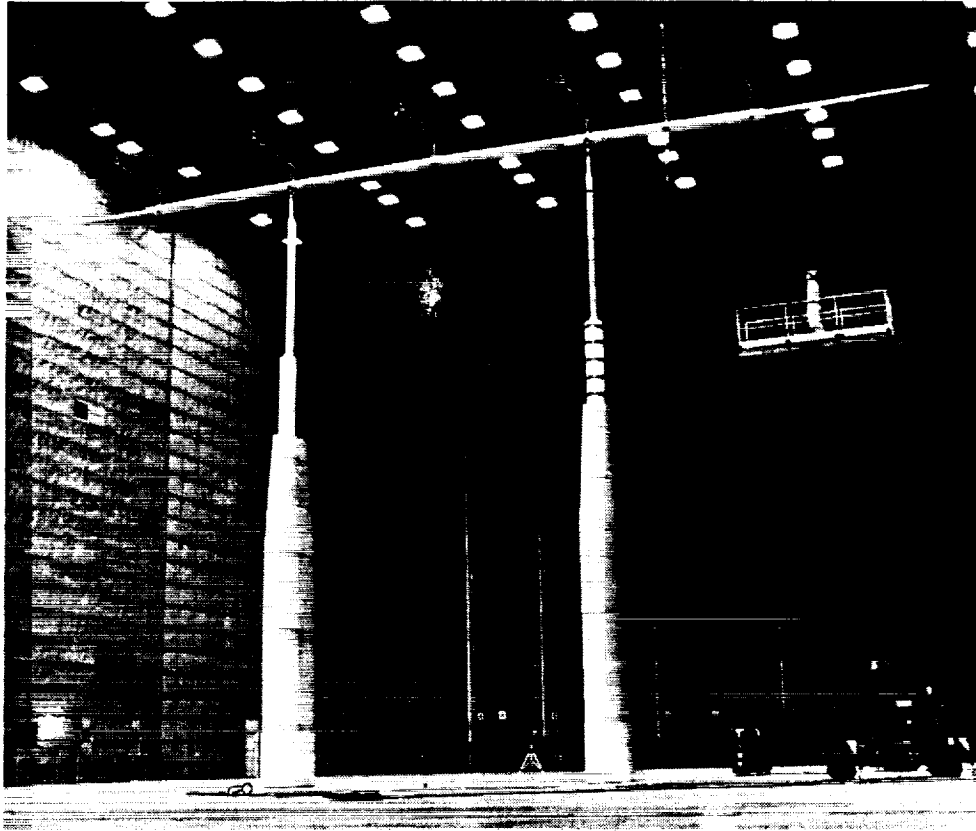


*Figure 12. Instrumentation boom at  $Z = 60$  ft height.*

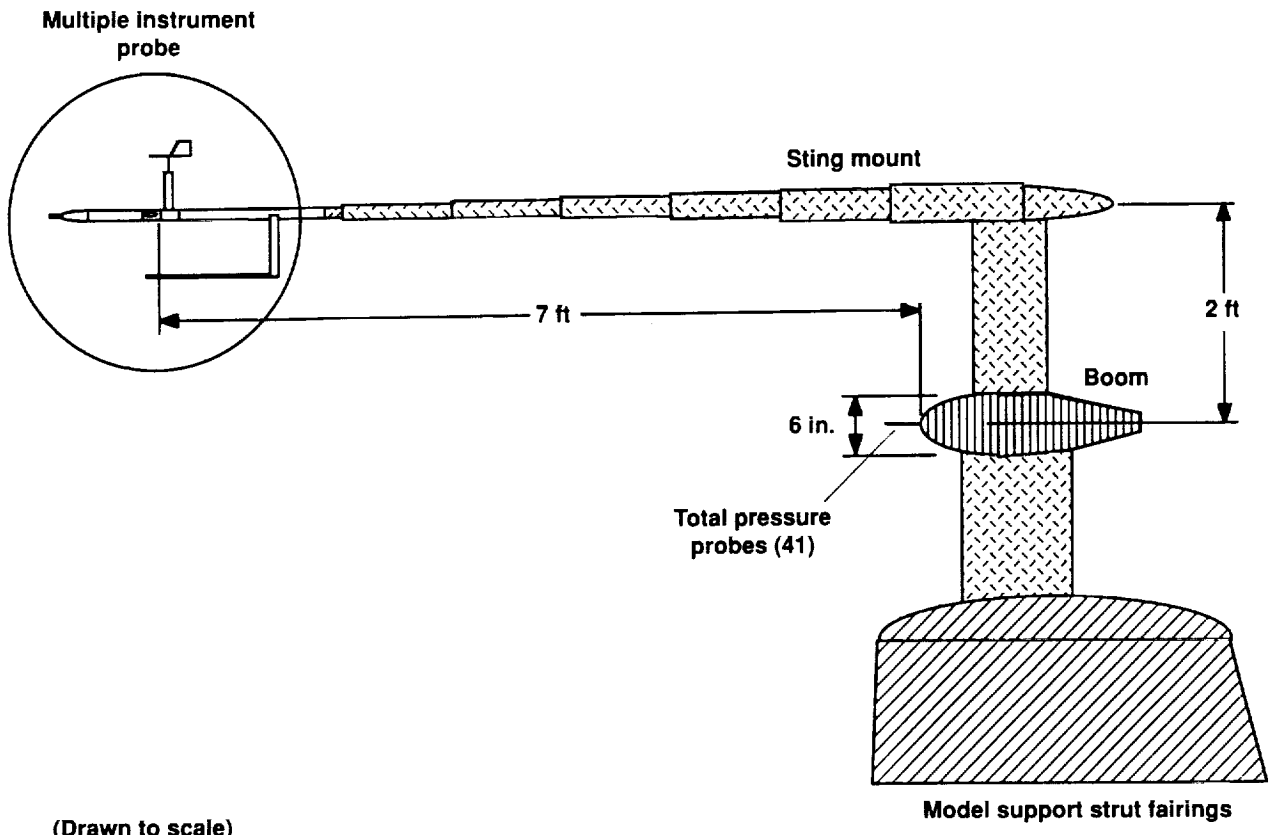
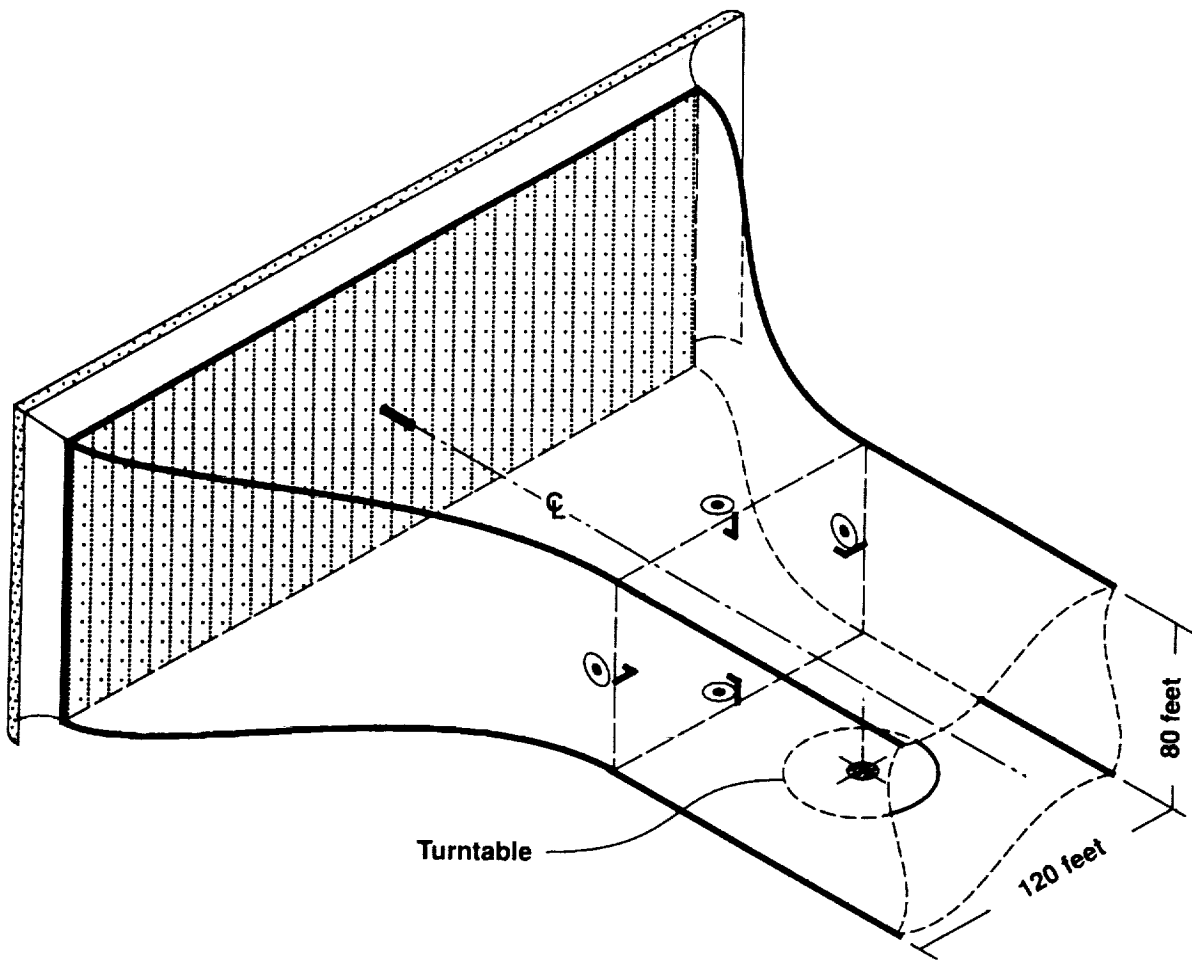


Figure 13. Multiprobe positioned ahead of the instrumentation boom.



**LEGEND**





Temperature sensor	
Total pressure probes (4-connected)	
Static pressure ports (4-connected)	
Relative humidity sensor	
<b>Note: Symbols not drawn to scale</b>	

Figure 14. Wind tunnel instrumentation for the 80- by 120-Foot Wind Tunnel.



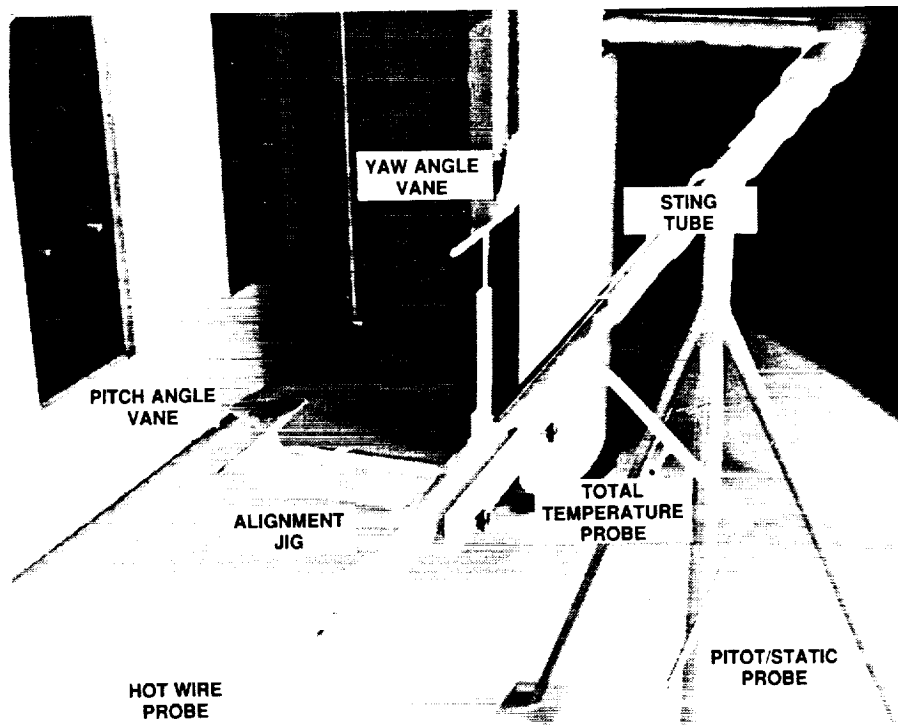
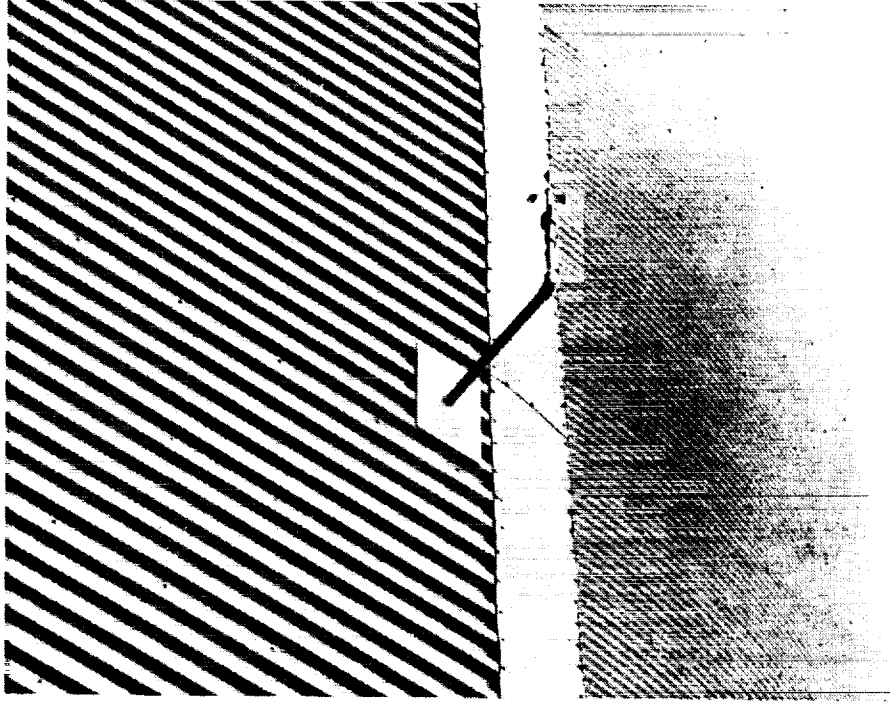
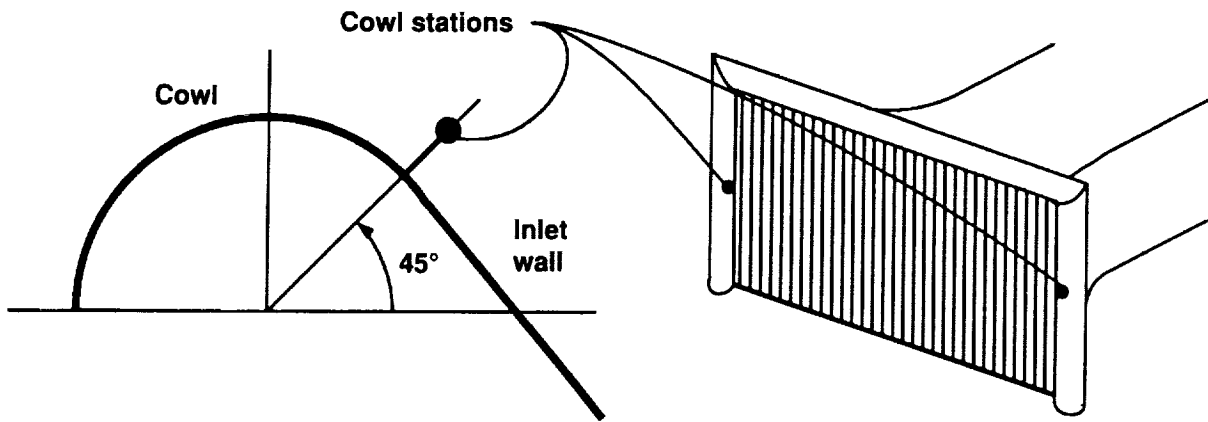


Figure 15. Multiprobe mounted on sting tube (note alignment jig on pitch vane).



(a) Anemometer on inlet cowl.



(b) Installation geometry.

Figure 16. Wind cup anemometer installation on the inlet cowls.

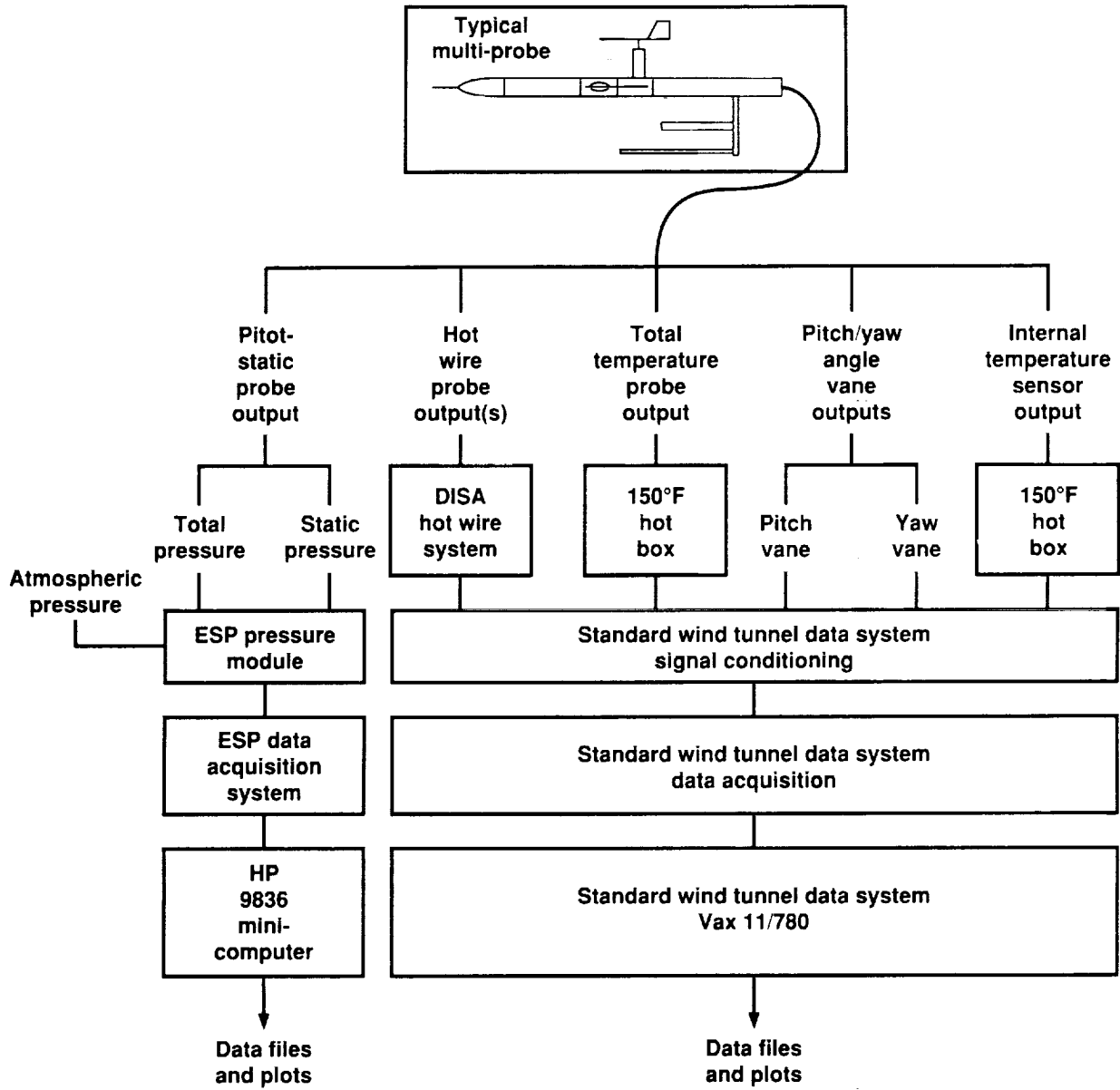
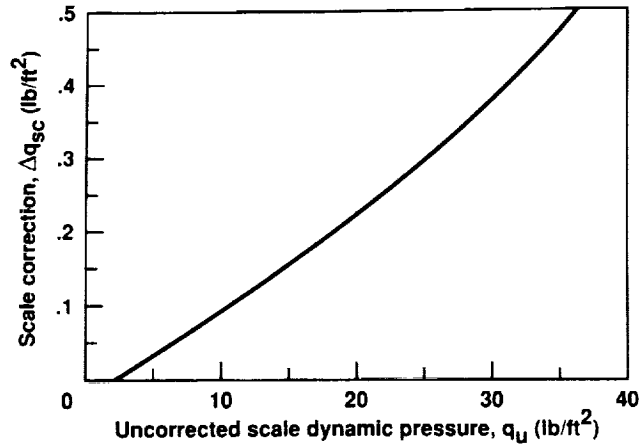
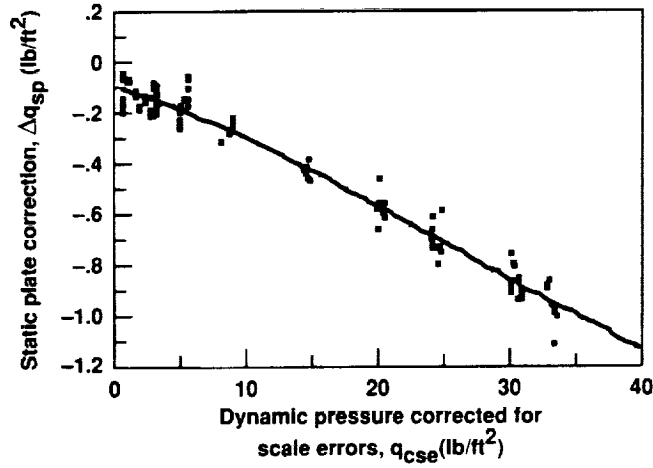


Figure 17. Data system flow chart for a typical multiprobe.



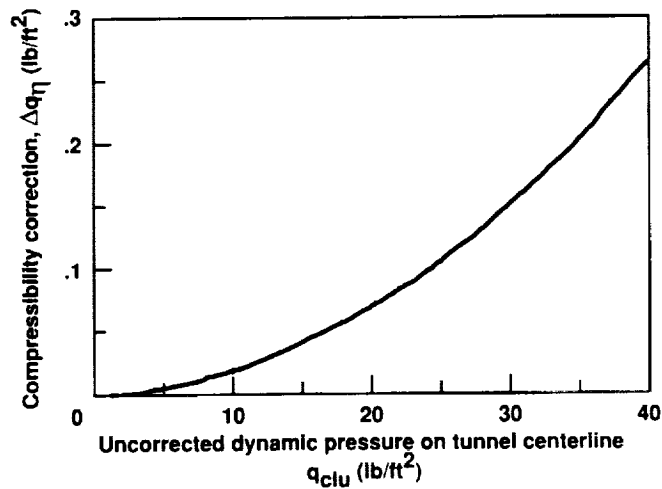
$$\Delta q_{sc} = -0.0152 + 0.0094 (q_u) + 1.309E-4 (q_u)^2 + 5.334E-8 (q_u)^3$$

Figure 18. Dynamic pressure scale correction.



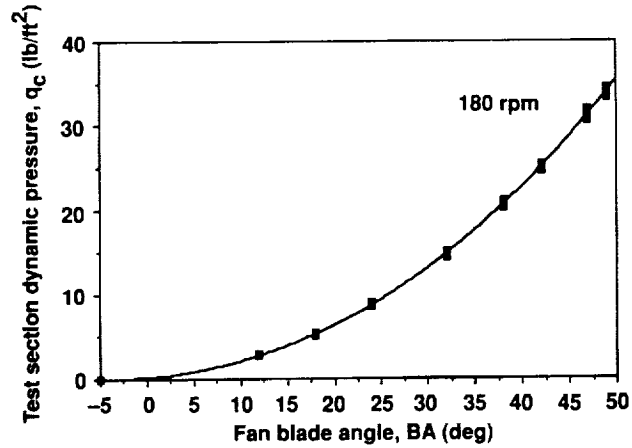
$$\Delta q_{sp} = -0.0441 - 0.0173 (q_u) - 5.394E-4 (q_u)^2 + 6.915E-6 (q_u)^3$$

Figure 19. Dynamic pressure static plate correction.



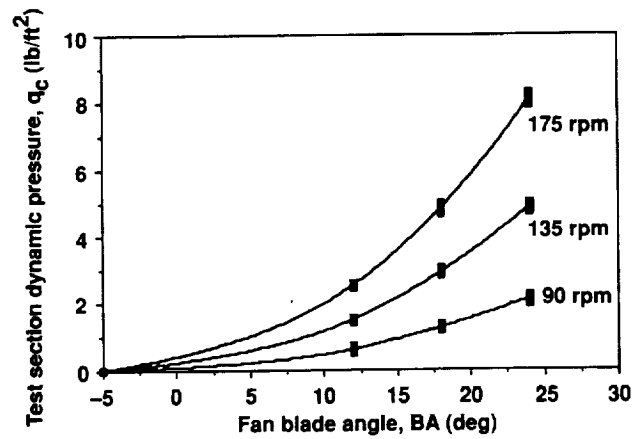
$$\Delta q_{\eta} = 1.688E-4 (q_{cse})^2$$

Figure 20. Dynamic pressure compressibility correction.



$$180 \text{ rpm } q_c = 0.1785 + 0.0862(BA) + 0.0103(BA)^2 + 4.063E-5(BA)^3$$

Figure 21. Corrected dynamic pressure on centerline versus fan blade angle (utility mode).

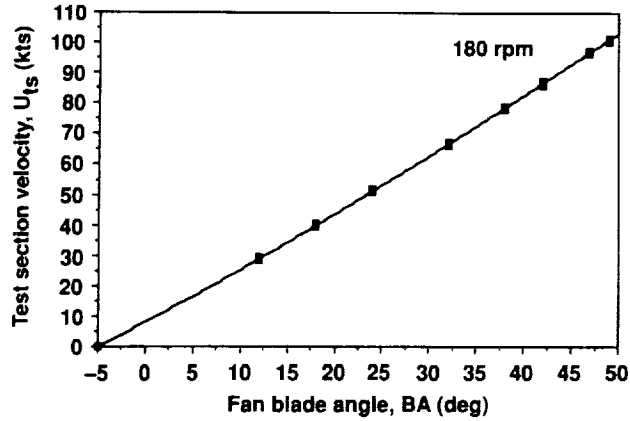


$$90 \text{ rpm } q_c = -0.0239 + 0.0133(BA) + 0.0035(BA)^2 - 1.545E-5(BA)^3$$

$$135 \text{ rpm } q_c = 0.0847 + 0.0452(BA) + 0.0058(BA)^2 + 2.810E-5(BA)^3$$

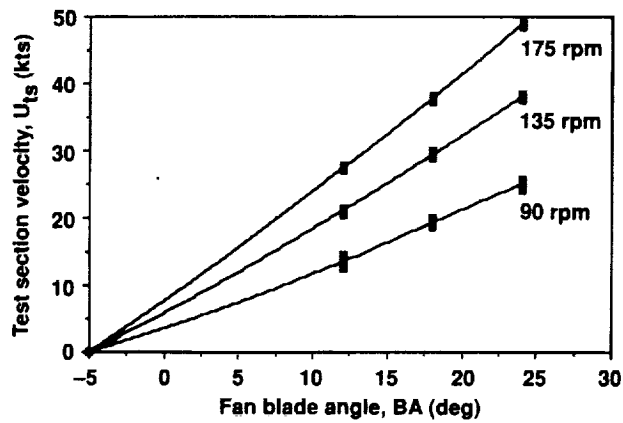
$$175 \text{ rpm } q_c = 0.1915 + 0.0807(BA) + 0.0088(BA)^2 + 6.562E-5(BA)^3$$

Figure 22. Corrected dynamic pressure on centerline versus fan blade angle (IFC mode).



$$180 \text{ rpm } U_{ts} = 8.0856 + 1.6525(BA) + 0.0065(BA)^2 - 2.938E-5(BA)^3$$

Figure 23. Corrected test section velocity on centerline versus fan blade angle (utility mode).



$$90 \text{ rpm } U_{ts} = 3.0856 + 0.7151(BA) + 0.0177(BA)^2 - 3.863E-4(BA)^3$$

$$135 \text{ rpm } U_{ts} = 5.6931 + 1.1897(BA) + 0.0096(BA)^2 - 1.216E-4(BA)^3$$

$$175 \text{ rpm } U_{ts} = 7.6403 + 1.5652(BA) + 0.0073(BA)^2 - 2.759E-5(BA)^3$$

Figure 24. Corrected test section velocity on centerline versus fan blade angle (IFC mode).

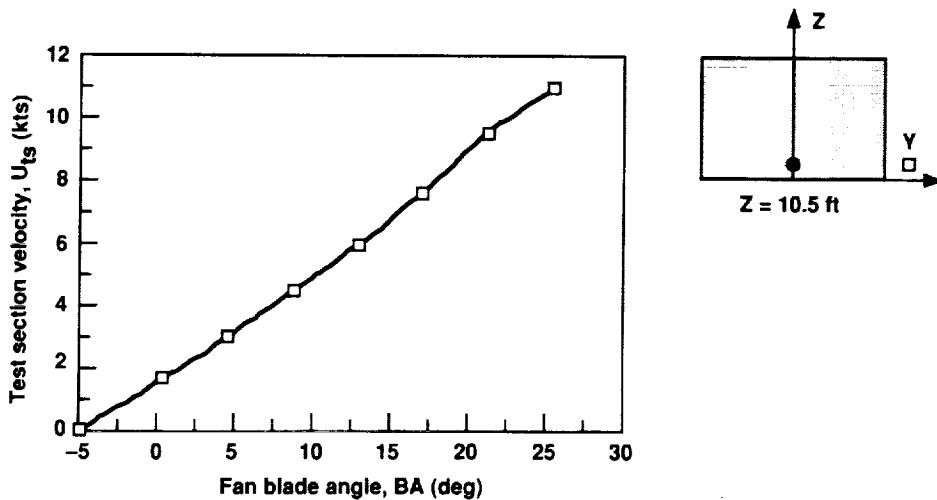


Figure 25. Test section velocity versus fan blade angle (IFC mode - 36 rpm).

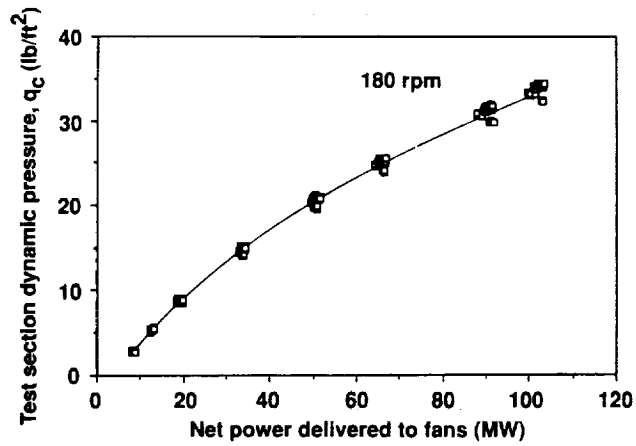


Figure 26. Corrected dynamic pressure on centerline versus net power delivered to fans (utility mode).

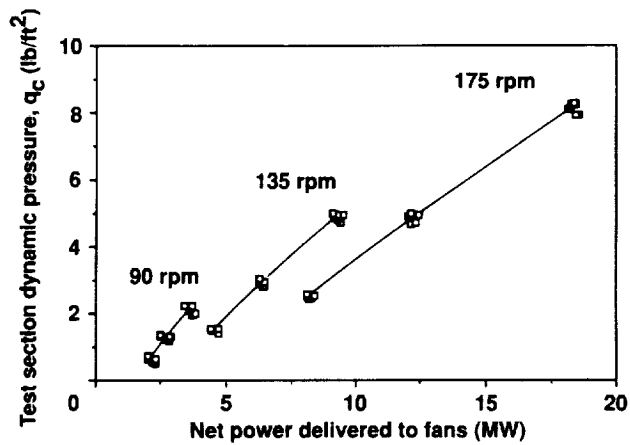


Figure 27. Corrected dynamic pressure on centerline versus net power delivered to fans (IFC mode).

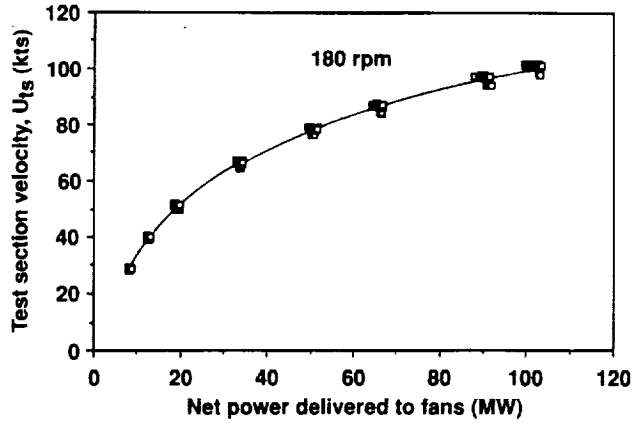


Figure 28. Corrected test section velocity on centerline versus net power delivered to fans (utility mode).

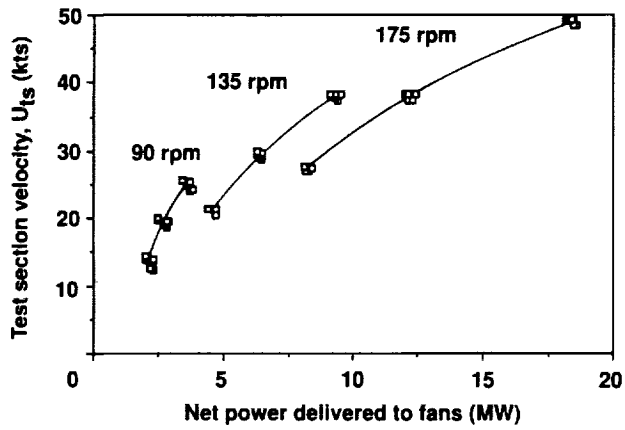


Figure 29. Corrected test section velocity on centerline versus net power delivered to fans (IFC mode).



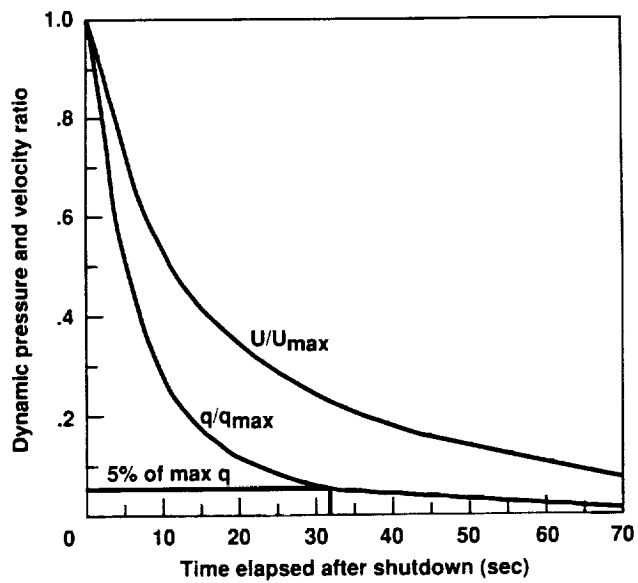


Figure 30. Dynamic pressure decay ( $q_{max} = 33$  psf).

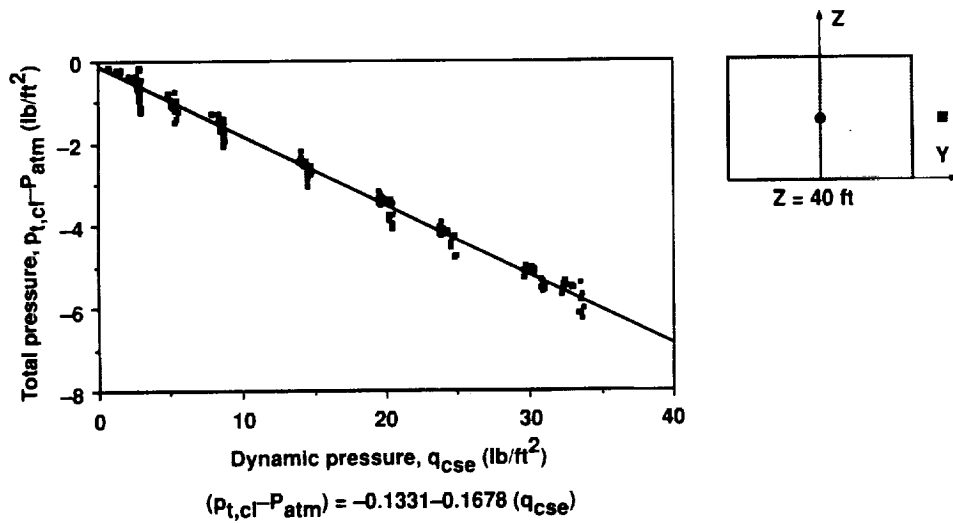


Figure 31. Indicated total pressure on centerline versus scale dynamic pressure ( $Z = 40$  ft).

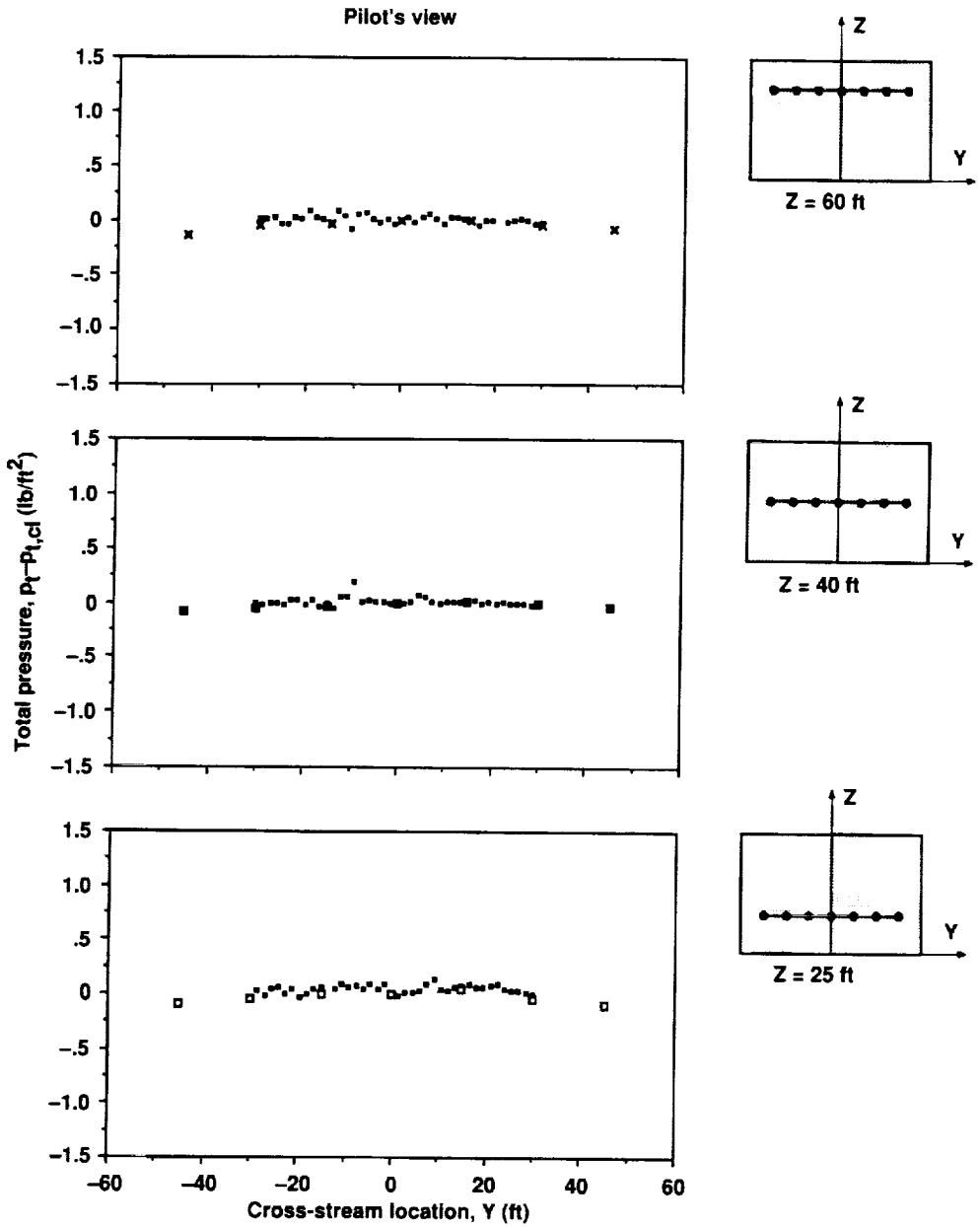


Figure 32. Test section total pressure distribution ( $U_{ts} = 50$  knots).

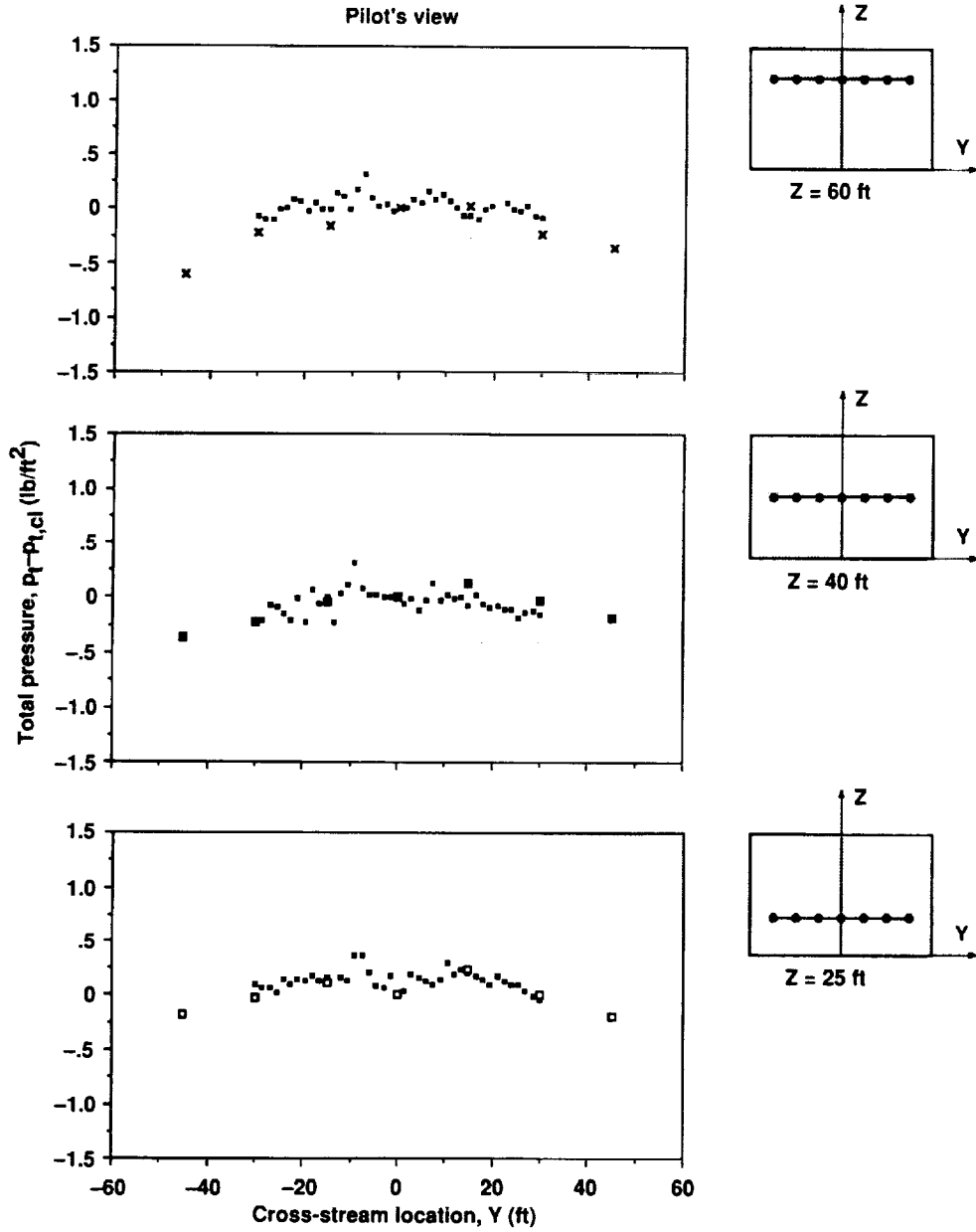


Figure 33. Test section total pressure distribution ( $U_{TS} = 100$  knots).

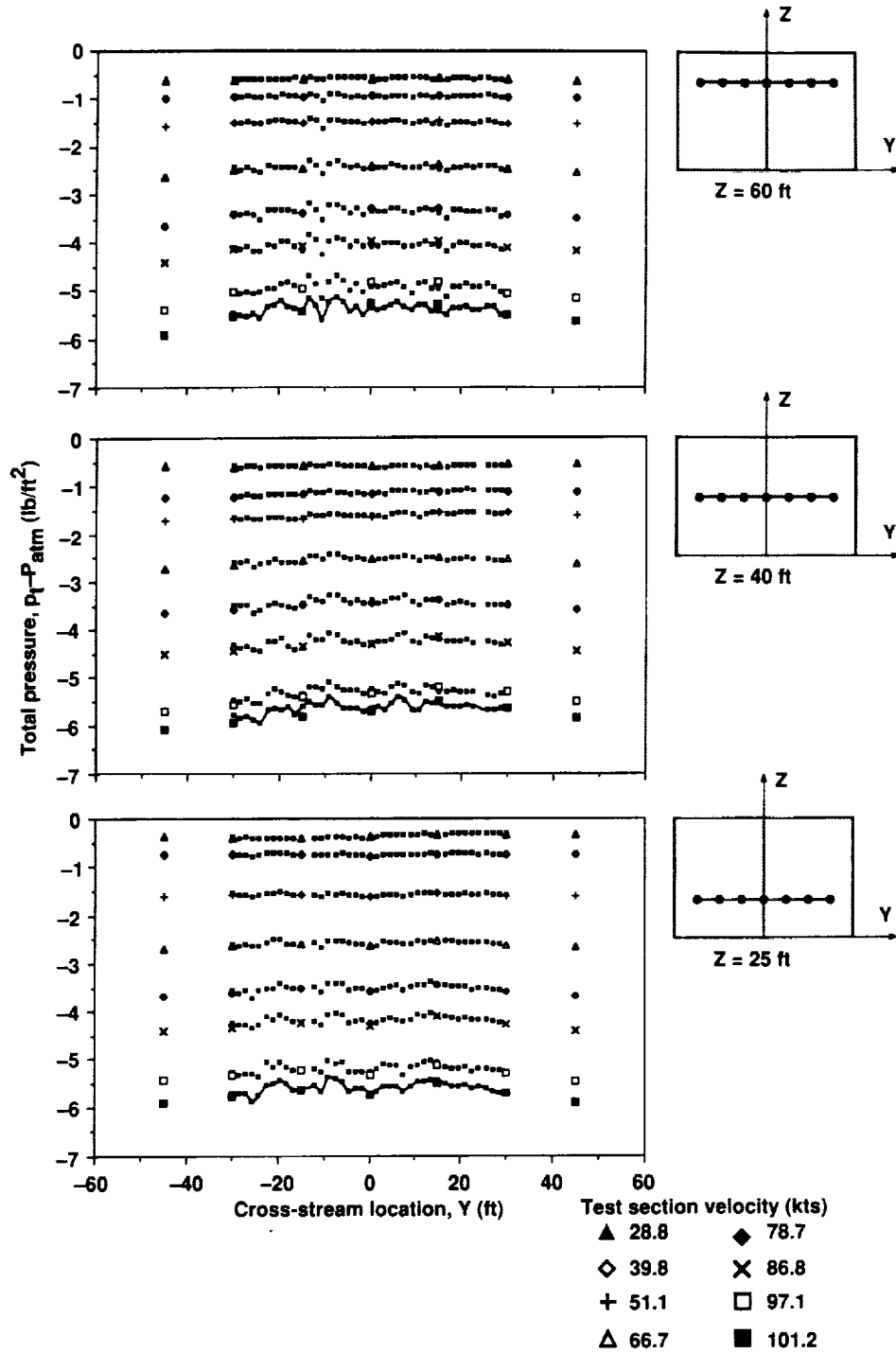
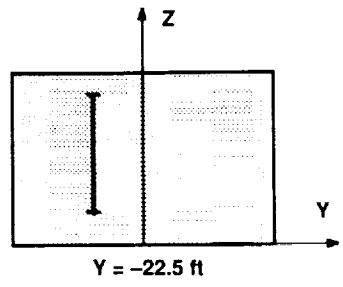
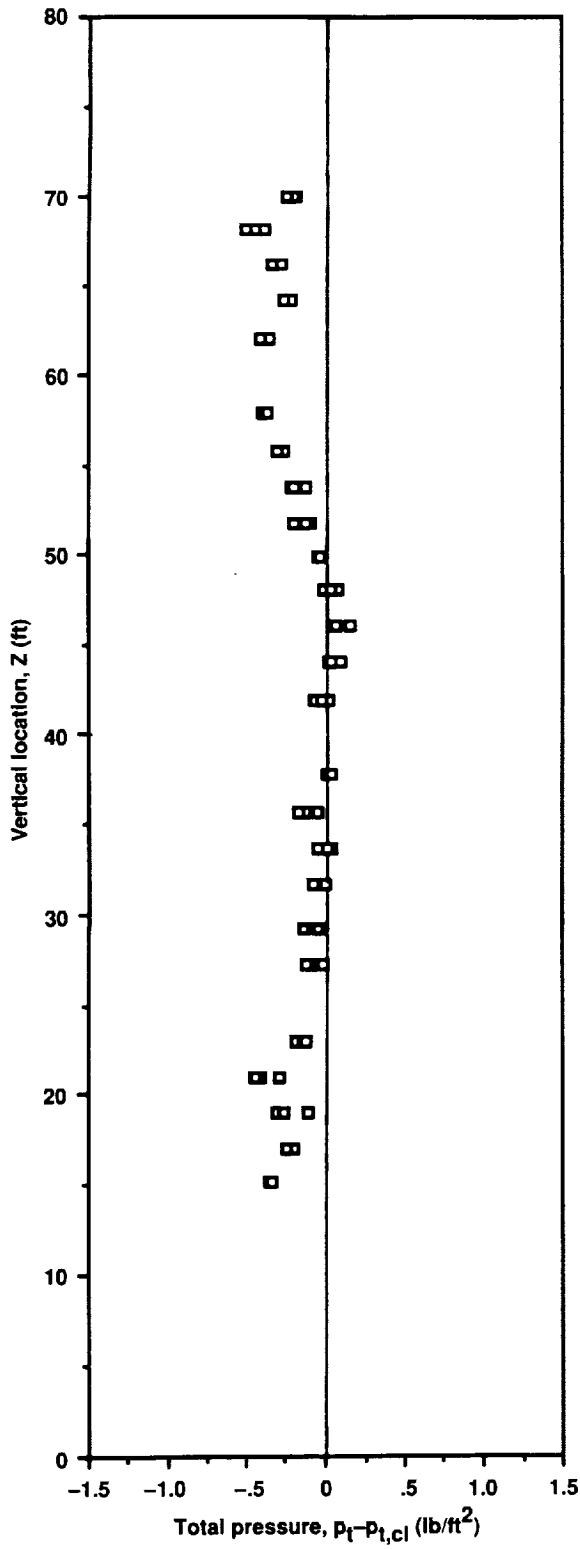


Figure 34. Total pressure distributions for various tunnel speeds.



( □ vertical rake )

Figure 35. Vertical total pressure distribution ( $U_{tS} = 100$  knots).

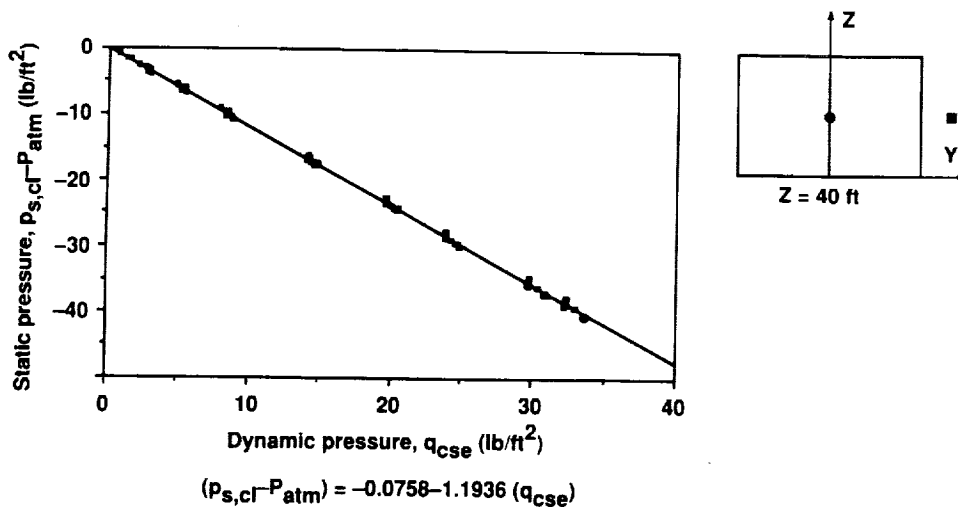


Figure 36. Indicated static pressure on centerline versus scale dynamic pressure ( $Z = 40$  ft).

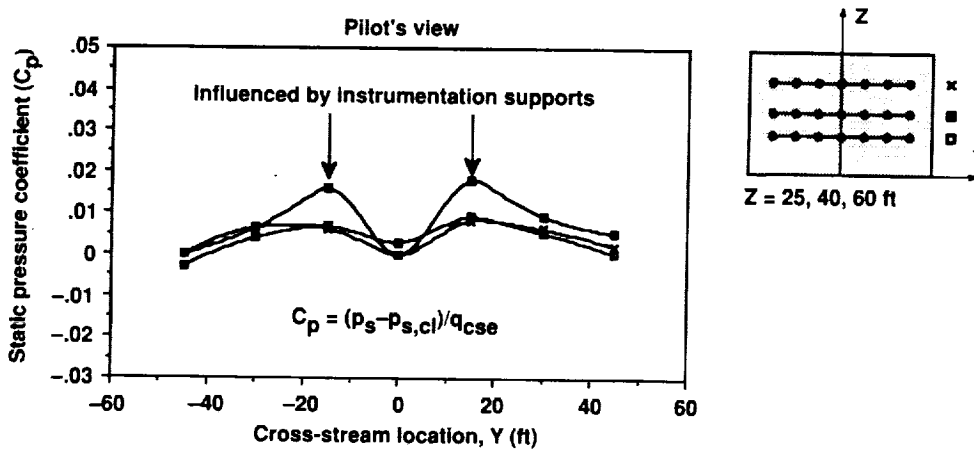


Figure 37. Static pressure coefficient distribution.

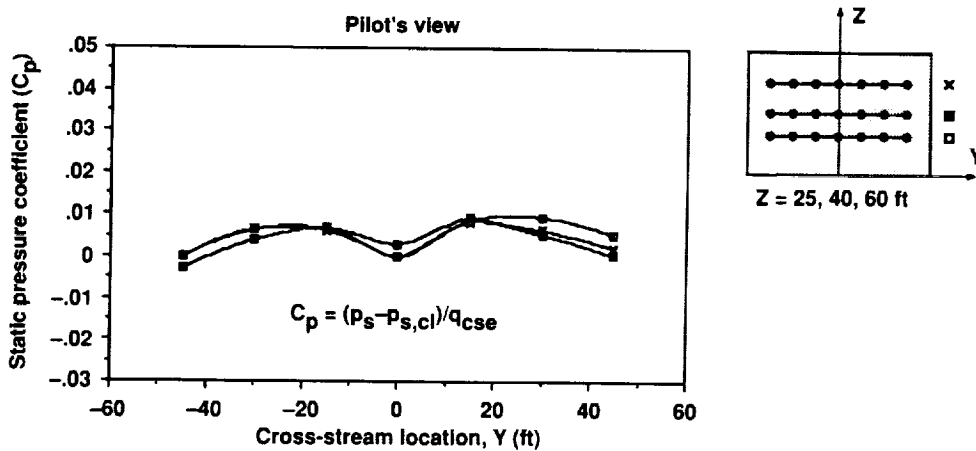


Figure 38. Static pressure coefficient distribution (corrected for aerodynamic interference of the instrumentation supports).

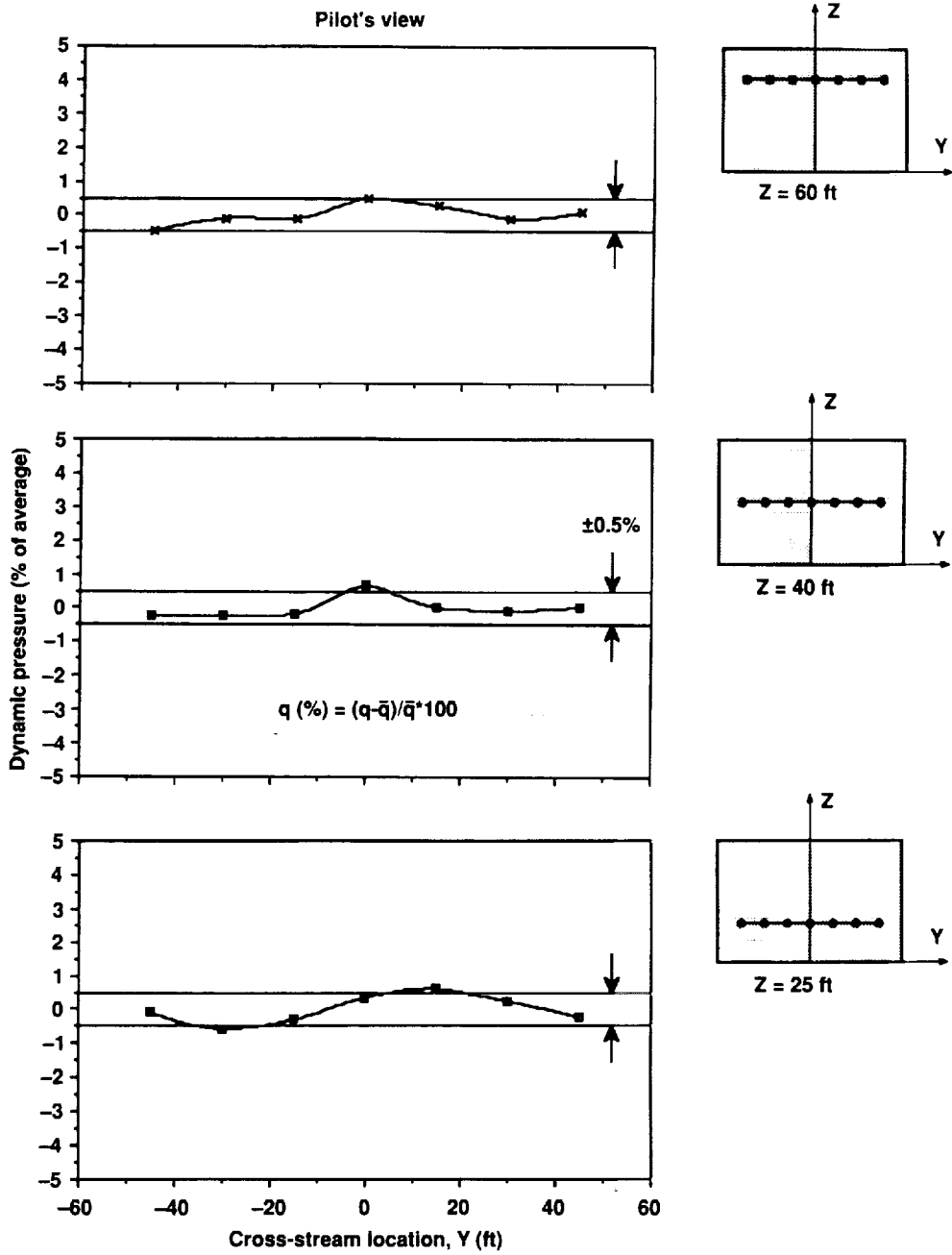


Figure 39. Dynamic pressure distribution ( $U_{ts} = 50$  knots).

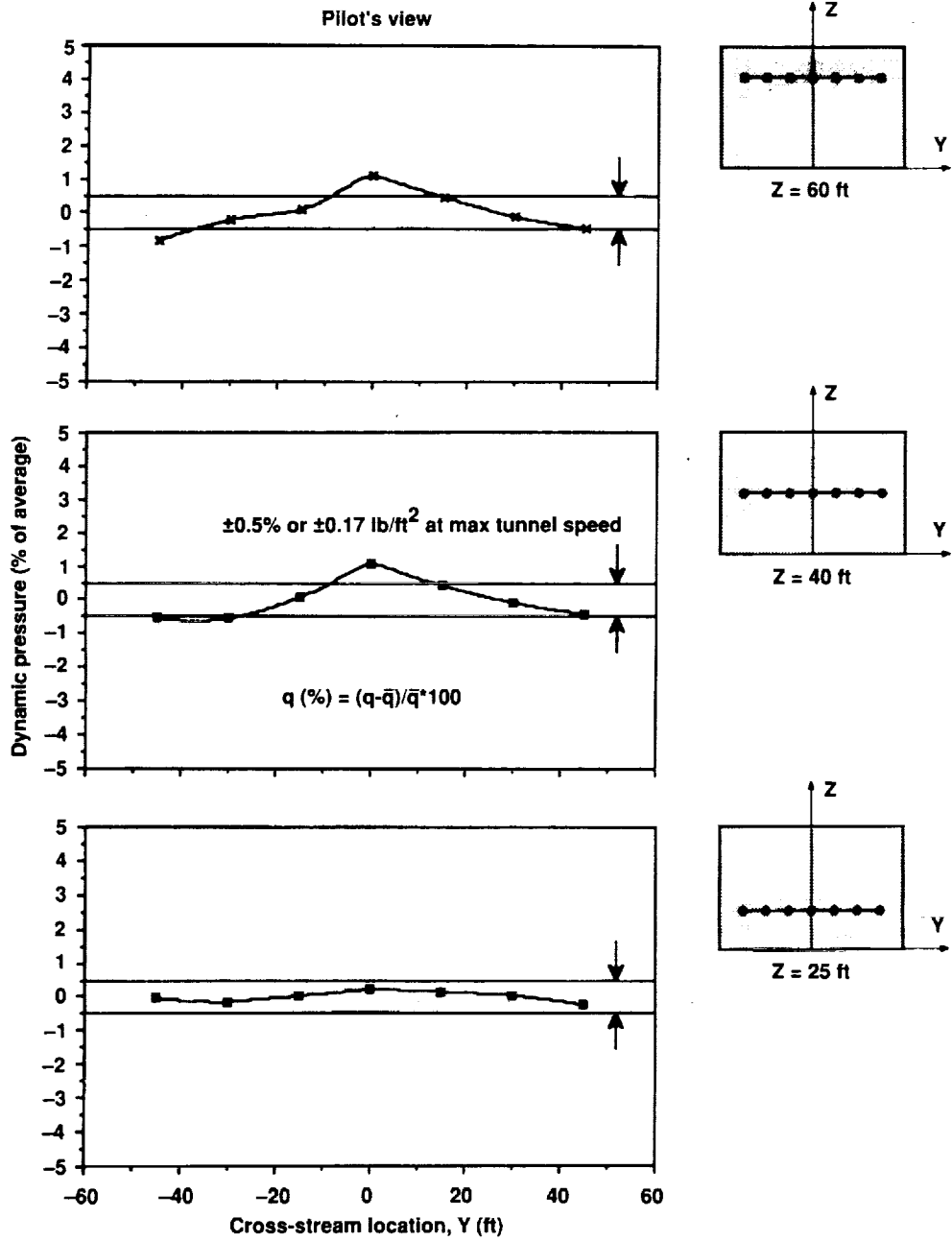


Figure 40. Dynamic pressure distribution for maximum tunnel speed ( $U_{TS} = 100$  knots).



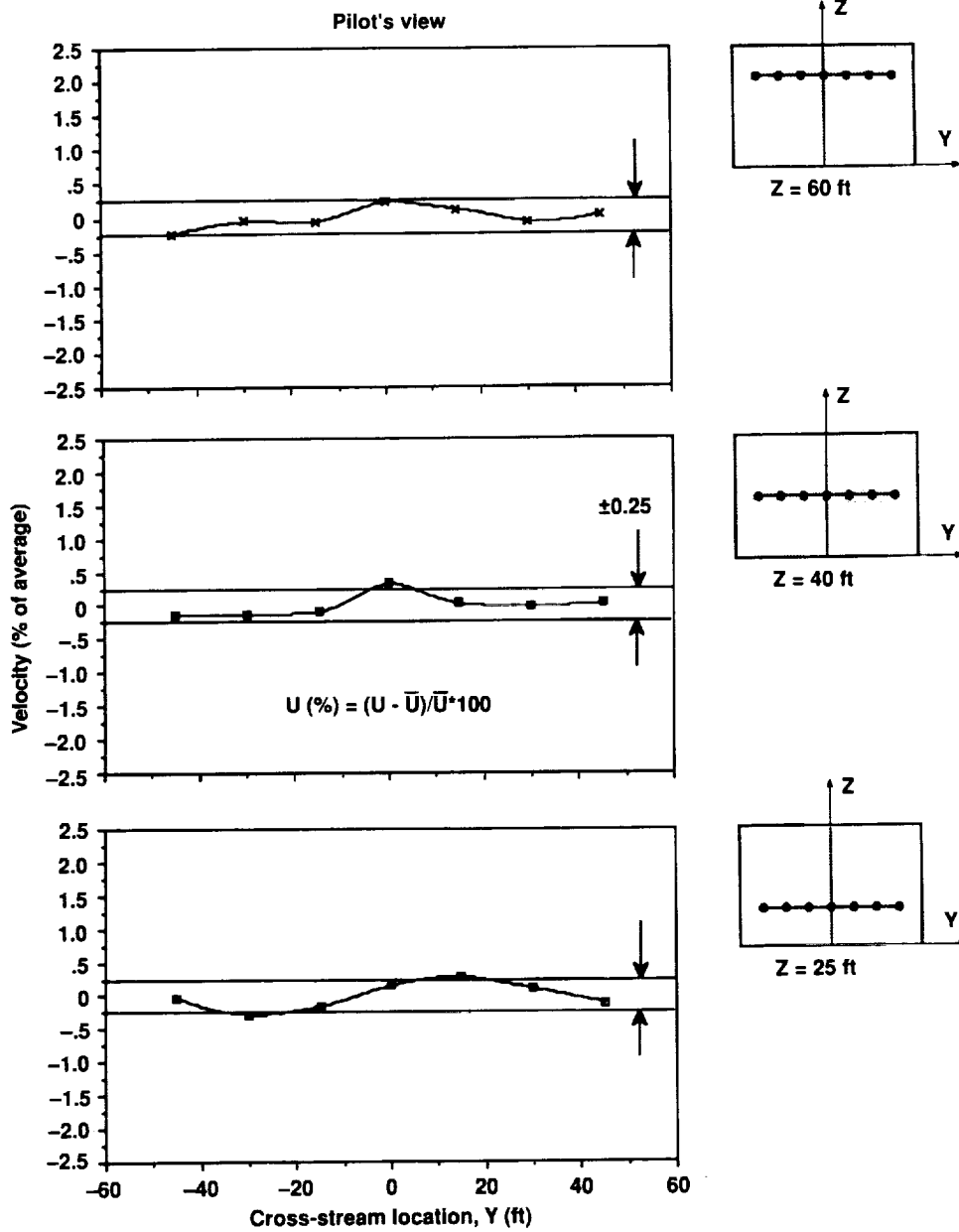


Figure 41. Velocity distribution ( $U_{TS} = 50$  knots).

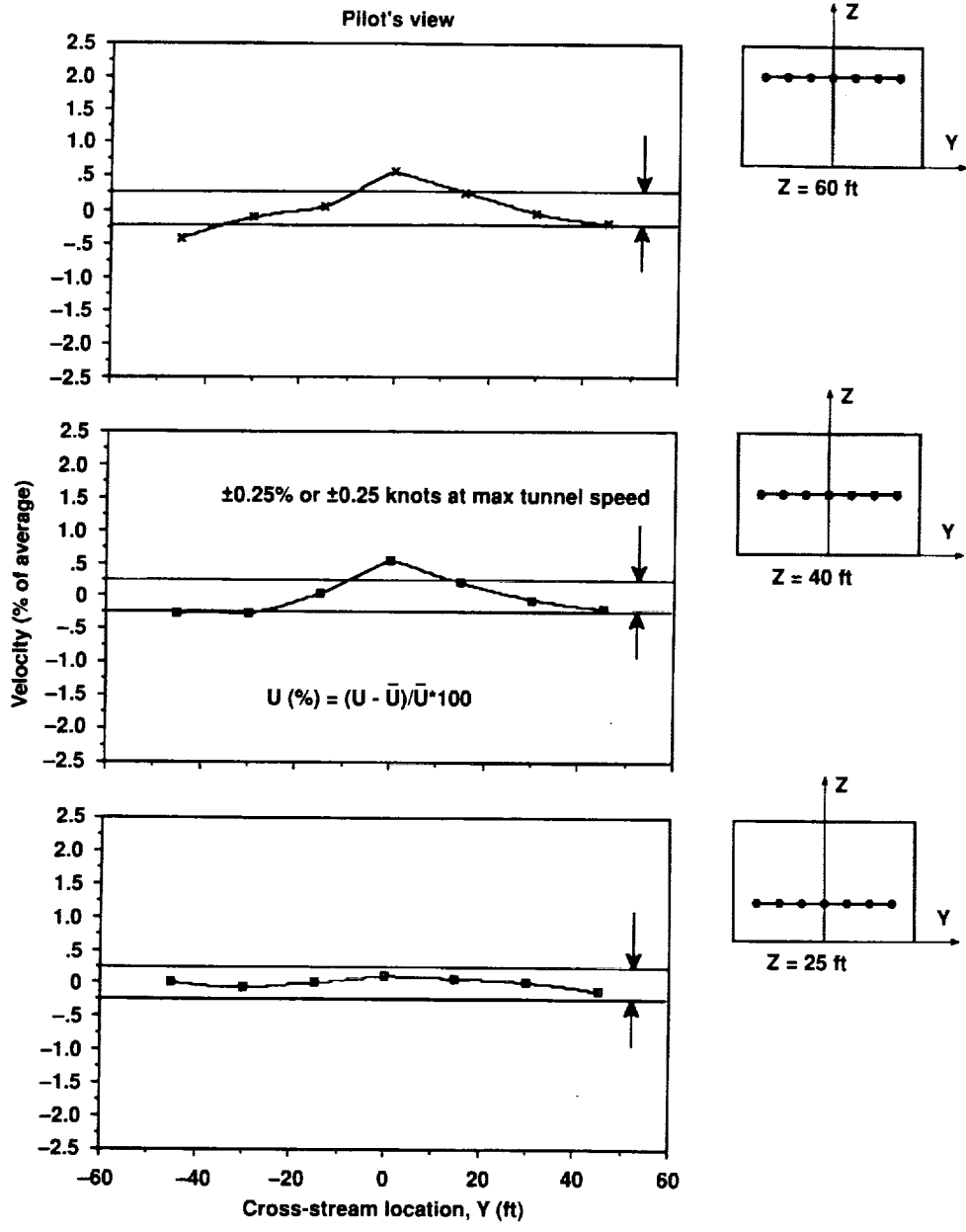


Figure 42. Velocity distribution for maximum tunnel speed ( $U_{TS} = 100$  knots).

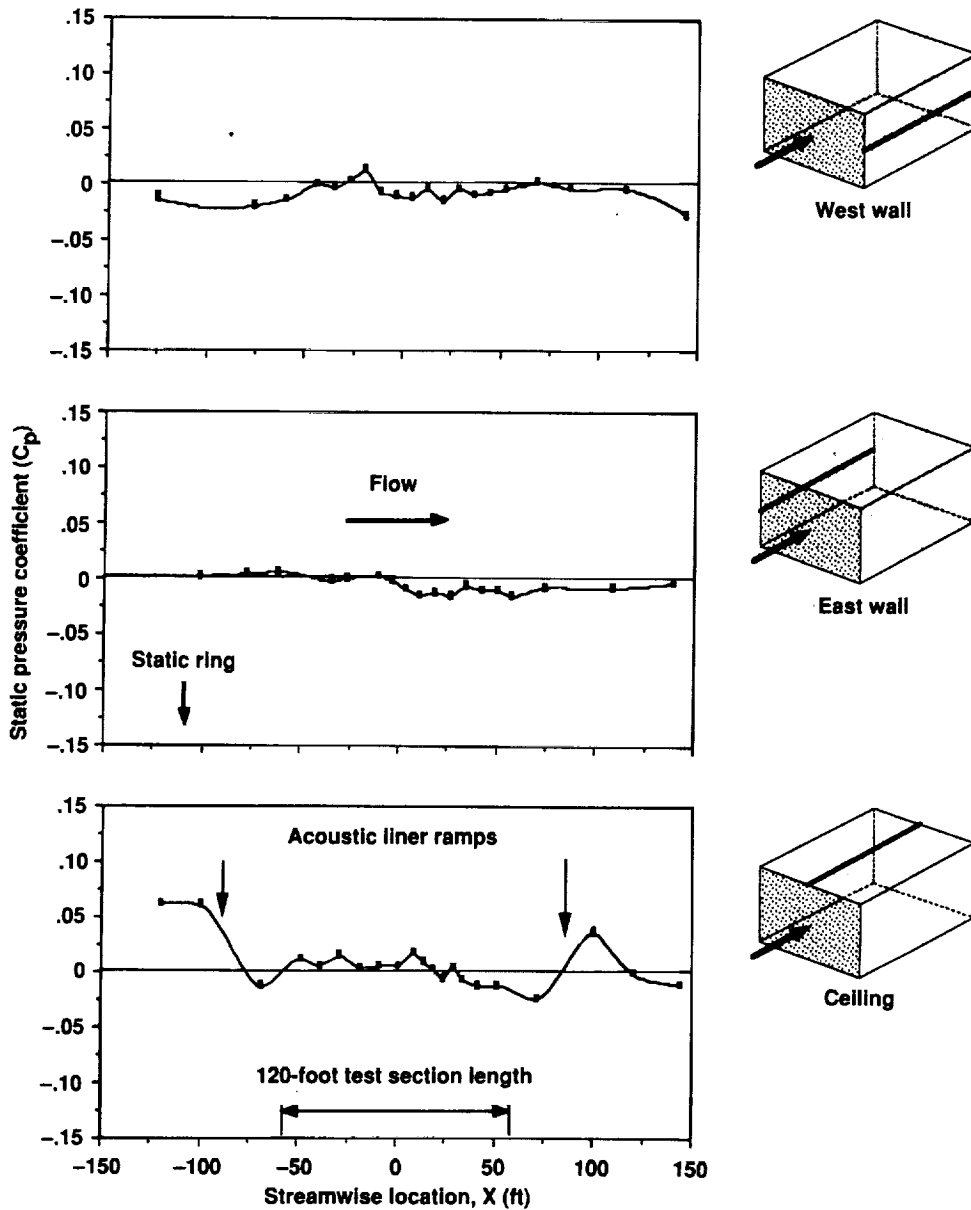


Figure 43. Streamwise wall static pressure coefficient distributions ( $U_{ts} = 100$  knots).

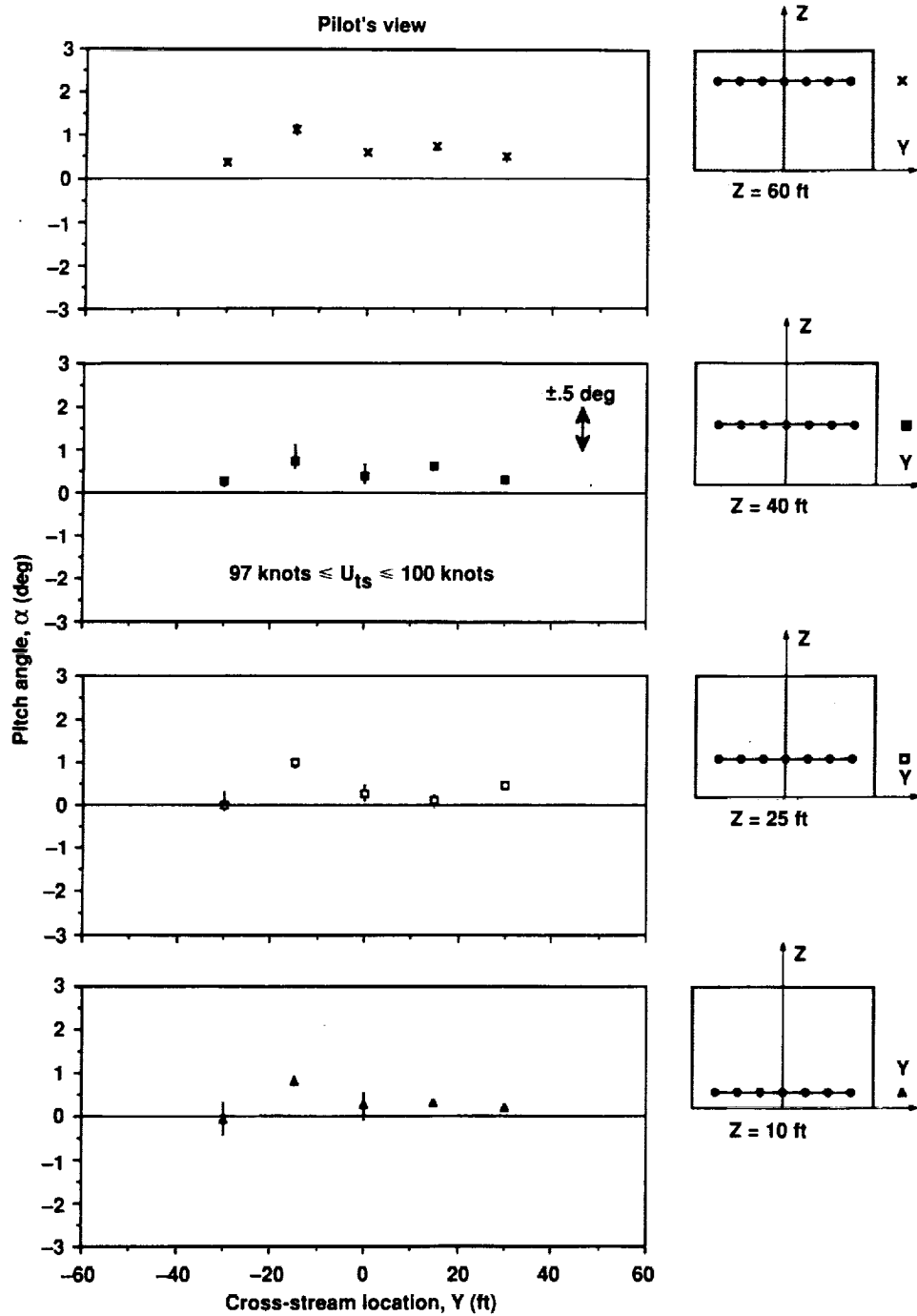


Figure 44. Pitch angle distributions ( $U_{ts} > 97$  knots).

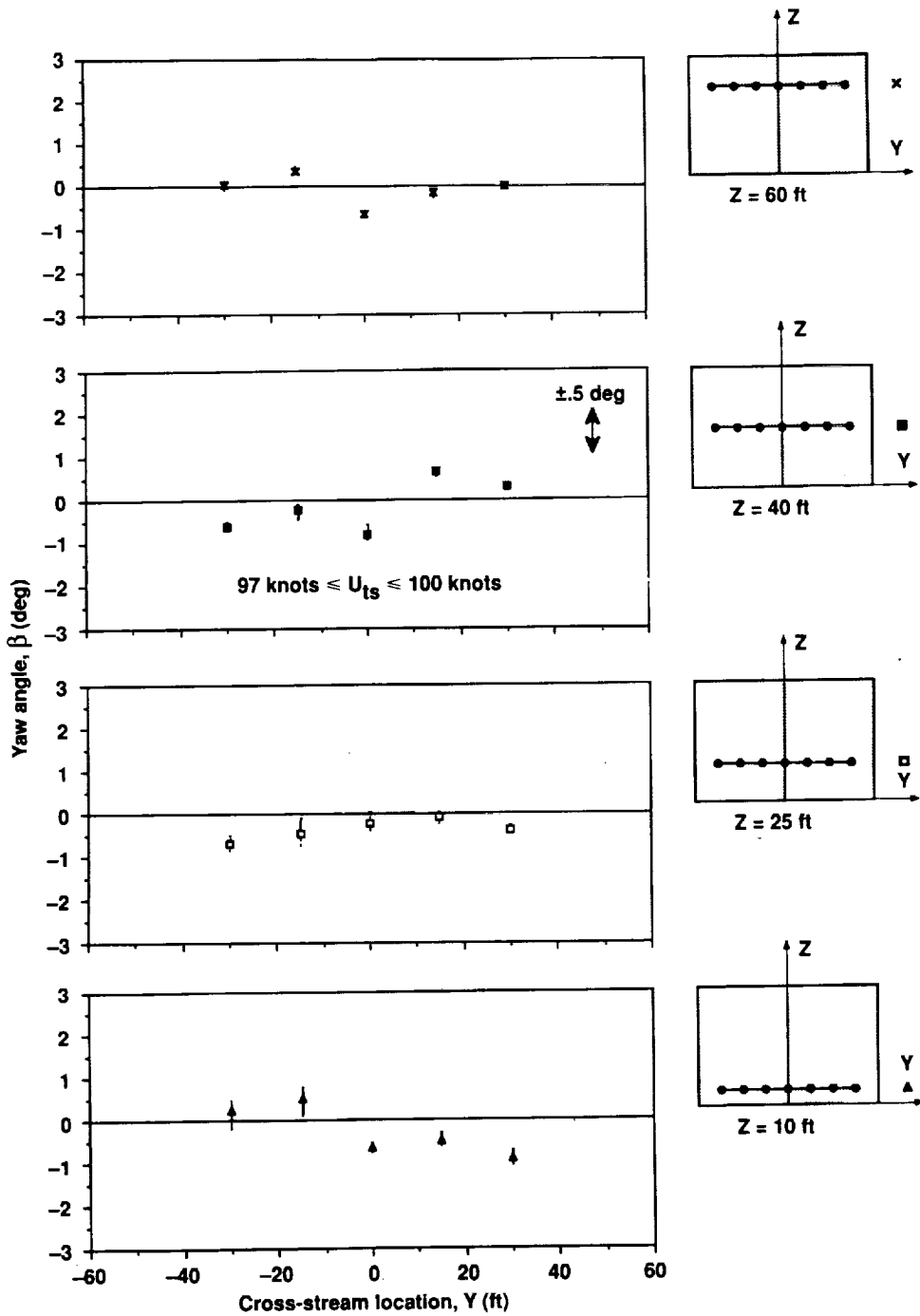


Figure 45. Yaw angle distributions ( $U_{ts} > 97$  knots).

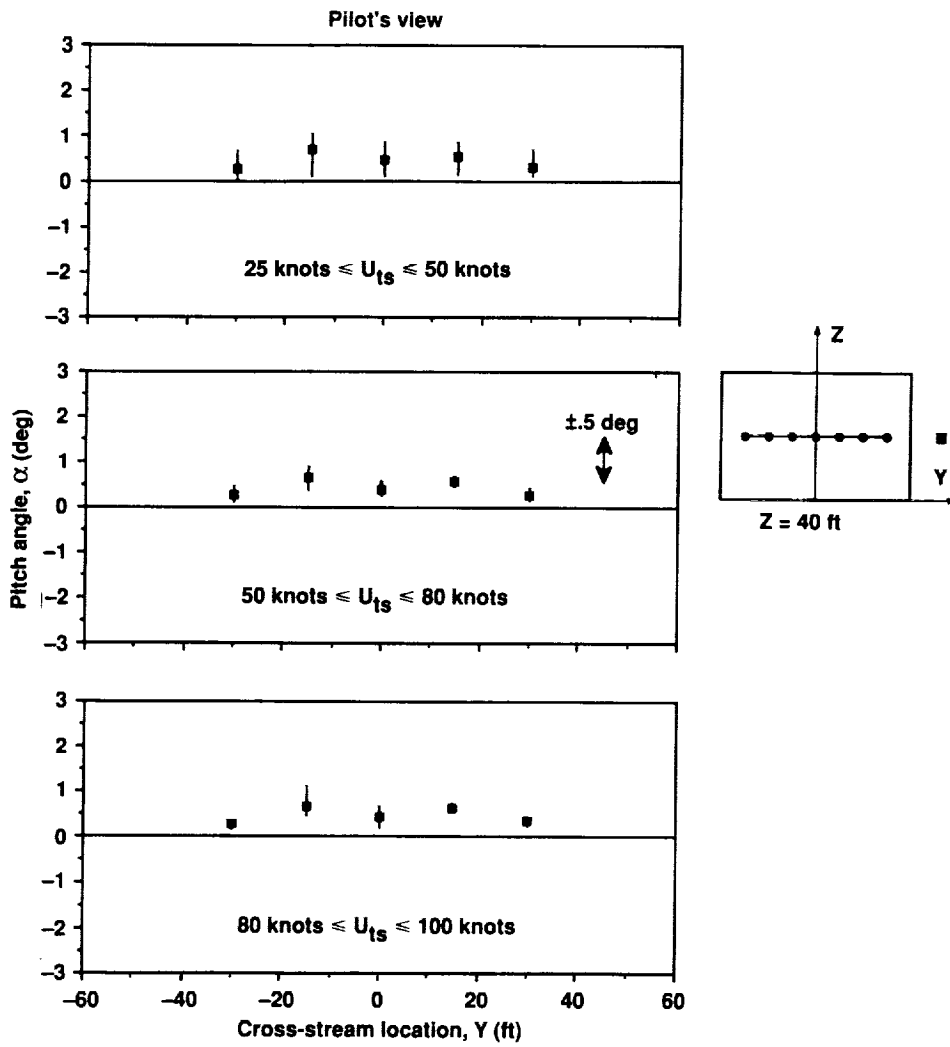


Figure 46. Pitch angle distributions for three speed ranges.

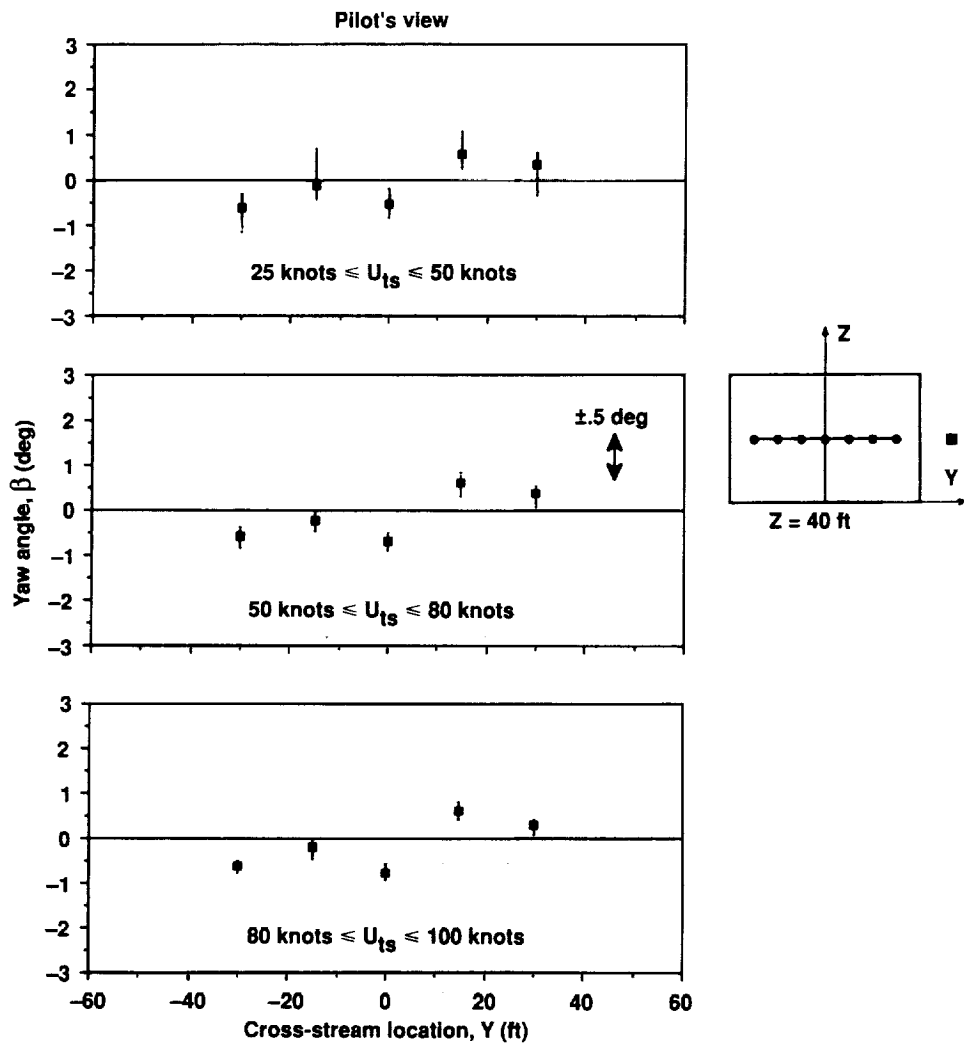


Figure 47. Yaw angle distributions for three speed ranges.

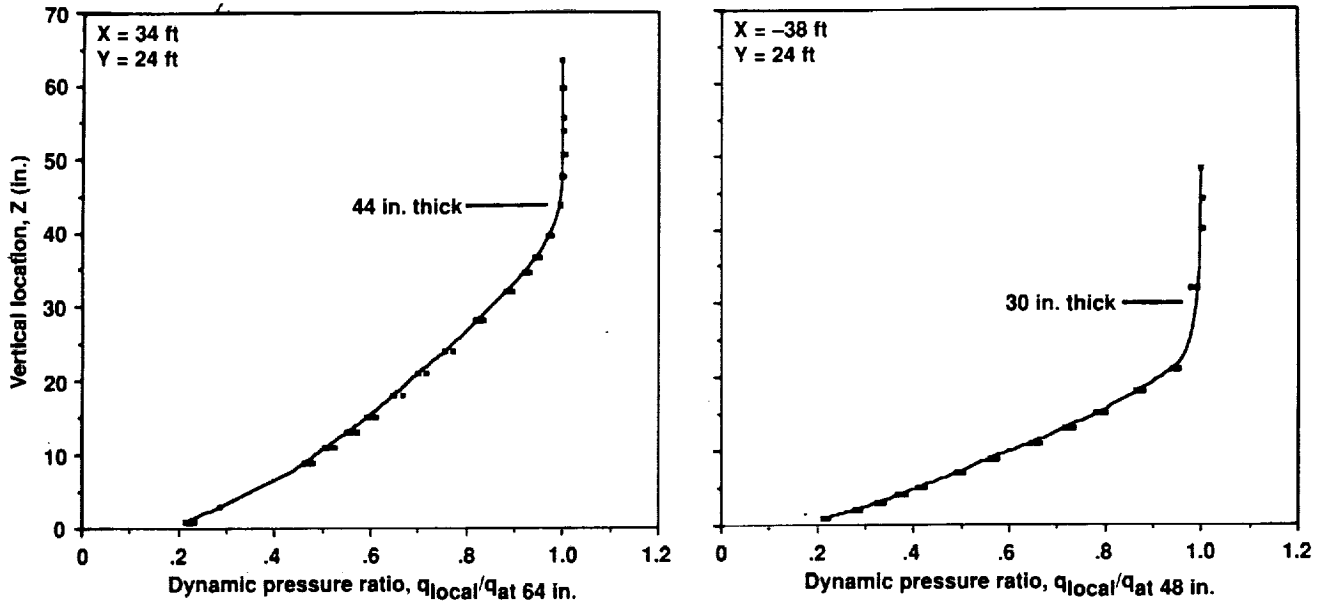


Figure 48. Dynamic pressure profiles from the fixed rakes on the test section floor ( $U_{TS} = 100$  knots).

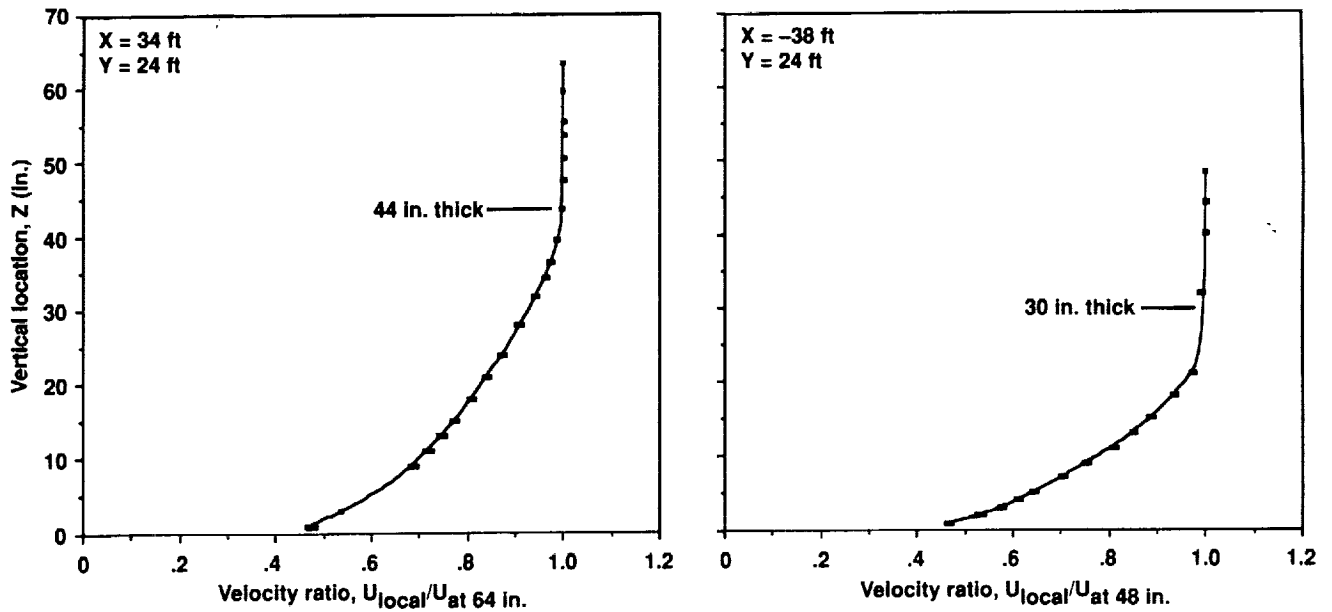


Figure 49. Velocity profiles from the fixed rakes on the test section floor ( $U_{TS} = 100$  knots).



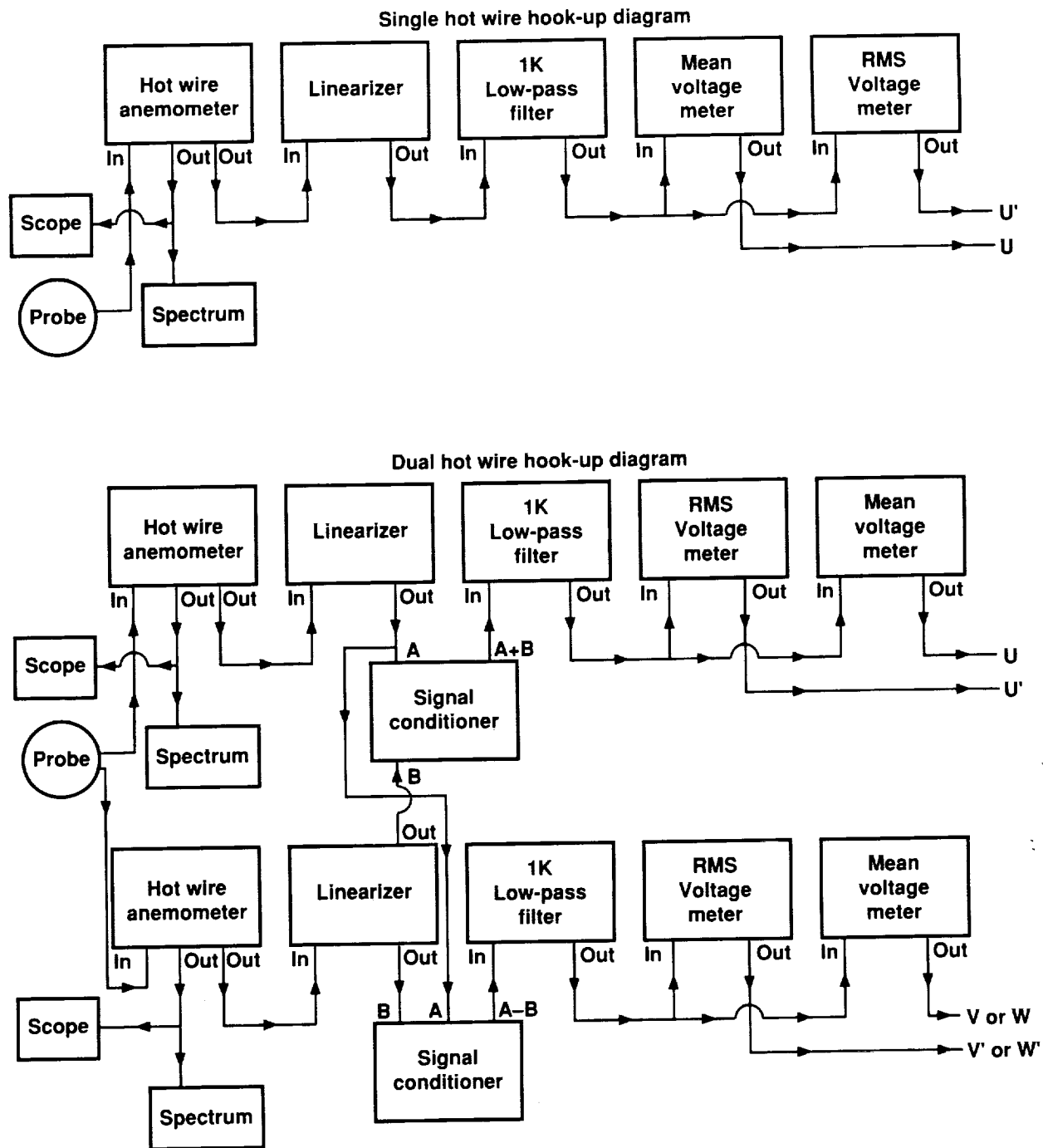


Figure 50. Hot wire anemometer instrumentation diagrams.

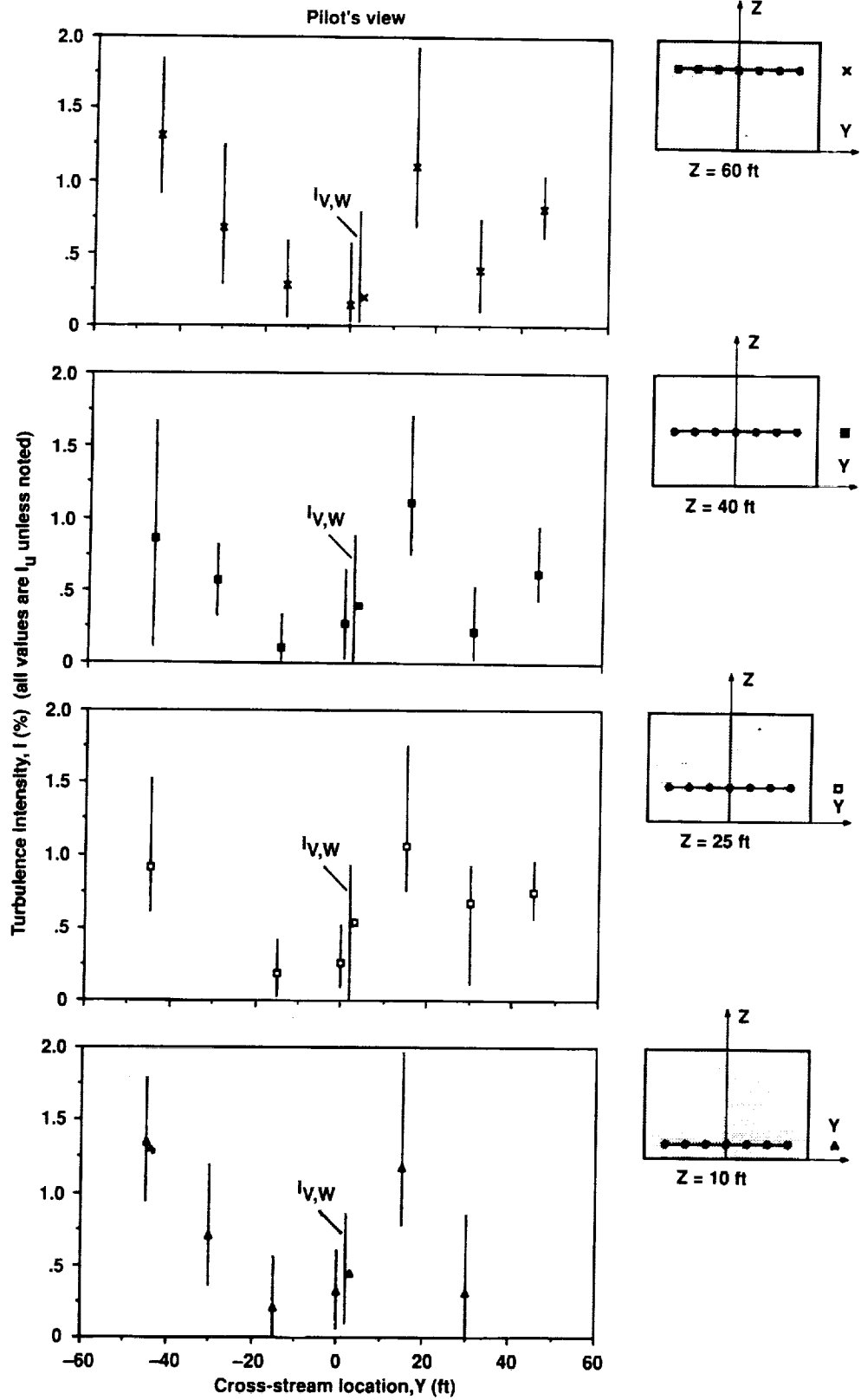


Figure 51. Turbulence intensity distribution ( $U_{TS} < 50$  knots).

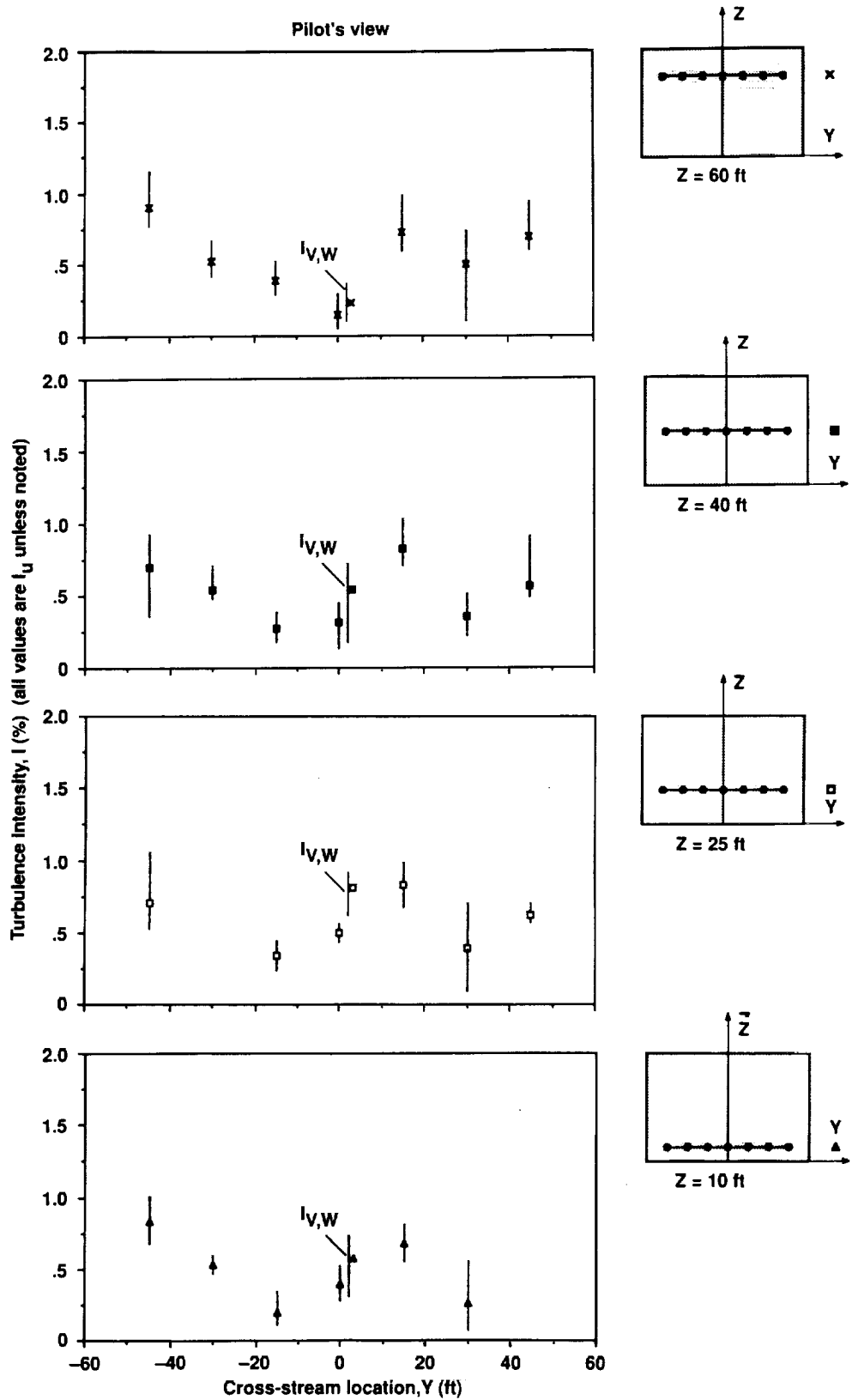


Figure 52. Turbulence intensity distribution ( $50 \text{ knots} < U_{TS} < 75 \text{ knots}$ ).

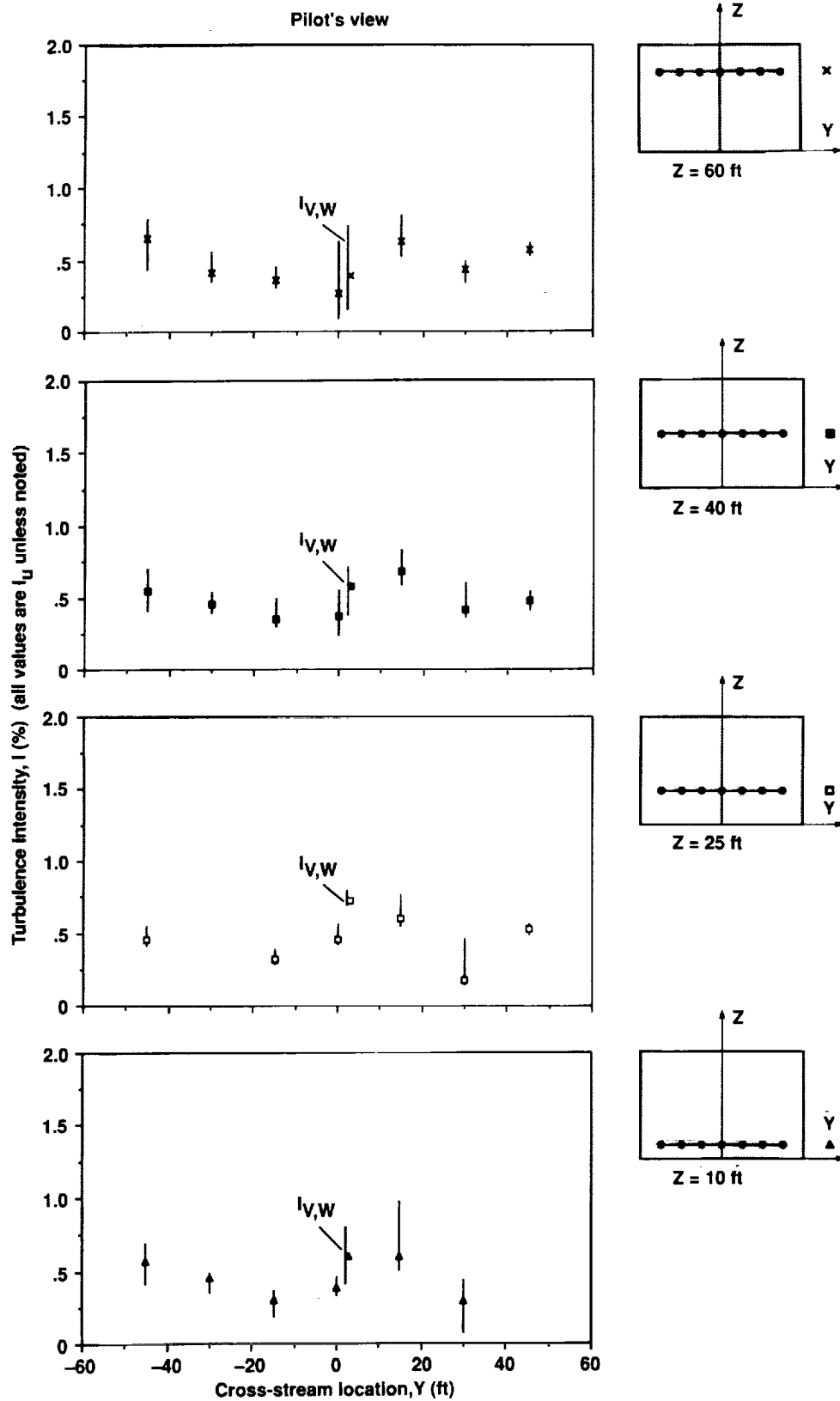
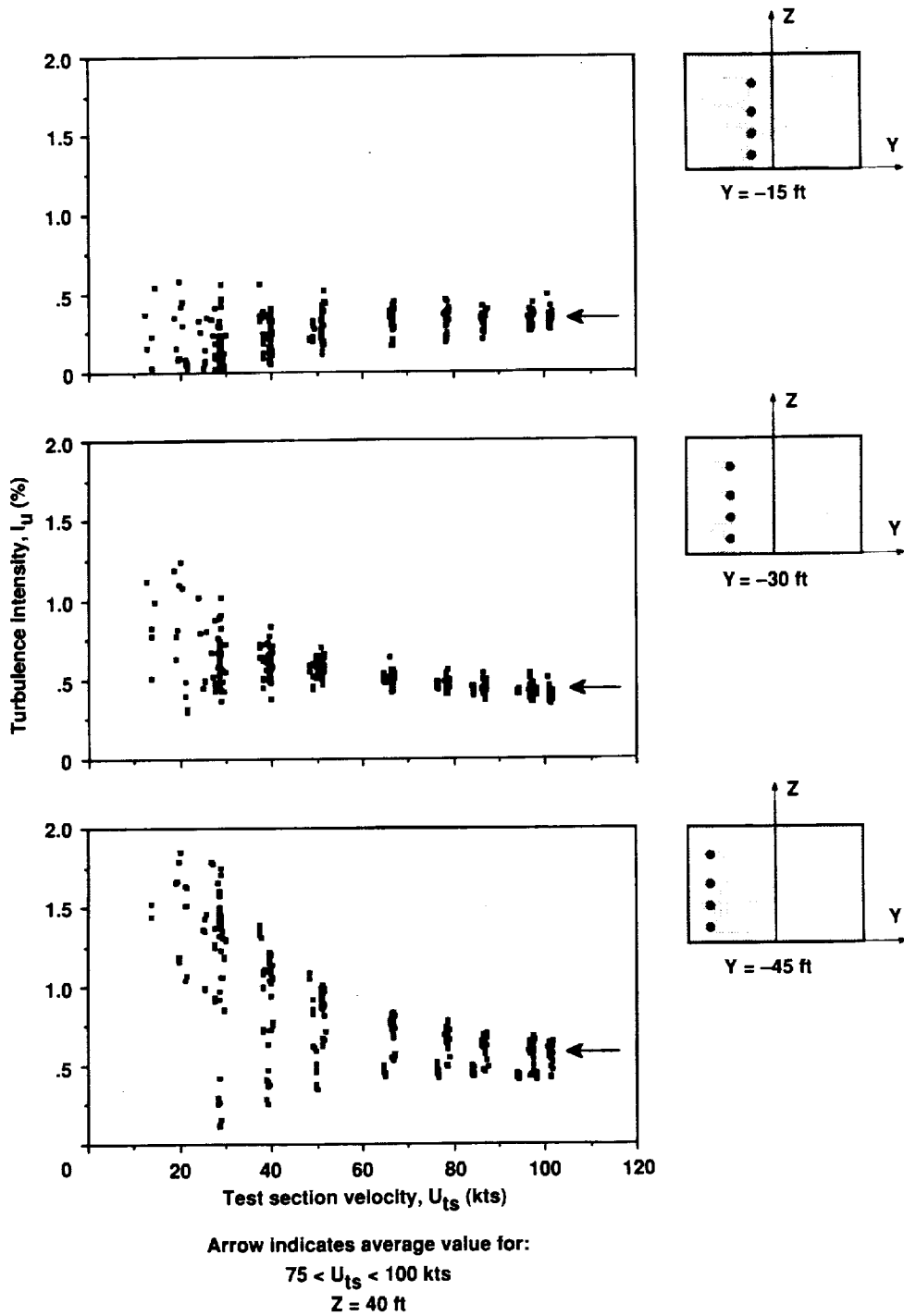
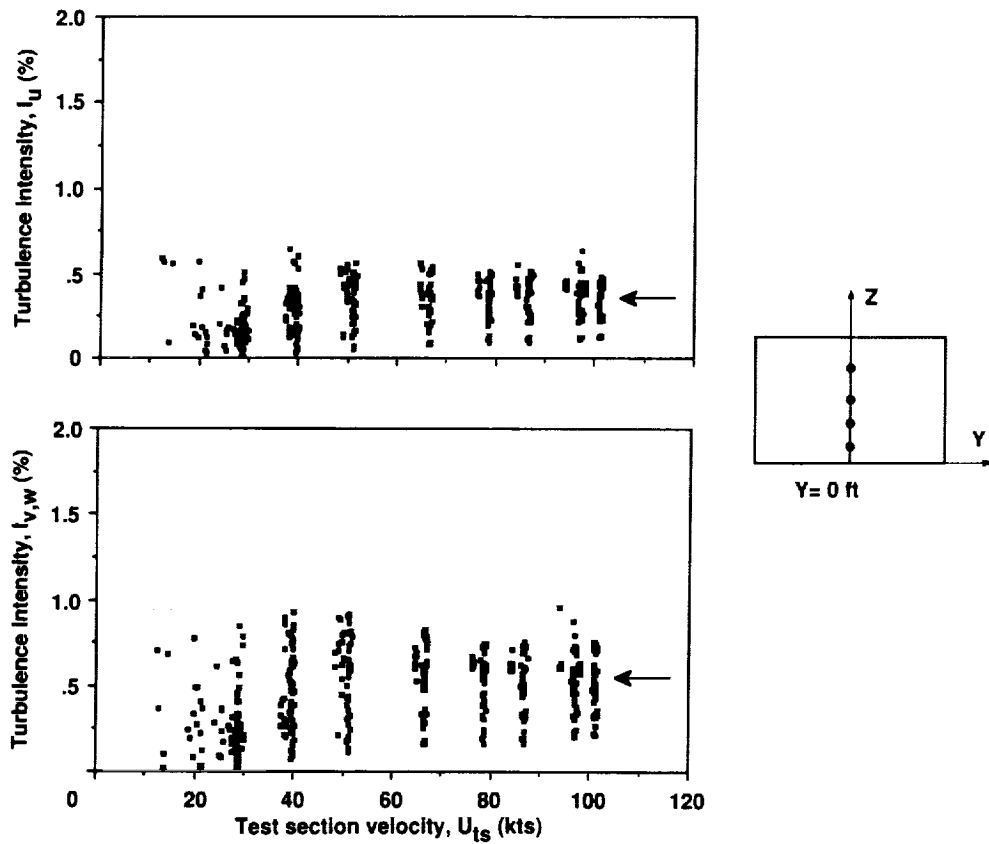


Figure 53. Turbulence intensity distribution ( $75 \text{ knots} < U_{TS} < 100 \text{ knots}$ ).



(a)  $Y = -15, -30, -45$ .

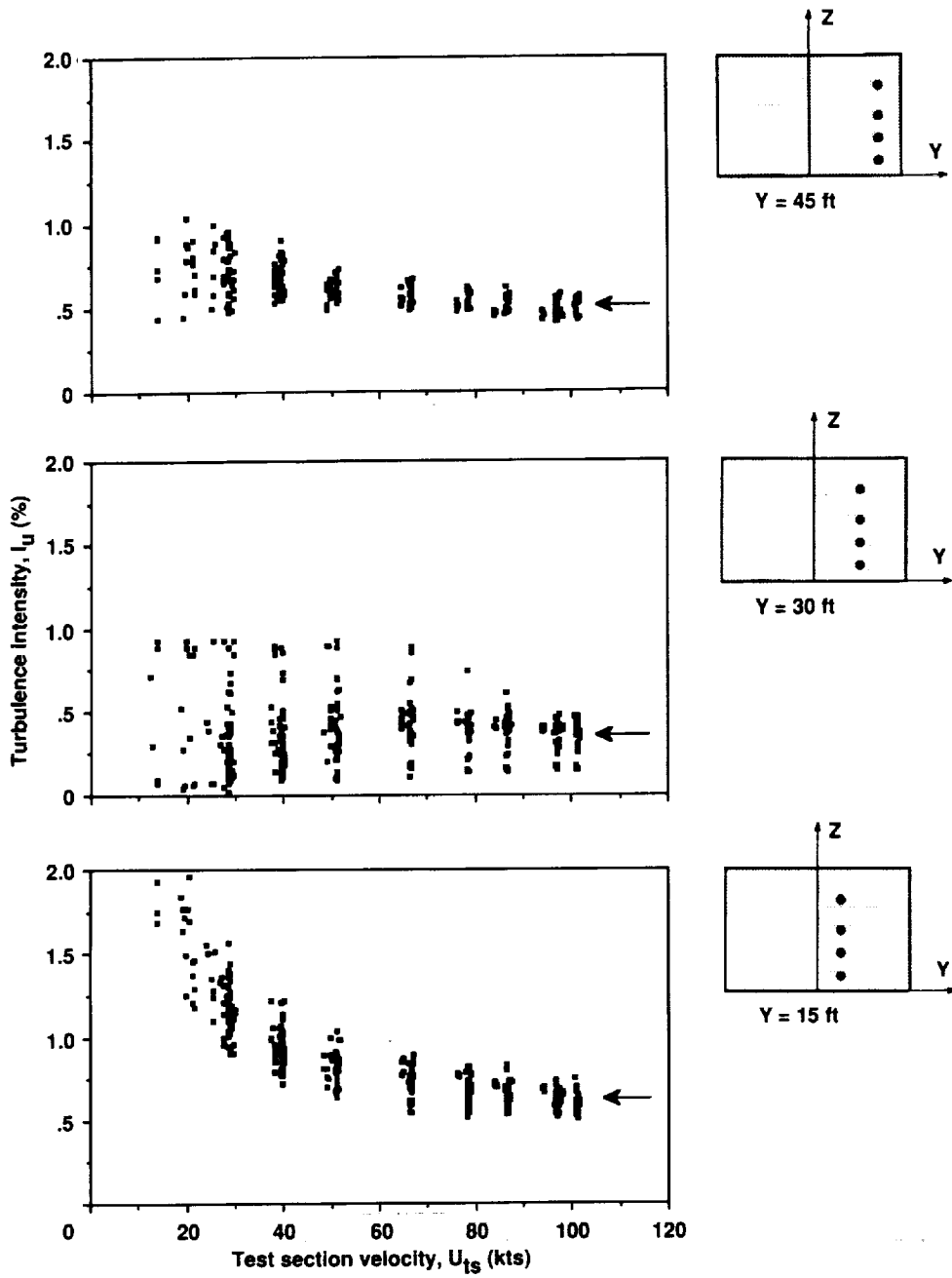
Figure 54. Turbulence intensity variation with test section velocity (all boom stations, all FLOCAL runs).



Arrow indicates average value for:  
 $75 < U_{ts} < 100$  kts  
 $Z = 40$  ft

(b)  $Y = 0$ .

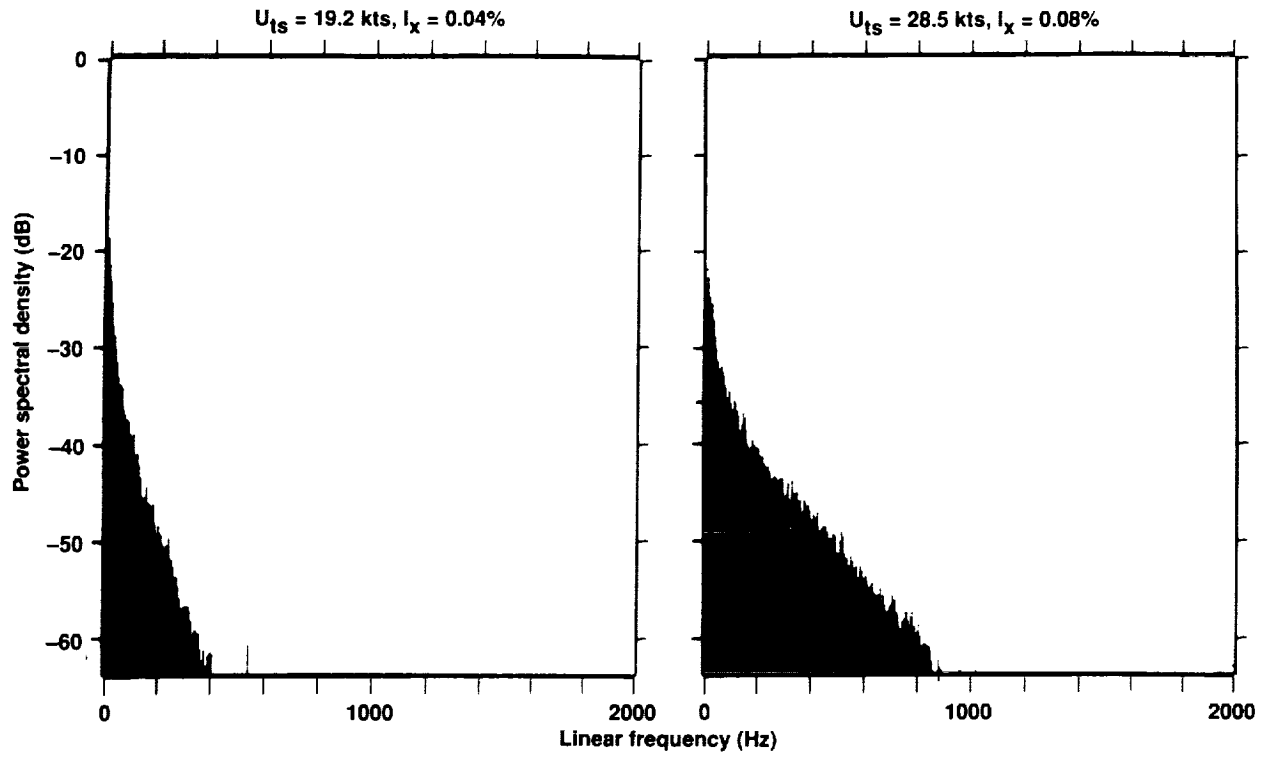
Figure 54. Continued.



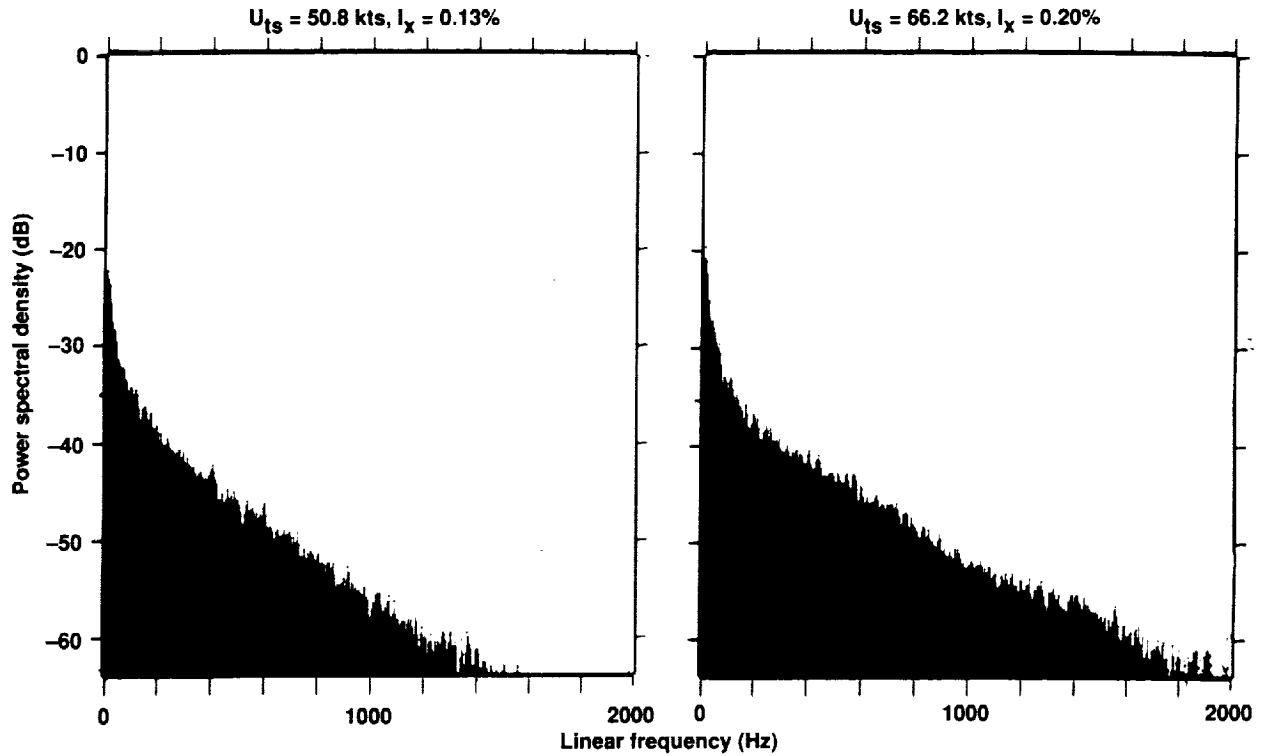
Arrow indicates average value for:  
 $75 < U_{ts} < 100$  kts  
 $Z = 40$  ft

(c)  $Y = 45, 30, 15$ .

Figure 54. Concluded.



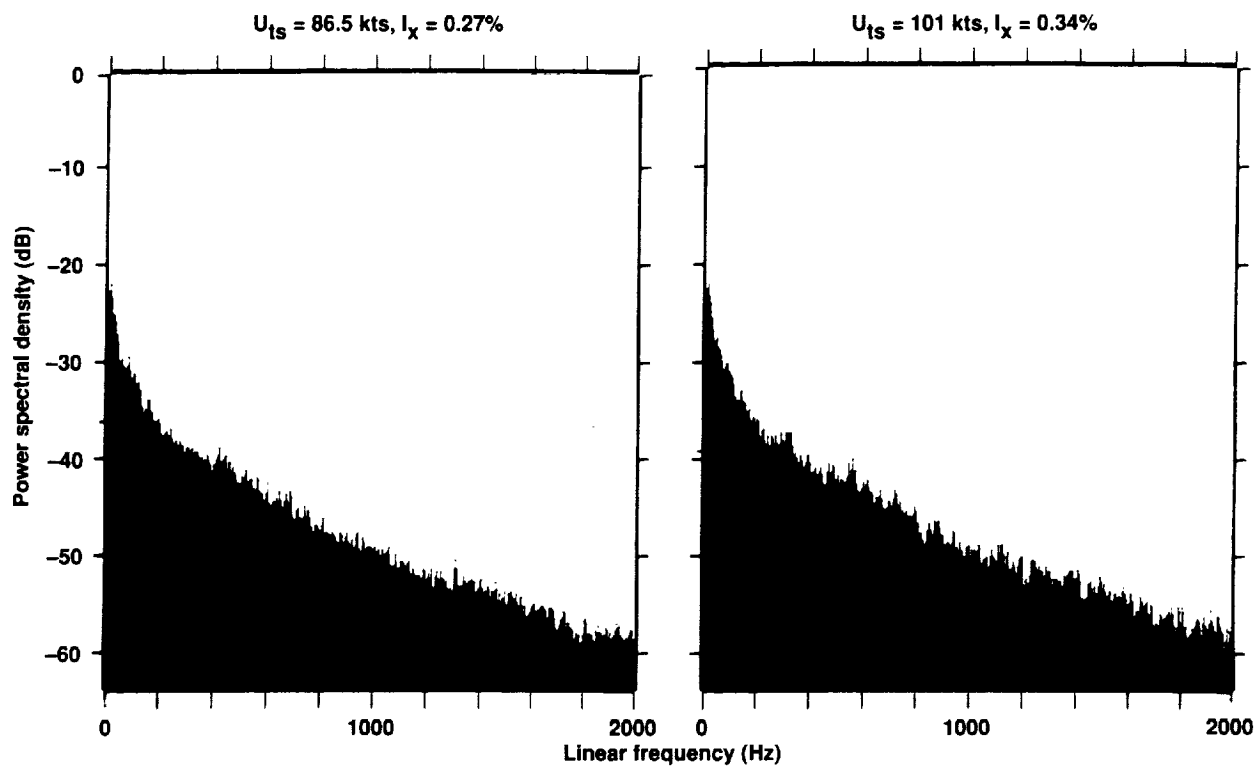
(a)  $U_{ts} = 19.2, 28.5$  knots.



(b)  $U_{ts} = 50.8, 66.2$  knots.

Figure 55. Turbulent energy spectra.





(c)  $U_{tS} = 100 \text{ knots}$ .

Figure 55. Concluded.

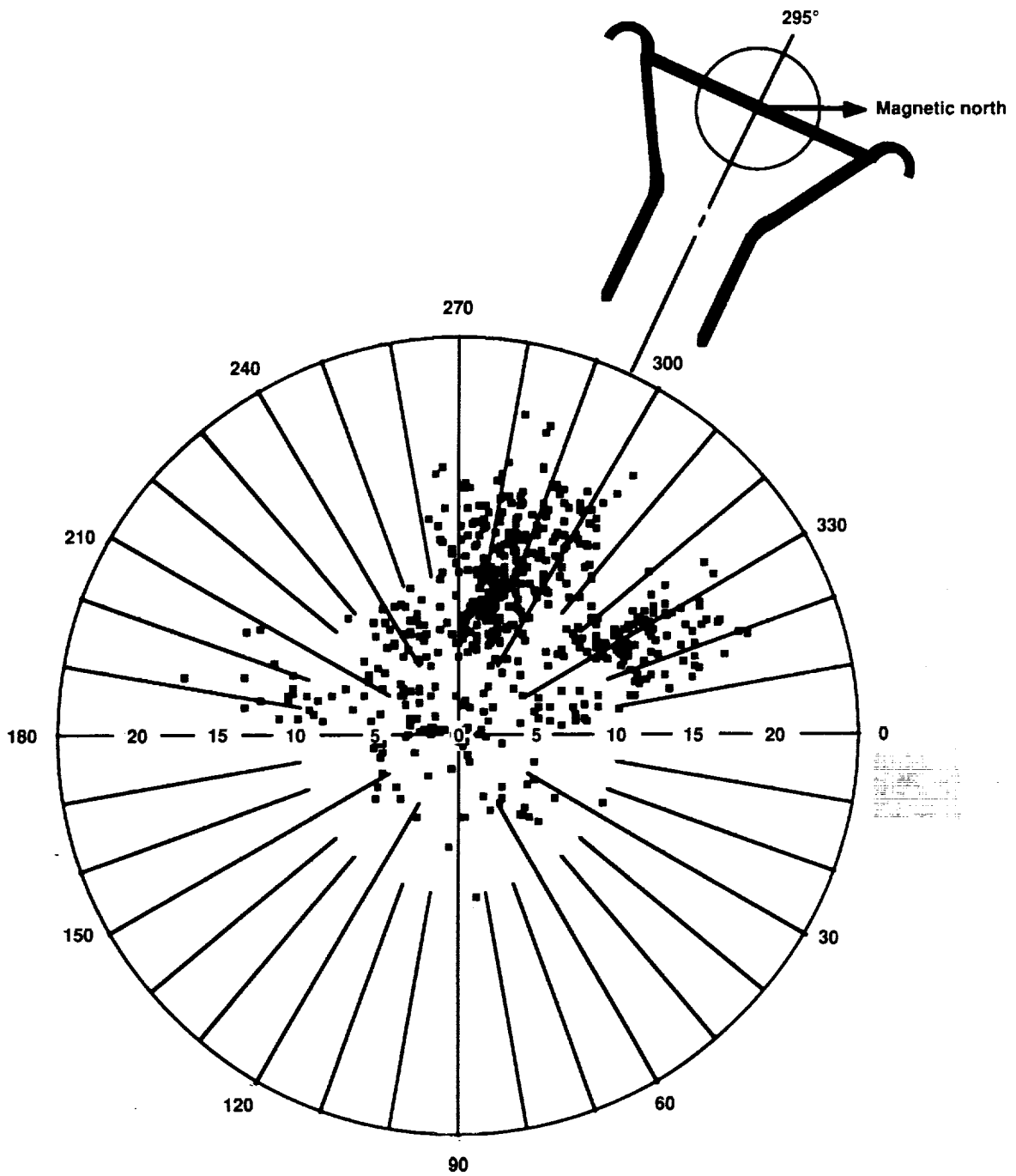


Figure 56. FLOCAL wind rose.

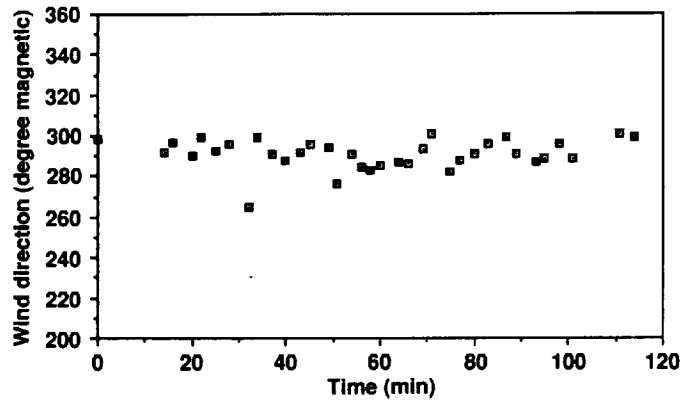
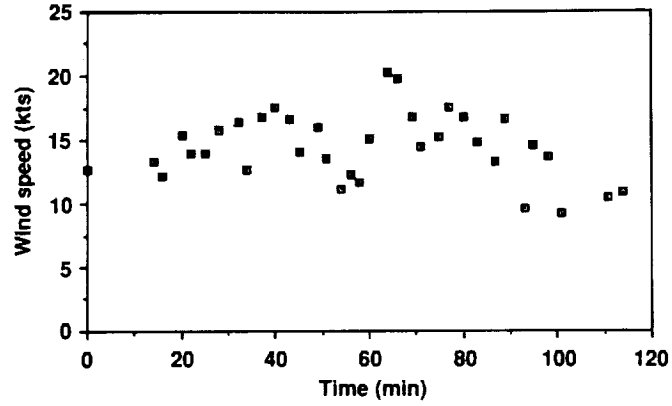


Figure 57. Variation of wind speed and direction during a typical FLOCAL run.

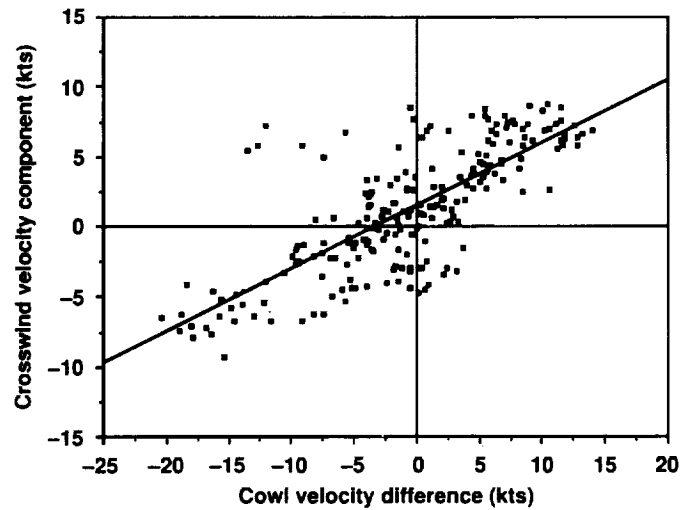


Figure 58. Difference in cowl velocity plotted against the wind velocity component aligned perpendicular to the tunnel centerline.

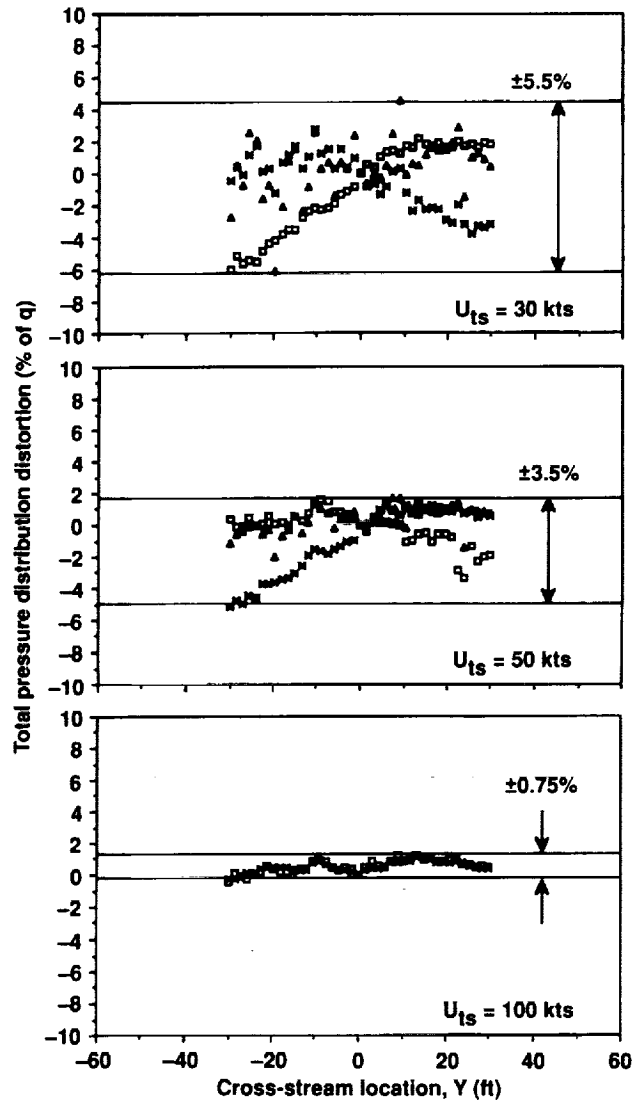


Figure 59. Total pressure distributions in percent of average  $q$  for three speed ranges and for various wind conditions.

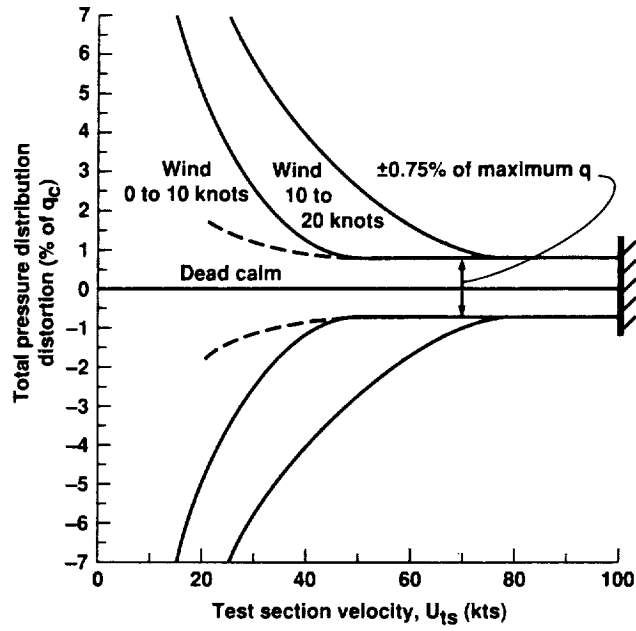


Figure 60. Total pressure distribution distortion versus test section velocity for various wind conditions.

# REPORT DOCUMENTATION PAGE

Form Approved  
OMB No. 0704-0188

Public reporting burden for this collection of information is estimated to average 1 hour per response, including the time for reviewing instructions, searching existing data sources, gathering and maintaining the data needed, and completing and reviewing the collection of information. Send comments regarding this burden estimate or any other aspect of this collection of information, including suggestions for reducing this burden, to Washington Headquarters Services, Directorate for Information Operations and Reports, 1215 Jefferson Davis Highway, Suite 1204, Arlington, VA 22202-4302, and to the Office of Management and Budget, Paperwork Reduction Project (0704-0188), Washington, DC 20503.

1. AGENCY USE ONLY (Leave blank)		2. REPORT DATE January 1993	3. REPORT TYPE AND DATES COVERED Technical Memorandum	
4. TITLE AND SUBTITLE Performance and Test Section Flow Characteristics of the National Full-Scale Aerodynamics Complex 80- by 120-Foot Wind Tunnel			5. FUNDING NUMBERS 505-50-28	
6. AUTHOR(S) Peter T. Zell			8. PERFORMING ORGANIZATION REPORT NUMBER A-92058	
7. PERFORMING ORGANIZATION NAME(S) AND ADDRESS(ES) Ames Research Center Moffett Field, CA 94035-1000			10. SPONSORING/MONITORING AGENCY REPORT NUMBER NASA TM-103920	
9. SPONSORING/MONITORING AGENCY NAME(S) AND ADDRESS(ES) National Aeronautics and Space Administration Washington, DC 20546-0001			11. SUPPLEMENTARY NOTES Point of Contact: Peter T. Zell, Ames Research Center, MS 221-5, Moffett Field, CA 94035-1000; (415) 604-3690	
12a. DISTRIBUTION/AVAILABILITY STATEMENT Unclassified — Unlimited Subject Category 09			12b. DISTRIBUTION CODE	
13. ABSTRACT (Maximum 200 words)  Results from the performance and test section flow calibration of the 80- by 120-Foot Wind Tunnel are presented. Measurements indicating the 80- by 120-ft test section flow quality were obtained throughout the tunnel operational envelope and for atmospheric wind speeds up to approximately 20 knots. Tunnel performance characteristics and a dynamic pressure system calibration were also documented during the process of mapping the test section flow field.  Experimental results indicate that the test section flow quality is relatively insensitive to dynamic pressure and the level of atmospheric winds experienced during the calibration. The dynamic pressure variation in the test section is within $\pm 0.75\%$ of the average. The axial turbulence intensity is less than 0.5% up to the maximum test section speed of 100 knots, and the vertical and lateral flow angle variations are within $\pm 0.5^\circ$ and $\pm 0.7^\circ$ , respectively. Atmospheric winds were found to affect the pressure distribution in the test section only at high ratios of wind speed to test section speed.				
14. SUBJECT TERMS Wind tunnel, Calibration, Flow			15. NUMBER OF PAGES 62	
			16. PRICE CODE A04	
17. SECURITY CLASSIFICATION OF REPORT Unclassified	18. SECURITY CLASSIFICATION OF THIS PAGE Unclassified	19. SECURITY CLASSIFICATION OF ABSTRACT	20. LIMITATION OF ABSTRACT	